Selected Aspects of Wireless Communication between Nano-devices

Selected Aspects of Wireless Communication between Nano-devices

Proefschrift

ter verkrijging van de graad van doctor
aan de Technische Universiteit Delft,
op gezag van de Rector Magnificus prof.dr.ir. K.C.A.M. Luyben,
voorzitter van het College voor Promoties,
in het openbaar te verdedigen op 19 november 2015 om 10:00 uur

door

Dmitriy Penkin

Master of Science (Electrical Engineering)
V.N. Karazin Kharkiv National University, Ukraine

geboren te Kharkiv, Ukraine

This dissertation has been approved by the:

Promotor: Prof. DSc. A. G. Yarovoy
Copromotor: Dr.ir. G.J.M. Janssen

Composition of the doctoral committee:

Rector Magnificus
Prof. DSc. A. G. Yarovoy, Delft University of Technology, promotor
Dr.ir. G.J.M. Janssen, Delft University of Technology, copromotor

Independent members:

Prof. dr. I. Niemegeers, Delft University of Technology
Prof. ing. F. Le Chevalier, Delft University of Technology
Prof. dr. G. Leus, Delft University of Technology
Prof. dr. W. Serdijn, Delft University of Technology
Prof. dr. A.B. Smolders, Eindhoven University of Technology

This research was supported by Delft University of Technology.

ISBN: 978-94-6186-571-7
Selected Aspects of Wireless Communication between Nano-devices.
PhD Dissertation, Delft University of Technology.

Author e-mail: dmitriynet@gmail.com

Dedicated to my beloved wife,
my family and my parents

Summary

Recently, the concept of a nanonetwork has attracted large attention of researchers as it potentially offers low-cost solutions for a wide spectrum of current applications and enables numerous emerging ones. At present, however, all the sensor networks consist of a relatively small number of macroscale devices with their positions carefully pre-determined. The typical nanonetwork, on the contrary, can be envisioned as a swarm of nanomachines that are distributed in a random manner, which also can reach covered places, accomplish sensing directly inside a phenomenon or equip an application with enhanced control capabilities. To operate and monitor within a macroscale application area, information sharing between nanonetwork entities is required (likewise data transfer among human cells). Electromagnetic waves at microwave frequencies can potentially enable wireless communication between nanomachines even in vicious and hazardous environments. However, the paradigms of traditional microwave communication must undergo a substantial revision before being applied to nanotechnology: due to space restrictions, nanomachines have very strong power limitations and should be capable to operate on an extremely tight energy budget. This places a very strong restriction on the communication link power budget. Moreover, networking-level techniques capable of describing a connectivity and signal propagation in the 'topology-less' nanonetwork are currently missing. These two open issues served as primary motivating factors for this doctoral dissertation, which broadly focuses on the feasibility and development of electromagnetic-based communications for nanonetworks.

The research starts with the analysis of the energy consumption demands to establish a conventional, bidirectional RF link between two nanomachines. A power gap between the communication needs of a nanomachine and its available energy budget, which was detected within this analysis, triggered research on antenna-based

and channel-based possible solutions to bridge it. In particular, research is focused on (1) the development of a highly efficient concept of an electrically small antenna for a nanomachine; (2) the advancement of electromagnetic theory for nanoscale fullerene structures and (3) modelling and analysis of the impact caused by a surface wave supporting interface on the power budget of the communication channel between nanomachines. At the networking level, connectivity of the nanonetwork and signal spreading in it is studied using percolation theory as well as the method to localize the message source in a nanonetwork is proposed.

The results obtained in this thesis provide solutions to key problems of nanonetworks at both the physical layer and the networking layer, demonstrate the potential of the nanonetworking concept and thus represent an important step forward in the development of nanonetworks.

Keywords: *nanonetworking, nanoscale node, wireless channel, electrically small antenna, fullerene structures, surface wave, percolation theory.*

Samenvatting

Recentelijk heeft het concept van een nanonetwerk veel belangstelling gekregen van onderzoekers, omdat het potentieel goedkope oplossingen biedt voor een breed scala van bestaande toepassingen en talloze nieuwe toepassingen mogelijk maakt. Op dit moment bestaan sensornetwerken uit een relatief klein aantal vrij grote apparaten waarvan de lokaties vooraf heel zorgvuldig vooraf bepaald zijn. Een typisch nanonetwerk daarentegen kan echter gezien worden als een zwerm van nanomachines die op een willekeurige manier verspreid zijn, dat een bepaald gebied bestrijkt, dat monitortaken kan uitvoeren in een afgeschermde omgeven of een toepassing kan voorzien van uitgebreide extra besturingsmogelijkheden. Om te kunnen opereren en monitoren binnen een grootschalig toepassingsgebied, is informatie-uitwisseling binnen het nanonetwerk vereist (vergelijkbaar met informatie-uitwisseling tussen menselijke cellen). Elektromagnetische golven op microgolf frequenties zijn in principe geschikt voor draadloze communicatie tussen nanomachines,,zelfs onder ongunstige en gevaarlijke omstandigheden. Echter, de paradigmas van traditionele microgolf communicatie dienen aanzienlijk te worden aangepast voordat deze kunnen worden toegepast op nanotechnologie: als gevolg van de beperkte ruimte zijn nanomachines enorm beperkt in hun energieverbruik en zullen moeten kunnen werken met een zeer krap energiebudget. Dit leidt tot een zeer beperkt vermogensbudget voor een communicatie verbinding. Daarbij komt dat technieken op netwerk niveau voor het beschrijven van de connectiviteit en de signaal propagatie op dit moment nog ontbreken. Deze twee open vragen vormen de primaire motivatie voor deze doctorale thesis, die breed ingaat op haalbaarheid en ontwikkeling van electromagnetisch gebaseerde communicatie voor nanonetwerken.

Het onderzoek start met de analyse van het benodigde energieverbruik voor het tot stand brengen van een conventionele bi/directionele RF verbinding tussen twee

nanomachines. Een door deze analyse ontdekt gat tussen het energieverbruik van een nanomachine en het beschikbare budget, leidde tot onderzoek naar mogelijke op antenne en verbindingsniveau gebaseerde oplossingen om dit probleem te overbruggen. In het bijzonder wordt het onderzoek gericht op (1) de ontwikkeling van een heel efficint concept voor een elektrisch-kleine antenne voor een nanomachine; (2) de uitbreiding van de elektromagnetische theorie voor fullereen structuren op nano niveau en (3) modellering en analyse van de invloed van een door een scheidingsvlak ondersteunde oppervlaktegolf op het vermogensbudget van een communicatiekanaal tussen nanomachines. Op netwerk niveau, wordt de connectiviteit van een nanonetwerk en de verspreiding van signalen hierin bestudeerd met gebruikmaking van de percolatietheorie en tevens wordt een methode voorgesteld om een berichtenbron binnen een nanonetwerk te lokaliseren.

De resultaten die in deze thesis verkregen zijn geven oplossingen voor sleutelproblemen van nanonetwerken, zowel op fysiek als netwerk niveau, laten de mogelijkheden van het nanonetwerkconcept zien, en vormen als zodanig een belangrijke stap voorwaarts in de ontwikkeling hiervan.

Sleutelwoorden: *nanonetwerken, nano-schaal knooppunt, draadloze verbindingen, elektrisch-kleine antenne, fullereen structuren, oppervlaktegolf, percolatietheorie.*

Contents

List of Figures

List of Tables

List of Acronyms and Symbols

Acronyms

2D	Two-dimensional
3D	Three-dimensional
BPSK	Binary Phase-Shift Keying
CMOS	Complementary metaloxide semiconductor
CNT	Carbon nanotube
DDA	Discrete dipole approximation
EM	Electromagnetic
ESA	Electrically small antenna
FET	Field effect transistor
GNR	Graphene nanoribbon
ICT	Information and communications technology
IOX	Infrared/Optical/X-ray
MEMS	Microelectromechanical systems
MoM	Method of moment
NFC	Near field communication
RF	Radio frequency
RFID	Radio-frequency identification

Chapter 1

Introduction

In December 1959, the concept of nanotechnology was for the first time addressed by the Nobel laureate physicist Richard Feynman in his famous speech entitled "There's Plenty of Room at the Bottom" [31]. In his talk, he pointed out how the handling of individual atoms and molecules would empower the creation of nanoscale machines. Fifty years later, nanotechnology is offering a set of tools and techniques capable of realising nanomaterials with novel properties not observed in macroscale counterparts. By taking advantage of these properties, nanotechnology is also focusing on the development of new nanoscale components with exceptional functionalities, e.g. nanosensors, nanoprocessors, nanobatteries and the like. It is foreseen that next generation nanotechnology will achieve the creation and design of nanomachines up to a few microns, which would include such nanocomponents in a single body and execute simple tasks such as sensing, actuation and computing [4]. However, to overcome their very limited coverage and performance, nanomachines are expected to cooperate and share information with a central controller and/or amongst themselves. The resulting nanonetwork (a swarm of interconnected nanomachines) could be deployed over large areas and reach remote places, providing extremely fine-grained sensing capabilities and execution of complex tasks. Such nanonetworks are thought to revolutionize a human life-style by enabling a new dimension of applications, which are not yet feasible.

1.1 Nanonetwork: Its Applications and Pecularities

Nanonetworks are meant to be deployed within an area to perform imperceptible sensing directly inside a phenomenon and/or yield specific tasks with superior control capabilities. There are numerous important applications where these systems could be employed. In particular, nanonetworks could be primarily applied for monitoring and smart control purposes in the following contexts:

- **Biomedicine and health.** Patient physiological data (e.g. body temperature, blood pressure, pulse, blood glucose level and the like) could be sensed and automatically transmitted by the nanonetwork to a physician interface, where it could be used for health status monitoring and medical exploration [16, 32]. Nanomachines operating in a blood stream could continuously analyse the blood, prevent coagulation/thrombosis as well as recognize cancer and other diseases at an early stage [138]. More capable nanomachines might also be implanted into a human body to deliver drugs to specific cells and even provide treatment for a number of illnesses, such as Parkinsons [39, 61]. Furthermore, nanonetworks capable of measuring gestures are able to support handicapped people and offer them a more independent living. Finally, these networks could assist in the performance of surgical procedures in unreachable areas as well as equip artificial limbs with a tactual sensation.

- **Environmental monitoring.** Nanonetworks could increase crop and livestock management by precisely controlling fertilizer concentrations [68]. The field of hydrochemistry for monitoring of freshwater quality has a compelling need for nanonetworks because of the difficulty to sample in unreachable locations or under adverse conditions [25]. By using nanomachines, dangerous levels of bacteria in food packaging could be detected at a much finer scale to control its freshness and shelf-life [130]. In military engineering, nanonetworks could enable advanced nuclear, biological and chemical defenses and sophisticated damage detection systems for soldiers and vehicles [58]. In particular, nanomachines could accurately explore and survey inhospitable environments such as remote geographic regions or toxic locations.

- **Civil engineering.** Nanonetworks can be deployed in different materials and structures, such as bridges, highways or plane wings, to detect and warn of structural weakness. Nanonetworks might enable a set of smart objects, like

e.g. car tires, which can measure their shape while driving through a large number of nanomachines embedded on the surface [125]. This could lead to a substantial enhancement in driving performance, road sensitivity and safety. In disaster recovery scenarios, buildings razed by an earthquake could be infiltrated with a set of nanomachines to locate signs of life. By employing nanonetworks, urban planners could track groundwater patterns and how much carbon dioxide cities expel, leading to better land-use decisions [113].

- **Smart structures.** Future robots for industry and private households might be equipped with nanonetworks, which could provide with a tactual sensation and allow them to execute highly complicated actions. Using smart gloves or similar devices equipped with nanomachines for gaming applications could lead to a far more engaging interaction. Potential industrial applications of nanonetworks also include cleaning of hardly reachable surfaces and early wear identification in machines [89]. Smart surfaces and paintable electronics would be another use of nanomachines: a large number of such devices is spread on a surface and the resulting ensemble auto-configures into a distributed computational network. This network would implement a range of innovative functions, such as high-resolution wall-sized displays, artificial skin, intelligent materials that respond to strain or stress (e.g. [69]), coatings with long-term memory and etc.

Considering all of the application domains above, it is clear that the concepts of nanonetworking are rapidly gaining popularity as such networks are potentially low-cost solutions to a variety of real-world challenges. In a similar way that happens with human cells, the sharing of information between nanomachines would allow the fulfillment of much more complex tasks and offer nanonetworks to cover and operate over macroscale application areas. Thus, the nanonetwork is envisioned to be a swarm of interconnected sensors and characterised by principal properties [19], such as:

[1] Self-organisation and decentralisation (plain hierarchy);

[2] Multihop routing: the collected data are forwarded throughout the network towards an end-user using intermediate nanomachines as relays;

[3] Dense deployment and cooperation among nanomachines;

[4] Dynamic topology due to fading and failures of nanomachines.

The last two characteristics make nanonetworks quite different from existing wireless random networks, such as ad hoc [110] or mesh [6] systems, and hence new networking-level problems should be addressed to enable nanonetworks in practice.

1.2 Primary Approaches to Interconnect Nanomachines

At present, four major types of communication among nanomachines are discussed: nano-mechanical, acoustic, molecular (also referred to as chemical) and electromagnetic communication [114]. In nano-mechanical communication, data are transmitted through hard junctions between linked nanomachines. Each of such physical linkages should precisely be mounted to establish and ensure a robust peer-to-peer connection. Since the manipulation of these junctions at nano-level is tough, nano-mechanical communication is a fair candidate to provide a few nanomachines with communication capabilities, but not the nanonetwork being a multitude of interconnected nanoscale devices. In acoustic communication, the transmitted message is encoded using ultrasonic waves. Such a communication requires the development of nanoscale ultrasonic transducers capable of sensing alterations in pressure produced by these waves and emitting acoustic signals as appropriate. However, the main principles of acoustic communication currently offer no way to design a feasible ultrasonic transceiver at nano-level [32]. In turn, molecular and electromagnetic approaches are regarded to be the most promising to enable data transfer between nanomachines [110] and they are discussed in details in Subsection 1.2.1 and 1.2.2, respectively.

1.2.1 Molecular Communication

The concepts of molecular communication are to use molecules or other microbiological matters to encode and transmit information among nanomachines [95]. Inspired by existing biological and natural systems, molecular communication has attracted a considerable attention in the recent years. The main advantage to such a communication technology is due to the fact that basic components of nanomachines and signal carriers (i.e., molecules, organelles and living cells) are already at nano-level. Since there is no need to downscale these entities, molecular communication is free of a number of scaling issues attributed to electromagnetic communication. Molecular communication also offers immense savings in energy consumption: in particular, a single molecular reaction capable of performing multiple computations consumes

10000 times less energy than an up-to-date microelectronic transistor [134]. Biocompatibility is another advantage of molecular-based nanonetworks as it offers a straightforward interaction with front-page medical applications [94]. Two different approaches are currently developed to enable molecular communication between nanomachines.

The traditional method exploits internal characteristics of molecules (e.g. relative positioning and polarization of molecular elements) to encode a message. By means of molecular motors [93], i.e., the proteins capable of generating movements using chemical energy, the encoded molecules are transported to a receiving side, where the transmitted data can be decoded. In general, this method is similar to the use of encrypted packets in macroscale communication networks, where an intended receiver is able to detect the information. However, some undesired interactions between a message-carrying molecule and other environmental molecules might appear. Such a noise in the interactions could modify the structure of the encoded molecule and thus lower the probability to detect and recognise the message.

The alternative approach [96] transfers a message relying on the concentration fluctuations of ions or specific molecules (similar to an amplitude and frequency modulation in traditional electromagnetic communication). For example, a molecular transmitter is able to encode a signal through modulating the concentration of Ca^{2+} ions. By measuring continuously such a concentration level (the number of received molecules per volume), a receiver decodes the delivered data. The noise in this case is subject to interference fluctuations, which might come from neighbouring transmitters. The second approach can directly be related to existing systems, where data are forwarded through a set of time-varying sequences.

Table 1.1: Electromagnetic Communication vs. Molecular Communication

Characteristic	Electromagnetic	Molecular
Communication carrier	Electromagnetic waves	Molecules
Propagation speed	$\sim 3 \times 10^8$ m/s	Extremely low
Medium conditions	Affect communication	Heavily affect communciation
Communication distance	Medium ($\sim$ m)	Very small ($\sim$ mm)
Other properties	High energy consumption (energy-per-bit $\sim$ nJ/bit)	Low energy consumption (energy-per-bit $\sim$ pJ/bit)

Being a new and immature communication paradigm, molecular communication has not been developed and formalised yet. In this regard, a number of fundamental problems and concerns (e.g. how to encode molecules in a reliable way, how to secure the molecular link from alterations in viscosity, temperature or pH) needs to be solved to realise a molecular link between nanomachines in practice. Moreover, molecular communication is subject to several limitations (Table 1.1). In particular, it only supports extremely low data rates and depends heavily on the environmental conditions, such as medium obstacles, wind, tide and the like.

1.2.2 Electromagnetic Communication

Due to the advances in wireless communication and MEMS technologies, the development of nanomachines suitable to communicate by means of electromagnetic waves is an ongoing process. To realise communication at nano-level, the engineering community is investigating two different electromagnetic spectra: RF and infrared/optical/X-rays range.

Communication with Infrared/Optical Waves/X-rays

The existing laser-emitting diodes integrate an oscillator, intensity modulator and antenna in a single entity and thus represent compact IOX transmitter. The size of such a transmitter is formally limited to the cavity with a dimension larger than a half-wavelength, which is known as the diffraction limit of a cavity [21]. Thanks to extremely small wavelengths in the IOX range, there are several approaches suitable to produce a laser-emitting diode at nanoscale. For example, by employing the metal-coating method, such a sub-micron transmitter has recently been proposed in [52]. An IOX receiver uses a photodetector array, which is composed of a large number of elementary cells (pixels). Due to the ability to convert an incident radiation into a proportional current, the photodetector array combines the functionality of a traditional antenna and detector and its implementation offers the realisation of smaller receivers. Although the recent advances enable the creation of a photodetector array at nano-level (the smallest array pixel has a dimension about 100 nm [87]), the utilization of CNT technologies [48, 55] would allow the development of IOX receivers even of smaller sizes.

Beside a possibility to manufacture a nanoscale transceiver, the IOX communication provides also several advantages over RF transmission systems. The IOX channel

in free space is in particular characterised by a lower energy-per-bit ratio, better resistance to jamming and higher data rates. Another benefit is the utilization of a large IOX band, which is unlicensed and unregulated today. Meanwhile, IOX communication is subject in matter to a set of limitations. Due to the extremely high operating frequencies, the IOX channel is described by high propagation losses. As the light penetration capabilities are weak, the IOX link requires an obstacle-free line-of-sight between transmitter and receiver. Since the IOX transmitters should generate highly directive radiation to compensate a very low sensitivity of nanoscale receiver, there will be a need to allocate and manipulate nanomachines in an application area which is not yet feasible in practice. Development of IOX antennas with reasonably wide radiation patterns might be able to relax the latter constrain.

Communication with RF Waves

Nowadays, RF waves (frequency up to 300 GHz; electronic circuits for higher frequencies at this moment are under development and their power efficiency is too low) are commonly exploited to interconnect wirelessly different macroscale devices, such as cellular phones, TV sets, satellites and so on, since they support high data rates and can establish a reliable connection at long distances. Thanks to recent progress in silicon technology, CNT and graphene electronics engineering, the development of nanoscale equipment capable of communicating via RF waves attracts a considerable attention [5, 153]. In particular, the possibility to employ the same antenna and electronic circuits for transmitting and receiving RF radiation leads to the design of smaller-scale transceivers, which can more effectively be integrated into nanomachines. However, the paradigms of traditional RF communication must undergo a substantial revision before being applied to connect nanomachines.

Since energy component replacement is not an option for networks with thousands of nodes, nanomachines must have a very long lifetime to perform networking tasks in an acceptable manner. Furthermore, as a consequence of space restrictions, the nanomachines would have very strong power limitations and must operate on an extremely tight energy budget. Therefore, the power demands of an RF transceiver integrated in a nanomachine should be kept very small to bridge with its restricted energy capabilities. This results in a need to equip such transceivers with low-energy electronics and efficient antennas for RF communication. From electrodynamics [9], it is known that an antenna can radiate in an effective fashion only when its size is in the order of the operating wavelength λ. In such case, the antenna impedance might have

	Circuit size (m^3)	Antenna size (m^3)	System size
Hitachi	1E−14	1E−08	1E−08
UCI CNT Radio	1E−23	1E−05	1E−03
France-Telecom	1E−09	1E−09	1E−09
Smart Dust	3.125E−09	1E−06	1E−06
SMS	NA	NA	1E−06
BioRasis	NA	NA	5E−09
ISSYS	NA	NA	1E−06
Potential single-chip radio			1E−14
Volume of single cell			1E−18
Potential nano radio			1E−21

Table 1.2: Comparison of major parameters for micro- and nano-nodes (from [17]).

a small imaginary part and this would entail an easy compatibility and minor losses with a transmitter to which the antenna is connected. As the operating wavelength alters from 100 km to 1 mm in RF band, the realisation of a nanoscale antenna capable of broadcasting RF waves, however, becomes a fundamental scaling issue. The tiniest RF transceivers available in practice are surveyed and presented in Table 1.2. In [17], the authors observe that electronic circuits can already be manufactured at nano-level with the CMOS technology, while the size of existing antennas for bidirectional RF communication are far beyond the nanomachine dimensions.

1.3 RF-based Nanonetworks

From an application perspective, nanonetworks are foreseen to be deployed over large macroscale areas (from a few square meters to kilometres). Characterised by the communication range from nm to mm, the molecular-based nanonetworks would therefore consist of an incredibly high number of nanomachines and could only be manageable in a cumbersome way. Due to a sufficiently large peer-to-peer communication distance (from cm up to several meters), electromagnetic-based nanonetworks would be composed of a much smaller number of nanomachines and thus offer a low-cost, controllable and robust solution to perform the application tasks. Meanwhile, since

nanonetworks would commonly operate in hazardous, vicious and nonuniform environments, the use of IOX waves become an inefficient or even infeasible (in case of non-transparent propagation medium) mean to establish connections among nanomachines. In this way, this thesis focuses on studying and modelling the communication paradigms of RF-based nanonetworks. Since such nanonetworks require nanomachines with a wireless communication component capable of both transmitting and receiving data, RFID, NFC and other technologies, which involve passive electronic circuits, are out of the scope of this work. Note that these communication techniques are however primary candidates to establish a connection between an 'active' macroscale unit and a 'passive' nanomachine as they offer the rapid miniaturisation of electronic devices by enabling battery-less solutions [17].

1.4 Research Challenges

To implement RF-based nanonetworks in practice, two novel fundamental problems, such as (1) how to establish a feasible bidirectional wireless link between nanomachines and (2) how to control a signal dispersion in such a large-scale and 'topology-less' system, should be treated (Fig. 1.1). To comprehensively approach the former issue, the approaches to bridge the gap between energy capabilities of a nanomachine and its power consumption demands need to be developed. To address the latter networking-level problem, we should ensure that the nanonetwork is connected and have a suitable model to describe the signal propagation in it. Hence, the relative challenges, their novelties and importances, are formulated and outlined below. Meanwhile, due to the interdisciplinary approach of this work, the state-of-the-art overview on each of these challenges and the selection of the methods are exclusively discussed in the corresponding thesis chapters.

In any type of potential applications, some of which are discussed in Section 1.1, the sustainability of a nanonetwork should be provided on a long-term or ideally permanent basis to offer an acceptable usability of this system. To enable autonomous operation of nanomachines, the implementation of an efficient RF wireless component at nano-level is required to meet the drastically constrained power capabilities of nanomachines. From a classical electromagnetics point of view, the wireless communication component with a conventional antenna, which is downscaled to a few hundreds of nanometers, would however operate in an inefficient manner. The impedance of such an electrically small antenna becomes mostly reactive and this causes huge mis-

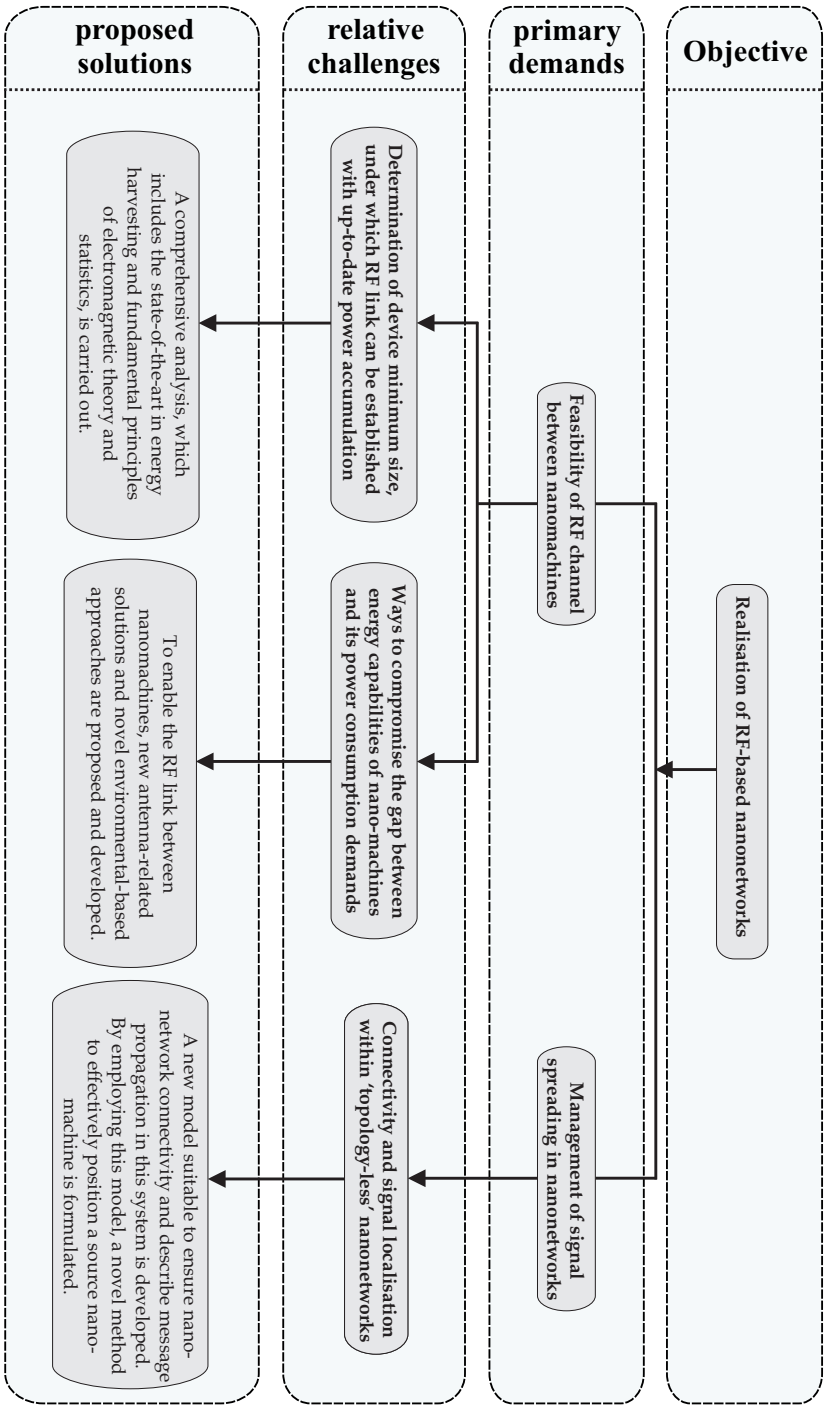

Figure 1.1: The block diagram of thesis challenges & approaches.

match losses between the antenna and an electronic circuit. The use of extremely high operating frequencies might compromise the feasibility of RF communication among nanomachines - the increase of antenna electrical size would lower the mismatch losses and thus implies a more effective communication link. Nonetheless, with enlarging the operating frequency f the free space propagation losses increase ($\sim f^2$). Therefore, we face the first challenge: **by considering state-of-the-art in power accumulation, how much is the gap between energy capabilities of nanomachine and its power consumption demands aimed to realise a conventional and bidirectional RF link with a similar device (i.e., the devices are in the far field of each other)?**

According to [24], the wave propagation velocity in GNRs and CNTs might be decreased up to one hundred times compared to the speed of light (it depends on the structural geometry, temperature and Fermi energy). In this way, the resonant frequency of graphene/CNT-based antennas can be up to two orders of magnitude below that of antennas built with traditional materials. Due to this finding accompanied by rapid advances in developing and manufacturing nanoscale GNR and CNT structures, there is strong interest in designing graphene/CNT-based antennas for the nanomachine communication block. In particular, such a nanoscale antenna is described by using the network analysis theory in [18]. Meanwhile, the performance of CNT-based dipoles is formally modelled from the classical electrodynamics point of view in [42,45]. When it comes to GNRs, the propagation model of electromagnetic waves on a graphene sheet is first formulated in [44]. Inspired by the developed models, a few advantageous graphene/CNT-based antenna designs, such as [22, 67, 71, 82, 128], are successfully proposed and investigated. In these classical-electrodynamics-based models, GNR and CNT structures are treated as continuous objects characterized by a frequency-dependent dielectric constant or conductivity. Unfortunately, this approach limits the minimum size of a nanoscale particle under analysis: it must contain a sufficient number of atoms and form a regular structure to determine its electromagnetic properties. Therefore, much smaller nanoscale objects (i.e., fullerenes [121]) received little attention by the scientific community because of no means to determine their electromagnetic properties. Since fullerenes and fullerene-based structures exhibit a great potential in designing antennas for nanomachines [135,159], we face the first challenge: **how to model and determine the electromagnetic properties of various fullerene derivatives in a formal way?**

Another idea on how to bridge the energy capabilities of a nanomachine with

its power consumption requirements is to use properties of a communication environment to maximise the received power. In particular, many application scenarios include the distribution of nanomachines over different surfaces (warning systems for airplane wings and highways, smart surfaces, paintable electronics and the like). The influence of this surface on the power budget of the communication channel between nanomachines might be substantial for the nanonetwork realisation: for example, the existence of a strong link gain provoked by the interface is observed in [160], where the authors established a connection between microchips due to a surface wave contribution. Note that actual wireless links between two macroscale devices located close to an interface are typically modelled disregarding the surface wave impact as the amplitude of this wave decreases exponentially as the separation between the transmitter/receiver and surface increases [105]. Conversely, as nanomachines might be located very close to the interface, the contribution of the surface wave to the received power becomes significant and cannot be neglected. Considering that the quantitative impact of the half-space, which supports a surface wave, on the wireless link between nanomachines is not elucidated in the literature, we approach the second challenge: **what is the impact of the underlying surface-wave supporting half-space on the power budget of the communication link between nanomachines?**

At present, actual sensor networks consist of a relatively small number of macroscale nodes with their positions carefully engineered or pre-determined and they perform various monitoring tasks, e.g. to protect a forest against fire, to control the water waste in homes and so on. As shown in Section 1.1, the nanonetwork is foreseen as a multitude of densely deployed nanomachines, which are randomly distributed within an application area. Moreover, the simple functionality of nanoscale nodes entails that the network topology cannot be retrieved (a nanomachine have no resources to reconnoitre its surroundings). Due to all these properties, the nanonetwork becomes very distinguishable from the existing sensor systems and thus new solutions at the networking level are required to make it operable. Since the positioning of the source node in nanonetworks is in particular relevant from an application perspective, we eventually approach the third challenge: **how to describe signal spreading in the nanonetwork and accomplish localisation of the signal source within such a 'topology-less' system?**

1.5 Thesis Organisation

The four fundamental questions described above have been selected in this thesis. To address these research challenges and following the research guide shown in Figure 1.1, the thesis structure is organised as follows:

- in Chapter 2, the promising battery-driven solutions and potential power scavenging technologies are surveyed in an exhaustive manner to foresee the energy level available in the nanomachine. As the power consumption of the nanomachine is shown to be nearly identical to that of the wireless communication component, a comprehensive model suitable to analyse the feasibility of a communication between two nanoscale devices linked by means of far-field RF waves is formulated. This model is developed as an integrated solution by combining the fundamental principles of the electromagnetic and communication theories and statistics, and provides with the detailed treatment of such a peer-to-peer wireless link. By relating the results obtained from numerical simulations with the capabilities of up-to-date power sources, we determine the gap between the power demands of the nanomachine and its energy budget provided by the most potent power source.

- In Chapter 3, the electromagnetic properties of a nanoscale object with a small number of atoms are studied. The field scattered by such an object is analysed by means of the integral equation approach. Based on the developed framework and assuming that a fullerene is represented as a sphere with a certain 'effective' radius due to its ball-like atomic constitution, the relative dielectric constant of well-known fullerene derivatives are evaluated for the first time. Inspired by the Yagi-Uda antenna principle, we also investigate directional capabilities of a nanoscale fullerene-based Yagi-Uda-type antenna (i.e., the parasitic elements are represented by different fullerenes) at ultraviolet and optical frequencies. It was found however that such antenna will operate in X-ray range.

- In Chapter 4, by using the standard electromagnetic methods, we analytically analyse the impact of plain surface-wave supporting substrate on both the wireless propagation link between nanomachines and the characteristics of an electrically small antenna. The formulated approach treats such an 'interface impact' problem from a general perspective, as this is no need to take care of the fields within the substrate, and can exclusively be used to determine the parameters

of the optimum communication scenario for nanomachines in the presence of the surface-wave supporting interface between two different media.

- In Chapter 5, the nanonetwork connectivity is investigated using the percolation theory. The goal is to determine the minimum node density required to assure nanonetwork connectivity with a probability greater or equal to some prespecified value. For a nanonetwork with a large number of nodes, an arbitrary node distribution in space and with sufficient connectivity, the message propagation is modelled relying on the properties of the percolating cluster. Last but not least, thanks to the developed model, an effective source-positioning method, which can localise a source node in the 'topology-free' nanonetwork without retrieving its topology (i.e., no energy is consumed to perform the prerequisite self-organization stage at which sensor nodes scout their surroundings) is proposed for the first time.
- Finally, the research results are summarized and future research directions are proposed in Chapter 6.

Chapter 2

RF Link between Nanomachines: Feasibility Analysis

2.1 Structure of Nanomachines

The RF-based nanonetwork is expected to continuously monitor and control an application area in an extremely fine-grained way and properly transfer the collected data to an end-user. Hence, likewise its macroscale counterpart (e.g., MICA mote [51]), the nanomachine should at least include sensor unit, processing core, transmission block and power supply component in order to interpret an input received by sensors and broadcast it through RF transceiver (Fig. 2.1). In the following, we overview different potential solutions for the implementation of each primary component composing the nanomachine.

Sensing unit. Nanomaterials (GNRs and CNTs) possess outstanding sensing capabilities and are used in designing nanoscale sensors of different natures. Due to the unique properties of nanomaterials, these sensors are able to identify and measure new types of events, such as the physical characteristics of structures just a few nanometers in size [131], chemical compounds in concentrations as low as one part per billion [15], or the presence of biological agents such as virus, bacteria or cancerous cells [143, 157]. Last but not least, the nanomaterial-based sensors provides with high accuracy and often operate in a passive manner (i.e., require no energy to perform their tasks).

Processing unit. At present, the rapid miniaturisation of CMOS FET devices in dif-

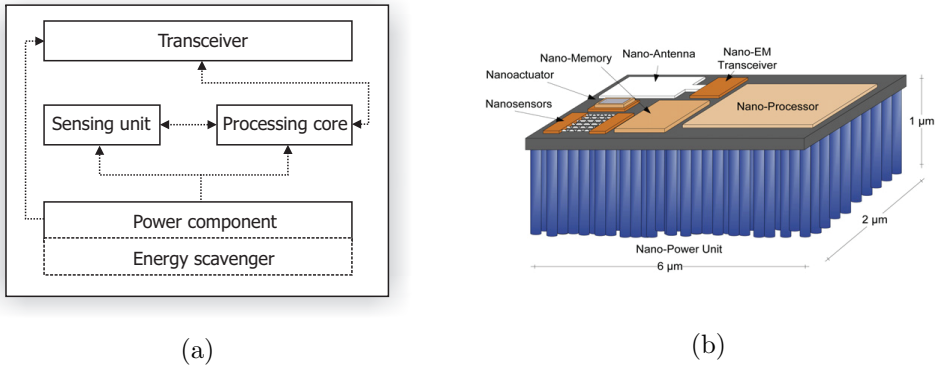

(a) (b)

Figure 2.1: (a) The typical architecture of the nanomachine. (b) the microscale sensor from [5].

ferent forms [10] enables the realisation of nanoscale processors. Nanomaterials, such as CNTs and GNRs, are also going to be employed to prototype control units in the nanometer scale. In particular, the smallest transistor has been manufactured using a thin graphene strip made of just 10 by 1 carbon atoms (i.e., less than 1 nm in all its dimensions) and experimentally tested [106]. Such a graphene-based transistors are not only tinier, but also able to operate at higher frequencies (as graphene exhibits almost ballistic transport of electrons, these particles can travel larger distances without being back-scattered). Meanwhile, next-generation processors made from nanoscale mechanical relays, which is currently under development, offers a significant reduction in power consumption since leakage current would be considerably lowered [78].

Power unit. Since the capabilities of conventional batteries are drastically restricted at nano-level, powering nanomachines requires new types of nanoscale energy storage. Hence, new concepts of energy supply unit (e.g. micro-fuel cells, micro-heat engines, radioactive sources and the like [116]) are actively being investigated to substitute the off-the-shelf battery technology. Nowadays, the most promising technique relies on the use of nanomaterials [147] and offers the volumetric capacity in the order of 45 $\mu\text{Ah}^{-1}\text{cm}^{-2}\mu\text{m}^{-1}$ proving their potential for driving nanoscale devices. However, with even such an expanded capacity there is a need to periodically recharge nanomachines, which cancels the usability of nanoscale batteries in realistic nanonetworks. To overcome the limitations of batteries in nanometer scale, the concept of self-powered nanomachines has recently been introduced [152] and attracts significant attention from the engineering community. The working principle of such devices is to convert the energy from some environmental source into electrical energy to con-

Table 2.1: Characteristics of promising environmental sources and harvested power.

Source	Source power	Efficiency	Harvested power
Ambient light			
Indoor	0.1 mW/cm^2	5-30%	10 μW/cm^2
Outdoor	100 mW/cm^2		10 mW/cm^2
Vibration/motion			
Human	100 μW/cm^2	1-10%	4 μW/cm^2
Industrial	2.5 mW/cm^2		100 μW/cm^2
Thermal energy			
Human	20 mW/cm^2	0.1%	20 μW/cm^2
Industrial	100 mW/cm^2	3%	3 mW/cm^2
RF			
Cell phone	0.3 μW/cm^2	50 %	0.15 μW/cm^2
WiFi	0.02 μW/cm^2		0.01 μW/cm^2

tinuously powering them. Since the most advanced secondary energy storage (i.e., graphene-based ultracapacitors [133]) possesses an energy density as high as that of a lithium-ion battery, the nanonetwork sensors are expected to be supplied only from an energy harvesting unit in order to have actual nanoscale dimensions.

Scavenging energy from the environment is thought to be the most useful solution for powering ultra-small devices as they might have infinite lifetime, provided that the energy harvesting and consumption processes are jointly designed. In particular, several potential ambient sources are being investigated to replenish the energy stored in microscale devices [116]. The powering capabilities of such environmental sources in micrometer scale is recently reviewed in [146] and presented in Table 2.1. As can be seen in this table, the existing ambient sources are not suitable to supply nanoscale electronic devices due to either an insufficient energy density and/or applicability restrictions. Such nanomachines are thus envisioned to be powered through a targeted energy delivery from a nearby rich source.

The emphasis in the discussion is on acoustic-driven power distribution as this approach are scalable into nanoscale domain and capable of transferring more power to nanomachines than other alternative methods: i.e., acoustic energy offers power densities on the order of 1 μW/cm^2 for a 100 dB wave or approximately 964 mW/cm^2 at 160 dB [115]. Moreover, acoustic-driven power delivery can maintain the oper-

ability of nanomachines both indoor and in harsh environments as well as causes no interference on wireless communications among such devices. At sub-mm scales, the energy harvesters exhibit resonance frequencies in the ultrasound range (above 20 kHz) and should thus be excited through ultrasonic acoustic waves. Although the use of ultrasound to deliver power for conversion back into electrical form attracts limited attention to date, there have already been implemented nanoscale generators, which are driven by ultrasonic waves and deliver ~ 10 nW of power to the nanomachine [151]. Due to the ongoing development of such acoustic-driven nanogenerators combined with the improvement of ultrasonic sources and advances in manipulation and processing of nanoscale materials, energy harvesting capabilities in the nanomachine are expected to be from several hundreds of nanowatts to a few microwatts. Therefore, the energy unit of nanomachine is hereinafter assumed to provide the power of 1 μW (or, -30 dBm).

Communication unit. To enable bidirectional communication via RF waves, each nanomachine should be equipped with a nanoscale transceiver. Such a wireless unit includes an electronic circuit for transmitting and receiving RF signals and antenna element. The former component can be manufactured in nanometer scale with the up-to-date CMOS technology [17], while the realisation of nanoscale antenna capable of radiating effectively at RF frequencies is formidable challenge: i.e., such an antenna is very electrically small compared to operating wavelengths in RF band and thus exhibits drastically reduced radiation performance. This fact actually implies that the communication unit is expected to consume the vast majority of energy provided by a nanoscale power scavenging component [83]. Since the overall power consumption of the nanomachine is appeared to be nearly identical to that of its wireless unit, we thus develop a formal model that comprehensively analyses RF communication link between two nanomachines in Chapter 2.2 in order to estimate the nanomachine power demands. Eventually, by relating the obtained results with power capabilities of state-of-the-art in energy harvesting, we would either demonstrate the feasibility of bidirectional communication between nanomachines via RF waves or express numerically the gap between energy features of nanomachine and its power consumption requirements.

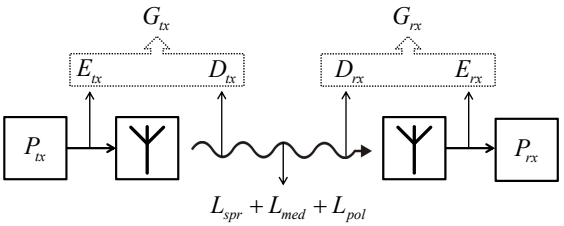

Figure 2.2: Major attenuation sources of radio communication channel.

2.2 Communication Demands of Nanomachine

To transmit a message via electromagnetic radiation, information is primarily modulated by systematically changing some property of RF waves, such as their amplitude, frequency, phase, or pulse width. When propagating radio waves strike the receiving antenna, the oscillating fields induce alternating currents in the conductor and eventually data in the waves can be extracted and transformed back into its original form. Hence, a peer-to-peer radio communication link depends upon characteristics of transmitting and receiving communication modules as well as is subject to several attenuation sources (Fig.2.2). The parameters $E_{tx/rx}$ and $D_{tx/rx}$ respectively correspond to the efficiency (i.e., the measure of mismatch between transmitter/receiver electronics and antenna) and directivity of transmitting/receiving antenna. Their product $G_{tx/rx}$, defined as an antenna gain, describes how well the antenna converts input power into radio waves headed in a specified direction (as a transmitting antenna) or indicates how well the antenna transforms RF radiation arriving from a certain direction into electrical power (as a receiving antenna). While propagating in a communication medium, radio waves primarily decays due to spreading loss L_{spr}, dissipation on environmental particles and inhomogeneities L_{med} and polarisation mismatch loss L_{pol}.

2.2.1 Friis-equation-based Analysis

Since a nanomachine's antenna of any design is very electrically small with respect to the operating radio wavelength λ, its radiation properties are similar to those of elementary dipole [9]: i.e., the nanomachine's antenna has a linear polarisation and is characterised by a torus-shaped radiation pattern with equal radiation in H-plane and maximum directivity $D = 1.76$ dBi. Therefore, to minimize the amount of power

required to establish bidirectional radio communication between two nanomachines, the transmitting and receiving antenna is regarded to be vertically polarised (there is no polarisation misalignment between the antennas $L_{pol} = 0$ dB) and other payload components of nanomachine make no impact on the channel budget. Moreover, the nanonetwork is assumed to be deployed in 2D plane and operates in free space: this would maximise the antenna's directivity $D_{tx/rx}$ and cause no attenuation of a radio signal passing between the nanomachines due to the propagation medium ($L_{med} = 0$ dB). In this way, the free space propagation of RF waves can be described by the Friis transmission equation [33] in dB domain as:

$$P_{tx}\ [dBm] = P_{rx}\ [dBm] + \underbrace{20\log_{10}\frac{4\pi R}{\lambda}}_{L_{spr}} - G_{tx}\ [dB] - G_{rx}\ [dB], \tag{2.1}$$

where P_{tx} is the output power of the transmitter, P_{rx} is the received power and R is the communication distance between nanomachines. In turn, the power P_{rx} is complex and obtained through the energy per bit to noise power spectral density ratio E_b/N_0, the data rate S and the noise spectral density N_0 as follows:

$$P_{rx}\ [dBm] = N_0\ [dBm] + E_b/N_0\ [dB] + S\ [dB]. \tag{2.2}$$

In an attempt to estimate the lower limit of transmitting power P_{tx}, we relax conditions on coefficients in Eq.(2.2) for numerical analysis as follows:

- Since BPSK modulation technique is optimum in terms of power consumption for microwave channel [137], it is exclusively applied to model the wireless link of interest and aids to assess P_{rx}. In particular, for BPSK modulation the maximum acceptable bit-error probability of 10^{-3} is achieved with the energy per bit ratio $(E_b/N_0)_{min} = 7$ dB. The thermal noise power spectral density is set to $N_0 = -174$ dBm/Hz as the communication takes place at room temperature ($T = 290K$). Meanwhile, the low data rate $S = 100$ bit/sec is used for the simulations as this value can satisfy the communication demands of nanonetworking applications.

- To apply the Friis-equation-based analysis, the receiving point should be located in the radiative region of transmitting antenna (i.e., the criterion $R \geq 10\lambda$ must be fulfilled as shown in [59]). Hence, the minimum valid distance $R = 10\lambda$ is employed in numerical calculations.

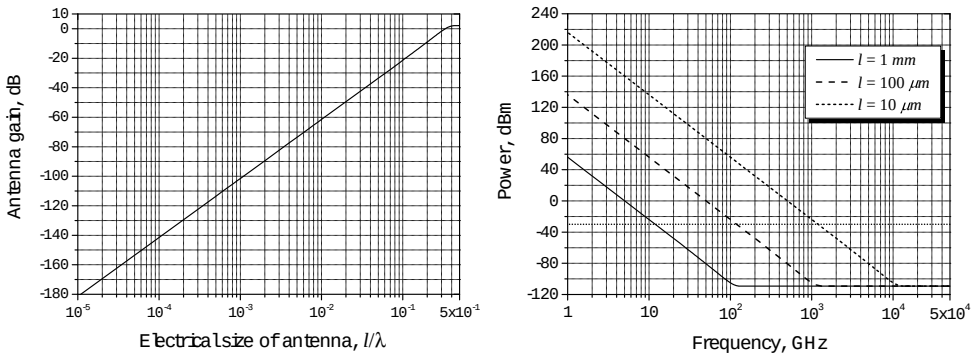

(a) (b)

Figure 2.3: (a) Dipole gain in azimuth plane versus its electrical size and (b) he

- The transmitting and receiving antennas are identical and fairly modelled as an electrically small vertical dipole with the length l and radius $r = l/10$. Based on the extensive simulations in the electromagnetic solver [1], the power gain of such a dipole in the azimuth plane is determined as a function of its electrical length l/λ (Fig.2.3a). Note that the calculations involve the assumption that the dipole antenna is connected and fed by a transceiver with non-reactive characteristic impedance $Z_0 = 50$ Ohm.

- The operating frequency is set to 300 GHz – the increase of antenna electrical size will lower the mismatch losses and increase the power gain. In this context, though the free space propagation losses also increases, the minimum amount of the transmitted power is calculated to decrease with enlarging the operating frequency. Higher frequencies are meanwhile technologically impracticable and thus not considered.

Eventually, the required amount of output power P_{tx} to maintain the peer-to-peer communication between devices with antennas of length $l = 1mm, 100\mu m, 10\mu m$ is evaluated over a broad frequency range and shown in Fig.2.3b. As shown in this figure, at the frequency $f = 300$ GHz the transmitted power $P_{tx} \cong 20$ dBm is needed to support the radio communication between antennas with $l = 10\mu m$, which is several orders greater than the capabilities of nanomachine's energy unit (-30 dBm). Nonetheless, the Friis-equation-based analysis is limited to model radio propagation in free space, requires supplementary data on antenna performance, which has to be collected using a third party solver, and cannot analyse the impact of statistical

properties of the nanonetworking channel. Therefore, a more general model capable of investigating the wireless channel between two nanomachines in an uniform medium and assessing its statistical nature is developed in the next subsection.

2.2.2 Green-function-based Model

The radio link between electrically small devices, which are defined by their position and orientation and communicate in a homogeneous environment, is under investigation. By means of the standard electromagnetic methods and using the Hertz potential formalism, we relate the transmitted power P_{tx} and received power P_{rx} in a closed-form way. In particular, the electric field $\vec{E}(x,y,z)$ is obtained through the Hertz potential $\vec{\Pi}^e(x,y,z)$ in a general form as [30]:

$$\begin{aligned}\vec{E}(x,y,z) &= \left[\text{graddiv} + k^2\varepsilon\mu\right]\vec{\Pi}^e(x,y,z) = \\ &= \frac{\left[\text{graddiv} + k^2\varepsilon\mu\right]}{4\pi i\omega\varepsilon_0}\int\limits_V \vec{j}^e(x',y',z')\cdot\widehat{G}^e(x,y,z;x',y',z')\mathrm{d}x'\mathrm{d}y'\mathrm{d}z',\end{aligned} \tag{2.3}$$

where $k = 2\pi/\lambda$ is the wavenumber, ε and μ stands for the dielectric permittivity and magnetic permeability of propagation medium, $\omega = 2\pi f$ is the angular frequency, ε_0 is the dielectric constant of free space and $\widehat{G}^e(x,y,z;x',y',z')$ corresponds to the electric tensor Green's function, which aids to calculate an electric field in the observation point (x,y,z) induced by a current source of volume V.

Without loss of generality, the transmitting antenna is assumed to be vertically polarised (i.e., located along the Z-axis). Since this antenna can be interpreted as an electrically small dipole of length l, the current distribution is modelled to be triangularly distributed over its aperture [77] and given by:

$$\vec{j}^e(x',y',z') = A\left(1 - \frac{z'-z_0}{l/2}\right)\delta\left(x'-x_0\right)\delta\left(y'-y_0\right)\vec{z}^0, \tag{2.4}$$

where A is the current amplitude, $\vec{z}^0$ stands for the unit direction vector of the dipole current (i.e., it is one-dimensional due to the small radius/length ratio of transmitting antenna), $\delta(x)$ is the Dirac delta function, (x_0,y_0,z_0) defines the dipole center, $z' \in [z_0 - l/2; z_0 + l/2]$ is a point of the antenna aperture. Next, by reducing the Green's function from tensor to scalar form (it is possible thanks to the one-dimensionality of the transmitting antenna), applying Eq.(2.4) in Eq.(2.3) and using $e^{i\omega t}$ time dependence, the components of the electric field at the observation

point (x, y, z) are expressed as follows:

$$\begin{aligned}
E_x &= -30Ali\frac{e^{-ik\sqrt{\varepsilon\mu}R}}{k\sqrt{\varepsilon\mu}R}\left[\frac{(z-z_0)(x-x_0)}{R^4}\left(-k^2\varepsilon\mu R^2+3ik\sqrt{\varepsilon\mu}R+3\right)\right];\\
E_y &= -30Ali\frac{e^{-ik\sqrt{\varepsilon\mu}R}}{k\sqrt{\varepsilon\mu}R}\left[\frac{(z-z_0)(y-y_0)}{R^4}\left(-k^2\varepsilon\mu R^2+3ik\sqrt{\varepsilon\mu}R+3\right)\right];\\
E_z &= -30Ali\frac{e^{-ik\sqrt{\varepsilon\mu}R}}{k\sqrt{\varepsilon\mu}R}\left[k^2\varepsilon\mu-\frac{ik\sqrt{\varepsilon\mu}}{R}-\frac{1}{R^2}+\right.\\
&\qquad\left.+\frac{(z-z_0)^2}{R^4}\left(-k^2\varepsilon\mu R^2+3ik\sqrt{\varepsilon\mu}R+3\right)\right];
\end{aligned} \tag{2.5}$$

where $R = \sqrt{(x-x_0)^2+(y-y_0)^2+(z-z_0)^2}$ is the communication distance between devices. As the transmitting dipole is situated along Z-axis, it is fair to consider only the dominant component E_z for subsequent analysis. Moreover, since the transmitting and receiving antenna is located in the far field region of each other, the field E_z can be simplified by considering only its radiating term and given by:

$$E_z = -30Ali\cdot k\sqrt{\varepsilon\mu}\frac{e^{-ik\sqrt{\varepsilon\mu}R}}{R}. \tag{2.6}$$

Since the receiving antenna is also modelled as an electrically small thin dipole of length l and thus experiences no change of electric field over its aperture, the current at the receiver block I_{rx} can be determined according to [9] as:

$$I_{rx} = \frac{1}{Z_a+Z_{rx}}\int\limits_{-l/2+z}^{l/2+z} E_\tau\left(1-\frac{|z''-z|}{l/2}\right)\mathrm{d}z, \tag{2.7}$$

where Z_{rx} is the complex impedance of the receiver electronic circuit, z and z'' corresponds to the Z-coordinate of the center and aperture point of the receiving dipole antenna. Under the assumption that such an antenna is aligned along an arbitrary vector $\vec{\tau}$, the electric field E_τ is the projection of the total field $\vec{E}_z$ available at the point (x, y, z) onto this vector and obtained as follows:

$$E_\tau = \left(\vec{E}_z, \vec{\tau}\right) = E_z\cdot\cos\gamma;\ \gamma\in[0;\pi], \tag{2.8}$$

where $\gamma = \left(\widehat{\vec{z^0}, \vec{\tau}}\right)$ is the directional angle between the vector $\vec{\tau}$ and Z-axis. In turn, the received power P_{rx} is simply determined through I_{rx} as:

$$P_{rx} = \frac{|I_{rx}|^2\,\Re(Z_{rx})}{2} = \frac{l^2\Re(Z_{rx})}{8\,|Z_a+Z_{rx}|^2}\,|E_\tau|^2. \tag{2.9}$$

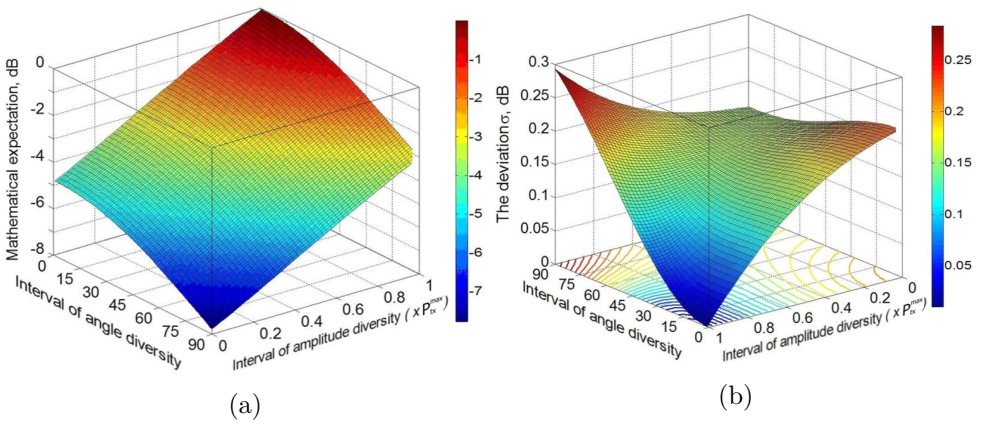

(a) (b)

Figure 2.4: (a) The mathematical expectation and (b) the standard deviation of the received power as a function of the variation of transmitted power and the polarisation mismatch between antennas.

Hence, by taking into account the mismatch between the antenna and transmitter as well as using Eq.(2.6) and Eq.(2.8), the final relationship between the received power P_{rx} and the transmitting power P_{tx} possesses the following form:

$$P_{rx} = \frac{225\Re(Z_{tx})\Re(Z_{rx})\cos^2\gamma}{4\left|Z_a + Z_{tx}\right|^2\left|Z_a + Z_{rx}\right|^2} \cdot \frac{k^2 l^4 \left|\varepsilon\mu\right| e^{-2kR\left|\sqrt{\varepsilon\mu}i\right|}}{R^2} P_{tx}, \tag{2.10}$$

where Z_{tx} indicates the impedance of the transmitter. The derived formula offers the straightforward evaluation of a total loss of the peer-to-peer radio channel between nanomachines in a homogeneous (possibly, lossy) medium. Moreover, by virtue of this expression we further analyse and assess statistical aspects of the nanonetworking channel, which may decrease its performance.

Since the nanonetwork would contain a huge number of nanomachines, it can only be distributed within an application area in a random manner or according to some predefined statistical distribution. In this way, a potential polarisation loss, caused by a misalignment between the transmitting and receiving antenna and thus characterised by the angle γ, will affect the channel budget and is addressed from a statistical perspective. In the meantime, as nanomachines are supplied with energy scavenged from variable environmental sources, we consider the transmitted power P_{tx} as a statistic quantity as well. In particular, both the parameters of interest are

modelled to be uniformly distributed and determined as follows:

$$\begin{aligned} f_1(P_{tx}) &= \frac{1}{P_{tx}^{max}}, \text{ where } P_{tx} \in [0...P_{tx}^{max}]\,; \\ f_2(u = \cos\gamma) &= \frac{2}{\pi\sqrt{1-u^2}}, \text{ where } u \in [0...1]\,. \end{aligned} \tag{2.11}$$

Since the multidimensional density of probability distribution for the received power P_{rx} can be given as a product of $f_1(P_{rx})$ and $f_2(\cos\gamma)$ according to the statistics theory and following Eq.(2.10), the mathematical expectation and standard deviation for P_{rx} is formally derived through simple algebra from Eq.(2.11). Subsequently, both these characteristics are calculated as a function of the transmitted power and the angle between the transmitting and receiving antenna and demonstrated in Fig.2.4. In particular, the polarisation loss is accessed in the case when the angle changes from $\gamma \in \left[0...90^0\right]$ and $P_{tx} = P_{tx}^{max}$ and equal to $L_{pol} = 3 \pm 0.3$ dB. The maximum mathematical expectation of the received power is equal to $M(P_{rx}) = -7.5$ dB if the transmitted power varies from $P_{tx}/P_{tx}^{max} \in [0...1]$ and the directional angle between the antennas alters as $\gamma \in \left[0...90^0\right]$. In other words, the received power calculated using Eq.(2.10) should be reduced by a factor of 5 (= 7 dB) at least due to the statistical impact.

2.3 Discussion

To predict the energy level available in the nanomachine, the promising battery-driven solutions and potential power scavenging technologies have been surveyed in an exhaustive manner. As a result, the most capable nanoscale energy unit has been predicted to deliver the power of 1 μW (or, -30 dBm) by harvesting it from environmental ultrasonic sources.

The power consumption of the nanomachine has been shown to be nearly identical to that of the wireless communication block. Hence, the model suitable to analyse the communication between two nanoscale devices linked by means of far-field RF waves has been developed. Based on the Friis transmission equation, this model offers the determination of the minimum transmitted power under relaxing conditions: (1) the antennas are allocated such that their directivity $D_{tx/rx}$ is maximised; (2) no polarisation misalignment between the antennas; (3) the communication takes place in free space and there thus is no attenuation of radio waves due to the propagation medium; (4) the communication distance is minimised in terms of the criterion $R \geq 10\lambda$ for the

far-field scenario. From the numerical analysis, the devices equipped with antenna of $l = 10\mu m$ have eventually been demonstrated to communicate at the highest radio frequency $f = 300$ GHz once the transmitted power $P_{tx} \geq 20$ dBm (which is even not feasible with the current technology).

In the meantime, we have developed more general formal model capable of addressing the radio link between electrically small devices, which are defined by any position and orientation and communicate in a homogeneous (possibly, lossy) medium. Based on the standard electromagnetic methods and the Hertz potential formalism, this model moreover offers the straightforward evaluation of statistical aspects of nanonetworking peer-to-peer channel, which might decrease its performance. In particular, the polarisation loss is accessed in a closed form and equal to $L_{pol} = 3 \pm 0.3$ dB. Once the transmitted power is also considered as a statistical parameter due to the variable environmental energy sources, the statistical nature of the nanonetworking channel lowers the received power up to 7.5 ± 0.15 dB.

To recap, the orthodox wireless communication block at nano-level would consume energy several orders of magnitude greater than that provided by the most functional nanoscale power source. Moreover, the transmitted power should be increased by a factor of 5 (= 7 dB) at least due to the potential statistical impact of a nanonetworking channel. The solutions, which aim to lower the power consumption of nanoscale radio communication unit to meet drastically reduced energy capabilities of nanomachines and enable the autonomous operation of nanonetworks, are urgent. In particular, such a conventional but effective solution could be the integration of an efficient ESA in the nanoscale communication component. In general, an antenna is considered electrically small once its largest dimension is at or under $\lambda/10$. When a traditional antenna operates at frequencies for which it is electrically small, the antenna becomes highly ineffective to convert an electric power into radio waves, and vice versa. To enhance the performance of ESA, Wheeler [155] proposed to use the volume it occupies in a more efficient way. In particular, the impedance resonance in this antenna is achieved due to its developed complex-shaped structure (e.g. [12,91]). Since it is questionable to realise such nontrivial ESAs at nano-level because of a lack of manipulation and handling means, Wheeler's approach is not further discussed. Another idea about the creation of efficient ESAs is coating a metal wire with a layer of dielectric or magnetic material, or both. The use of a dielectric/magnetic coating would lower the wave propagation velocity and, as a result, enable the implementation of an efficient and durable antenna at a smaller scale [62]. Thanks to the increasing

interest in the development of portable devices, the design of ESAs which include a dielectric/magnetic layer, already attracts a considerable attention of the scientific community [145]. However, the existing solutions for macroscale antennas do not fulfill nanomachine requirements in terms of implementation and usability.

In Appendix A, we propose the design of a high performance ESA which is intended to be integrated and operate in nanomachines. This antenna is dipole-like and possesses the resonance properties thanks to a thin, highly magnetic layer coating a metal enclosure. From a nanoscale antenna perspective, the proposed 'encapsulated antenna' concept is advantageous compared to the rest of antenna alternatives due to the following properties: (1) thanks to the simple architecture, the nanoscale prototype of the encapsulated antenna is feasible and could be manufactured in an unconstrained manner; (2) due to its smooth-faced profile, the encapsulated antenna would provide a durable operation under various environmental conditions and might thus be employed in many nanonetwork applications; (3) owing to a small operational bandwidth, the encapsulated antenna becomes very frequency selective and thus a more space-saving nanomachine design excluding a filter circuit could be realisable (note that the bandwidth is acceptable due to extremely high operating frequencies and low data rate demands). Moreover, the promising nanomachine design implies the placement of other payload device components into the nanoscale antenna body. Such a nanomachine architecture is beneficial as it is very space-efficient, can maximise the antenna aperture and safely preserve other delicate components of the nanomachine. In particular, a macroscale sensor device inspired by this design has recently been developed within the e-CUBES (6th European Framework ICT) project [112]. Unlike any other counterparts, the encapsulated antenna possesses a sufficiently large, interior hollow/usable space (due to the thin magnetic covering) and, as a consequence, its usage could enable the realisation of nanomachines with such an optimum design. Last but not least, the proposed antenna has resonance properties even when its length is much smaller than the operating wavelength and, thus, facilitates the realisation of a smaller device while keeping its power consumption at a constant level. However, taking into account the minimum level of the transmitted power determined in this work, other novel and unorthodox approaches should be also considered to meet the drastically reduced energy capabilities of nanomachines and enable a truly autonomous operation of nanonetworks.

Chapter 3

Electromagnetic Properties of Fullerenes: Mathematical Model

Recent advances in the field of nanotechnology have enabled the development of so-called optical antennas, which consist of a cluster of nanoscale particles [101]. Likewise traditional RF antennas, optical antennas are aimed to convert propagating optical waves into conducted electrical signals and vice versa. These antennas should intensify light-matter interactions to improve the performance of light-emitting diodes, biosensors and solar cell batteries as well as to detect DNA structures and single molecules [14]. Optical antennas capable of radiating a near-diffraction-limited beam might be used in microscopy as alternatives to conventional focussing and objective lenses [23]. Meanwhile, the usage of nanomaterials might also enable the development of efficient nanoscale antennas for microwave band. In particular, GNRs and CNTs can decrease the wave propagation velocity up to one hundred times compared to the speed of light [24] and, as a consequence, efficient graphene/CNT-based antennas would be up to two orders of magnitude smaller those built with traditional materials.

Experience has shown that interactions between electromagnetic waves and nanomaterials can reliably be modelled by using the standard electrodynamics methods and by considering peculiarities of nanoscale particles. In particular, the fundamental transmitting properties of CNTs were firstly described at RF and optical frequencies in [42] and [126] based on the classical integral equation accompanied by the axial quantum mechanical description of CNT conductivity [24]. In the course of anal-

ysis of CNTs as potential dipole antennas, the standard electrodynamics methods were successfully employed to determine the performance and radiating characteristics of CNT-based antennas in the RF and THz ranges [18, 43, 67, 127] as well as the near-infrared and optical bands [46, 70, 72, 124]. These methods solve Maxwell's equations by treating nanoscale particles as continuous objects characterized by a frequency-dependent dielectric constant. By describing a free electron gas subject to an external electromagnetic field, the Drude model [7] can estimate the dielectric constant of nanoscale particles over a very broad frequency spectrum and have widely been implemented in the papers listed above.

The Drude model is based on the statistical treatment, which implies a large number of electrons in an object and its regularity. Hence, one must be careful in using this model for a nanoscale object as it might contain an insufficient number of atoms to generate enough electrons or form a regular structure. In particular, the Drude model cannot handle a nanoscale particle with the size the same as the electron mean free path since the electron collision rate incomprehensibly increases due to the electron scattering from the particle surface [35]. Moreover, the Drude model is limited to calculate the electromagnetic properties at frequencies up to the visible spectrum as it does not consider the interband transitions between the valence and the conduction bands. In [64], the Drude model was particularly tested by experiments for the noble metals and it was observed that the model is not capable of describing gold and silver probes at frequencies higher than 484THz($\backsim$ 620nm) and 968THz($\backsim$ 310nm), respectively.

At present, a majority of nanoscale antenna designs employs CNTs of a few hundreds of nm. Such CNTs are large enough to possess a regular structure: i.e., their electromagnetic properties can safely be estimated by the Drude model and incorporated in the standard electrodynamics methods to investigate the CNT radiation performance in the infrared and optical ranges. Although other, smaller nanoscale particles, such as fullerenes, exhibit a great potential in optical and microwave antenna applications [135, 159], they attracted little attention due to absence of an adequate electromagnetic model describing interaction between electromagnetic fields and nanoscale particles. Thanks to the same reasoning, a small number of publications is devoted to the analysis and the design of antennas operating in the ultraviolet and X-ray band, though such systems are required to provide a better control over photochemical reactions and to advance biosensing/bioimaging applications by directly accessing to biomolecular resonances, native fluorescence and resonant Raman

scattering interactions [63, 85, 161].

In this chapter, we propose a novel electromagnetic model, which represents separate atoms in a nanoscale particle as scattering centers and aims to determine its relative dielectric constant. Under the assumption that the atom size is much smaller than the operating wavelength, a novel model employs the integral-equation-based techniques capable of describing the scattering of electromagnetic waves by electrically small bodies [111]. Due to the extremely small radius of an atom ($\backsim 10^{-10}$m on average), the model can calculate the dielectric constant of a nanoscale object at wavelengths up to 1nm and is thus applicable throughout the entire ultraviolet region. Furthermore, our model effectively handles a nanoscale particle with a small number of atoms due to reduced computation time and basically complements the Drude model to offer the evaluation of electromagnetic parameters for an object of any size over the very broad frequency spectrum (up to soft X-rays). Several types of fullerene can be characterized as a sphere with a certain 'effective' radius owing to the ball-like atomic constitution and the relative dielectric constant of such a sphere is calculated by means of the proposed model for the first time. Based on the obtained results and inspired by the concept of the Yagi-Uda antenna [108], we eventually introduce an exceedingly small fullerene-based Yagi-Uda-type antenna which possesses directional capabilities in X-ray band.

The remainder of this chapter is organized as follows. The integral-equation-based model aimed to determine the received electromagnetic field in the presence of a number of electrically small scattering spheres is formally developed in Section 3.1. The model is employed in Section 3.2 to investigate a fullerene structure from an atomic perspective and determine electromagnetic properties of various fullerene derivatives in the very broad electromagnetic spectrum. The design of the directional fullerene-based antenna and its performance in the ultraviolet region is discussed in Section 3.3. Finally, conclusions have been drawn in Section 3.4.

3.1 Integral-Equation-based Model

In the model, the Cartesian coordinates and $e^{i\omega t}$ time dependence are used throughout. The propagation and diffraction of electromagnetic waves take place in the free half-space with parameters $\varepsilon_0 = (36\pi)^{-1} \times 10^{-9}$ F/m and $\mu_0 = 4\pi \times 10^{-7}$ H/m. As shown in Fig.3.1, the initial field is produced by a vertically polarised point-source with frequency f (wavelength λ), amplitude A_0 and coordinates (x_0, y_0, z_0). This field

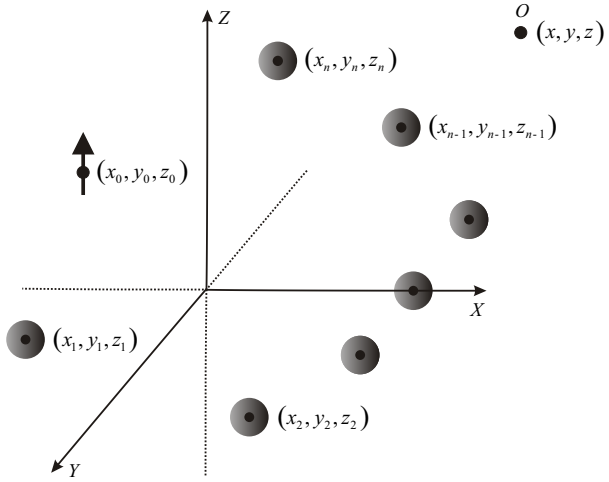

Figure 3.1: Problem geometry.

scattered by n spheres is intercepted by a vertically polarised point-receiver placed in (x, y, z). The scattering spheres represent n atoms, the nanoscale particle is made up of. Hence, the sphere's radius r_s is equal to that of the particle's atom, while the spheres' centres are located in coordinates $(x_{1...n}, y_{1...n}, z_{1...n})$ to fairly model the atomic organisation of nanoscale particle. To incorporate the electromagnetic impact of nanoscale particles, each sphere is assumed to be uniform, characterised by the relative dielectric constant ε_s and non-magnetic ($\mu_s = 1$). The sphere's size is kept much smaller than the operating wavelength to safely assume that both the field incident on the sphere and its internal field are homogeneous. To determine the relative dielectric constant ε_f of a fullerene C_n, such a carbon molecule is naturally modelled in the form of the sphere with its radius r_f and centre with coordinates (x_f, y_f, z_f). This radius and the centre point are obtained based on the known coordinates of n carbon atoms of C_n fullerene and through using a geometric representation.

For a single non-magnetic sphere with a volume V and relative dielectric constant ε_s located in free space, a total electromagnetic field outside the sphere is viewed as the sum of an incident field and a scattered field. The electric and magnetic components of this field can formally be derived by simplifying the integral equations

of macroscopic electrodynamics [53] and given by:

$$\begin{cases} \vec{E}_\Sigma(\vec{r},\vec{r}_0) = \vec{E}_0(\vec{r},\vec{r}_0) + \dfrac{(\varepsilon_s-1)}{4\pi}\cdot\left(\text{graddiv}+k^2\right)\displaystyle\int_V \vec{E}(\vec{r'},\vec{r}_0)\widehat{G}(\vec{r},\vec{r'})\mathrm{d}r' \\ \vec{H}_\Sigma(\vec{r},\vec{r}_0) = \vec{H}_0(\vec{r},\vec{r}_0) + \dfrac{ik\,(\varepsilon_s-1)}{4\pi}\cdot\text{rot}\displaystyle\int_V \vec{E}(\vec{r'},\vec{r}_0)\widehat{G}(\vec{r},\vec{r'})\mathrm{d}r' \end{cases}, \quad (3.1)$$

where $\vec{E}_0(\vec{r},\vec{r}_0)$ and $\vec{H}_0(\vec{r},\vec{r}_0)$ correspond, respectively, to the incident electric and magnetic fields, which are directly delivered to a point-receiver characterised by the radius-vector $\vec{r}$ from a point-source with radius-vector $\vec{r_0}$. The scattered field is described through the wavenumber $k = 2\pi/\lambda$ (where λ is the wavelength), the sphere's internal field $\vec{E}(\vec{r'},\vec{r}_0)$ caused by the point-source and the tensor Green's function $\widehat{G}(\vec{r},\vec{r'})$. The use of the Cartesian coordinate system implies that the Green's function tensor for a homogeneous medium is defined only in terms of its diagonal elements as:

$$\widehat{G}(\vec{r},\vec{r'}) = \begin{vmatrix} \dfrac{e^{-ik\left|\vec{r}-\vec{r'}\right|}}{\left|\vec{r}-\vec{r'}\right|} & 0 & 0 \\ 0 & \dfrac{e^{-ik\left|\vec{r}-\vec{r'}\right|}}{\left|\vec{r}-\vec{r'}\right|} & 0 \\ 0 & 0 & \dfrac{e^{-ik\left|\vec{r}-\vec{r'}\right|}}{\left|\vec{r}-\vec{r'}\right|} \end{vmatrix}, \quad (3.2)$$

where $\left|\vec{r}-\vec{r'}\right| = \sqrt{(x-x')^2+(y-y')^2+(z-z')^2}$. By incorporating Eq.(3.2) into Eq.(3.1) and employing the electromagnetic field superposition principle, the electric and magnetic fields originated by the source in (x_0,y_0,z_0) and received at the point (x,y,z) in the presence of n scattering spheres of the same volume and dielectric constant have the following representations:

$$\begin{cases} \vec{E}_\Sigma(\vec{r},\vec{r}_0) = \vec{E}_0(\vec{r},\vec{r}_0) + \dfrac{(\varepsilon_s-1)}{4\pi}\displaystyle\sum_{i=1}^{n}\left(\text{graddiv}+k^2\right)\int_V \vec{E}_i(\vec{r'},\vec{r}_0)\widehat{G}(\vec{r},\vec{r'})\mathrm{d}r' \\ \vec{H}_\Sigma(\vec{r},\vec{r}_0) = \vec{H}_0(\vec{r},\vec{r}_0) + \dfrac{ik\,(\varepsilon_s-1)}{4\pi}\displaystyle\sum_{i=1}^{n}\text{rot}\int_V \vec{E}_i(\vec{r'},\vec{r}_0)\widehat{G}(\vec{r},\vec{r'})\mathrm{d}r' \end{cases}. \quad (3.3)$$

In the subsequent analysis, the electric field in Eq.(3.3) is merely considered as the electromagnetic problem of interest involves only electric-type antennas. Since the

scattering spheres are electrically small, the integration field $\vec{E}_i(\vec{r'}, \vec{r}_0)$ in Eq.(3.3) is assumed to be a constant value (as it slowly varies throughout the volume V) and, as a consequence, the Green's function can be approximated as:

$$\widehat{G}(\vec{r}, \vec{r'}) = \frac{e^{-ik\left|\vec{r}-\vec{r'}\right|}}{\left|\vec{r}-\vec{r'}\right|} = \frac{e^{-ik|\vec{r}-\vec{r}_i|}}{|\vec{r}-\vec{r}_i|}, \tag{3.4}$$

where $\vec{r_i}$ stands for the geometric centre of the i-th scattering sphere with coordinates (x_i, y_i, z_i). For the sake of convenience, an electric field transformation tensor $\widehat{f}(\vec{r}, \vec{r_i})$ is introduced in this work as follows:

$$\widehat{f}(\vec{r}, \vec{r_i}) \times \vec{A} = \left(\text{graddiv} + k^2\right) \left[A_x \frac{e^{-ik|\vec{r}-\vec{r}_i|}}{|\vec{r}-\vec{r}_i|}\vec{x}^0 + A_y \frac{e^{-ik|\vec{r}-\vec{r}_i|}}{|\vec{r}-\vec{r}_i|}\vec{y}^0 + A_z \frac{e^{-ik|\vec{r}-\vec{r}_i|}}{|\vec{r}-\vec{r}_i|}\vec{z}^0\right]. \tag{3.5}$$

All the elements of this 3x3 tensor are determined in Appendix C, while its use allows to rewrite the field $\vec{E}_\Sigma(\vec{r}, \vec{r}_0)$ in Eq.(3.3) in a more straightforward way and given by:

$$\vec{E}_\Sigma(\vec{r}, \vec{r}_0) = \vec{E}_0(\vec{r}, \vec{r}_0) + \underbrace{\frac{(\varepsilon_s - 1)}{4\pi} \sum_{i=1}^{n} \int_V \widehat{f}(\vec{r}, \vec{r_i}) \times \vec{E}_i(\vec{r'}, \vec{r}_0) \mathrm{d}r'}_{\vec{E}_s(\vec{r}, \vec{r}_0)}. \tag{3.6}$$

Hence, to obtain the explicit expression for the received field $\vec{E}_\Sigma(\vec{r}, \vec{r}_0)$, the closed-form equations of the incident field $\vec{E}_0(\vec{r}, \vec{r}_0)$ and the total scattered field $\vec{E}_s(\vec{r}, \vec{r}_0)$ must preliminary be derived.

3.1.1 Incident Field Calculation

The incident field $\vec{E}_0(\vec{r}, \vec{r}_0)$ in Eq.(3.6) represents the field that is intercepted by the point-receiver at (x, y, z) from the source located in (x_0, y_0, z_0). As there is no polarisation mismatch between the transmitter and receiver, the dominant (with respect to the vertical polarization) electric field produced by the point-source with the amplitude A_0 is derived by using the classic electromagnetic approaches [60] as follows:

$$\vec{E}_0(\vec{r}, \vec{r}_0) = \frac{A_0}{4\pi i\omega\varepsilon_0} \left[\left(\text{graddiv} + k^2\right) \widehat{G}(\vec{r}, \vec{r}_0)\right] \times \vec{z}^0, \tag{3.7}$$

where $\omega = 2\pi f$ is the angular frequency. Applying Eq.(3.5) to Eq.(3.7), the incident field $\vec{E}_0(\vec{r}, \vec{r}_0)$ can be determined through the revised expression as:

$$\vec{E}_0(\vec{r}, \vec{r}_0) = \frac{A_0}{4\pi i\omega\varepsilon_0} \left[f_{xz}(\vec{r}, \vec{r}_0)\vec{x}^0 + f_{yz}(\vec{r}, \vec{r}_0)\vec{y}^0 + f_{zz}(\vec{r}, \vec{r}_0)\vec{z}^0\right]. \tag{3.8}$$

3.1.2 Total Scattered and Received Field Determination

In this chapter, the total scattered field $\vec{E}_s(\vec{r},\vec{r}_0)$ is determined using the Rayleigh-theory-based solution for the scattering of electromagnetic waves by small particles [79]. Since each scattering sphere is considered homogeneous and electrically small, both the field $\vec{E}_{0i}(\vec{r'},\vec{r}_0)$ incident on the i-th sphere and its internal field $\vec{E}_i(\vec{r'},\vec{r}_0)$ are uniform. By applying the zero-order approximation (assume no coupling between any two scattering spheres), the relationship between the incident and internal fields in the free space is given by:

$$\vec{E}_i(\vec{r'},\vec{r}_0) = \frac{3}{\varepsilon_s+2}\vec{E}_{0i}(\vec{r'},\vec{r}_0). \tag{3.9}$$

Each scattering sphere is small enough with respect to the operating wavelength so that it can be regarded as a point with coordinates $(x_{1\ldots n}, y_{1\ldots n}, z_{1\ldots n})$. Applying Eq.(3.9) to Eq.(3.6), the total scattered field is therefore given by:

$$\begin{aligned}\vec{E}_s(\vec{r},\vec{r}_0) &= \frac{3\,(\varepsilon_s-1)}{4\pi\,(\varepsilon_s+2)}\sum_{i=1}^{n}\widehat{f}(\vec{r},\vec{r_i})\times\vec{E}_{0i}(\vec{r_i},\vec{r_0})\int\limits_V \mathrm{d}r' \\ &= \frac{r_s^3\,(\varepsilon_s-1)}{\varepsilon_s+2}\sum_{i=1}^{n}\widehat{f}(\vec{r},\vec{r_i})\times\vec{E}_{0i}(\vec{r_i},\vec{r_0}),\end{aligned} \tag{3.10}$$

where r_s is the radius of a scattering sphere. Since the field $\vec{E}_{0i}(\vec{r_i},\vec{r_0})$ incident on the i-th sphere from a point-source located in (x_0, y_0, z_0) is described using Eq.(3.8), the received field $\vec{E}_\Sigma(\vec{r},\vec{r}_0)$ can thus be determined as follows:

$$\begin{aligned}\vec{E}_\Sigma(\vec{r},\vec{r}_0) = \frac{1}{4\pi i\omega\varepsilon_0}\Big(&A_0 f_{xz}(\vec{r},\vec{r}_0)\vec{x}^0 + A_0 f_{yz}(\vec{r},\vec{r}_0)\vec{y}^0 + A_0 f_{zz}(\vec{r},\vec{r}_0)\vec{z}^0 + \\ &+\frac{r_s^3\,(\varepsilon_s-1)}{\varepsilon_s+2}\sum_{i=1}^{n}\widehat{f}(\vec{r},\vec{r_i})\times\left[A_0 f_{xz}(\vec{r_i},\vec{r}_0)\vec{x}^0 + A_0 f_{yz}(\vec{r_i},\vec{r}_0)\vec{y}^0 + A_0 f_{zz}(\vec{r_i},\vec{r}_0)\vec{z}^0\right]\Big).\end{aligned} \tag{3.11}$$

The zero-order approximation does not take into account the field interactions between scattering spheres: that is why the diffraction field in Eq.(3.10) only includes the field incident from the point-source. To improve the model accuracy and reliability, proper allowance must be made for such interactions. Their account can be realized by using the iterative approach described below.

Since Eq.(3.11) allows to calculate the received field at any space point, the field delivered to the centre of the i-th sphere can be obtained using the zero-order ap-

proximation as follows:

$$\vec{E}_{\Sigma}(\vec{r}_i,\vec{r}_0)=\vec{E}_0(\vec{r}_i,\vec{r}_0)+\frac{r_s^3\,(\varepsilon_s-1)}{\varepsilon_s+2}\sum_{j=1}^{n}\widehat{f}(\vec{r}_i,\vec{r}_j)\times\vec{E}_{0j}(\vec{r}_j,\vec{r}_0) \tag{3.12}$$

where index j indicates the summation over all n scattering particles excluding the considered sphere (i.e., $j\neq i$). Therefore, in terms of the first-order approximation, the field $\vec{E}_{0i}(\vec{r_i},\vec{r_0})$ incident on the i-th scattering sphere in Eq.(3.10) should be estimated using not Eq.(3.8) but Eq.(3.11) to consider the coupling between scattering spheres. In such a case, the more precise received field $\vec{E}^1_{\Sigma}(\vec{r},\vec{r}_0)$ can be derived as:

$$\begin{aligned}
&\vec{E}^1_{\Sigma}(\vec{r},\vec{r}_0)=\vec{E}_0(\vec{r},\vec{r}_0)+\frac{r_s^3\,(\varepsilon_s-1)}{\varepsilon_s+2}\sum_{i=1}^{n}\widehat{f}(\vec{r},\vec{r_i})\times\vec{E}_{\Sigma 0}(\vec{r_i},\vec{r_0})=\\
&=\vec{E}_0(\vec{r},\vec{r}_0)+\frac{r_s^3\,(\varepsilon_s-1)}{\varepsilon_s+2}\sum_{i=1}^{n}\widehat{f}(\vec{r},\vec{r_i})\times\left[\vec{E}_0(\vec{r}_i,\vec{r}_0)+\frac{r_s^3\,(\varepsilon_s-1)}{\varepsilon_s+2}\sum_{j=1}^{n}\widehat{f}(\vec{r}_i,\vec{r}_j)\times\vec{E}_{0j}(\vec{r}_j,\vec{r}_0)\right]=\\
&=\vec{E}_{\Sigma}(\vec{r},\vec{r}_0)+\underbrace{\left(\frac{r_s^3\,(\varepsilon_s-1)}{\varepsilon_s+2}\right)^2}_{\overline{\alpha}^2}\sum_{i=1}^{n}\widehat{f}(\vec{r},\vec{r_i})\times\left[\sum_{j=1}^{n}\widehat{f}(\vec{r}_i,\vec{r}_j)\times\vec{E}_{0j}(\vec{r}_j,\vec{r}_0)\right],
\end{aligned} \tag{3.13}$$

where $\vec{E}_{0j}(\vec{r}_j,\vec{r}_0)$ is determined using Eq.(3.8). As can be seen, the refined field $\vec{E}^1_{\Sigma}(\vec{r},\vec{r}_0)$ includes the supplementary term with the squared coefficient $\overline{\alpha}$. By extending for higher-order approximations, the received field can be shown to be expressed as a power series in terms of the expansion parameter α, which includes $\overline{\alpha}$. To safely rely on the zero/first-order approximation, this series expansion parameter is demanded to be small ($\ll 1$) as only in such a case the higher-order terms of the series contribute negligibly and neglecting them has no problem. Hence, before the developed model is implemented, the limits of its applicability should be recognized in terms the parameter α. To keep the model creditable, according to [136] the criterion in Eq.(3.14) must be fulfilled (R is the distance between source and observation point). The same result can be drawn by investigating the components of the tensor $\widehat{f}(\vec{r},\vec{r}_i)$ in Appendix C: i.e., the electric field varies in inverse proportion to the distance R and the highest power of R in the field expression is cubed.

$$\alpha=\frac{\overline{\alpha}}{R^3}=\left(\frac{r_s}{R}\right)^3\frac{\varepsilon_s-1}{\varepsilon_s+2}<\left(\frac{r_s}{R}\right)^3\ll 1. \tag{3.14}$$

Our geometric-based analysis of different fullerene structures [26] demonstrates that the minimum distance between two neighbouring carbon atoms $R=1.4$Å, while the

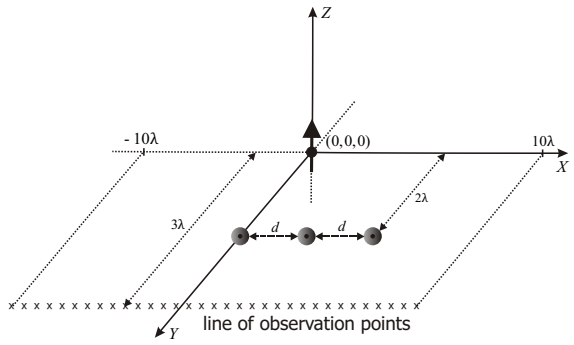

Figure 3.2: Special scattering case.

radius of carbon atom is set to be equal 0.67Å [38]. In this way, as the maximum series expansion parameter $\alpha < (0.67/1.4)^3 = 0.11$ is small to meet the criterion in Eq.(3.14), the zero-order approximation is capable of analysing a fullerene and accurately determining its electromagnetic properties as long as the scatterer size is small enough compared to the operating wavelength. However, before making the fullerene-related estimates, we need to prove the validity and the correctness of the developed model.

3.1.3 Model Verification

The model's results are compared to those generated by means of the electromagnetic numerical solver [1]. To be independent from the point-source amplitude A, the considered outcome is the ratio Δ between the received and the incident field magnitudes (in dB):

$$\Delta = 20 \log_{10} \left(\frac{\left| \vec{E}_{\Sigma}(\vec{r}, \vec{r}_0) \right|}{\left| \vec{E}_0(\vec{r}, \vec{r}_0) \right|} \right). \tag{3.15}$$

The incident field $\vec{E}_0(\vec{r}, \vec{r}_0)$ is calculated by applying Eq.(3.8), whilst the received fields $\vec{E}_{\Sigma}(\vec{r}, \vec{r}_0)$ in the zero-order and the first-order approximations are computed using Eq.(3.11) and Eq.(3.13), respectively. For the simulations in FEKO, such fields are directly obtained by analysing the corresponding numerical models.

For comparison analysis, a particular asymmetrical scattering problem is examined (see Fig.3.2). The point-source is located at the coordinate origin $(0, 0, 0)$. Each of

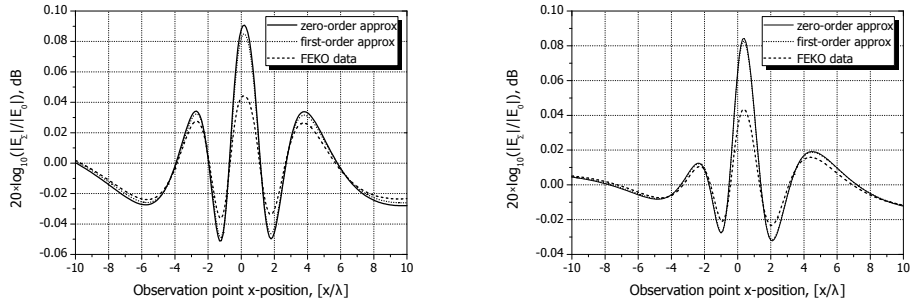

(a) (b)

Figure 3.3: The ratio between the received and the incident field magnitudes for (a) $d = 0.01\lambda$ and (b) $d = 0.1\lambda$.

three scattering spheres is modelled as a perfectly conducting body ($\varepsilon_s = 1 - i\infty$) with radius $r_s = 0.05\lambda$. The leftmost sphere is placed on the y-axis, while the x-axis separation between two neighbouring spheres are denoted as d. The y- and z-coordinates of all the spheres are the same and equal to 2λ and 0, respectively. A number of observation points are located along a line with coordinates $(-10\lambda...10\lambda, 3\lambda, 0)$. Thanks to a good agreement of the analytic predictions with the numerical calculations in FEKO (see Fig.3.3), we recap that the diffraction field, caused by several objects with maximum linear dimension less or equal to $\lambda/10$, can fairly be estimated using the developed model. Moreover, this limitation can be relaxed since our analysis indicates that the disagreement between the model's results and those computed in FEKO becomes significant only when such a maximum linear dimension exceeds $\lambda/5$. Once the interactions between the scattering objects are strong (Fig.3.3a), the use of the first-order approximation is more preferable as it substantially refines the results. If the scattering objects are spaced far enough apart from each other to keep these interactions weak (Fig.3.3b), the zero-order approximation could be applied due to its reliable accuracy and low computational costs.

3.2 Dielectric Constant of C_n fullerene

Since a majority of fullerene structures has a ball-like atomic constitution (Fig.3.4), in many electromagnetic problems it is convenient to represent a fullerene as a

spherical object. The geometric parameters of this object, such as the coordinates $\vec{r}_{cf} = (x_f, y_f, z_f)$ of its centre and the effective radius r_f, can straightforwardly be determined based on the known coordinates of n carbon atoms of the C_n fullerene as follows:

$$\begin{cases} x_f = \dfrac{\sum\limits_{i=1}^{n} x_i}{n}, \quad y_f = \dfrac{\sum\limits_{i=1}^{n} y_i}{n}, \quad z_f = \dfrac{\sum\limits_{i=1}^{n} z_i}{n}; \\ r_f = \dfrac{\sum\limits_{i=1}^{n} \sqrt{(x_i - x_f)^2 + (y_i - y_f)^2 + (z_i - z_f)^2}}{n}, \end{cases} \tag{3.16}$$

where $(x_{1\cdots n}, y_{1\cdots n}, z_{1\cdots n})$ are the coordinates of the atom centres.

Evidently, the relative dielectric constant ε_f of a fullerene sphere should be such that the field scattered by this sphere is the same as the diffraction field produced by all n carbon atoms of the fullerene. By assuming that each carbon atom is represented as a sphere with radius r_a and permittivity ε_a and using Eq.(3.10) for the zero-order approximation, the following expression is obtained:

$$\frac{r_f^3\,(\varepsilon_f - 1)}{\varepsilon_f + 2}\left[\widehat{f}(\vec{r}, \vec{r}_{cf}) \times \vec{E}_0(\vec{r}_{cf}, \vec{r}_0)\right] = \frac{r_a^3\,(\varepsilon_a - 1)}{\varepsilon_a + 2}\left[\sum_{i=1}^{n} \widehat{f}(\vec{r}, \vec{r}_i) \times \vec{E}_0(\vec{r}_i, \vec{r}_0)\right] \tag{3.17}$$

Suppressing the algebra, the expression for ε_f can be written in the following form:

$$\varepsilon_f(\vec{r}, \vec{r}_0) = \frac{\tau_0 + 2\tilde{F}_0(\vec{r}, \vec{r}_0)}{\tau_0 - \tilde{F}_0(\vec{r}, \vec{r}_0)}, \text{ where } \tau_0 = \frac{r_f^3\,(\varepsilon_a + 2)}{r_a^3\,(\varepsilon_a - 1)}, \ \tilde{F}_0(\vec{r}, \vec{r}_0) = \frac{\sum\limits_{i=1}^{n} \widehat{f}(\vec{r}, \vec{r}_i) \times \vec{E}_0(\vec{r}_i, \vec{r}_0)}{\widehat{f}(\vec{r}, \vec{r}_{cf}) \times \vec{E}_0(\vec{r}_{cf}, \vec{r}_0)} \tag{3.18}$$

Once both the source and the observation point are placed quite far from a fullerene molecule, the assumption $\widehat{f}(\vec{r}, \vec{r}_i) \times \vec{E}_0(\vec{r}_i, \vec{r}_0) = \widehat{f}(\vec{r}, \vec{r}_{cf}) \times \vec{E}_0(\vec{r}_{cf}, \vec{r}_0)$ is valid and Eq.(3.18) reduces as follows:

$$\varepsilon_f = \frac{\tau_0 + 2n}{\tau_0 - n} \tag{3.19}$$

This equation implies that when $\tau_0 \gg n$, the outlying C_n fullerene causes no electromagnetic influence on the environment due to its dielectric constant $\varepsilon_f \approx 1$. As can be also seen from Eq.(3.18), for any disposition of the source and the observation point $\varepsilon_f = 1$ as long as $\varepsilon_a = 1$. This result makes intuitive sense: a system must produce no electromagnetic impact once its entities cannot influence electromagnetic fields.

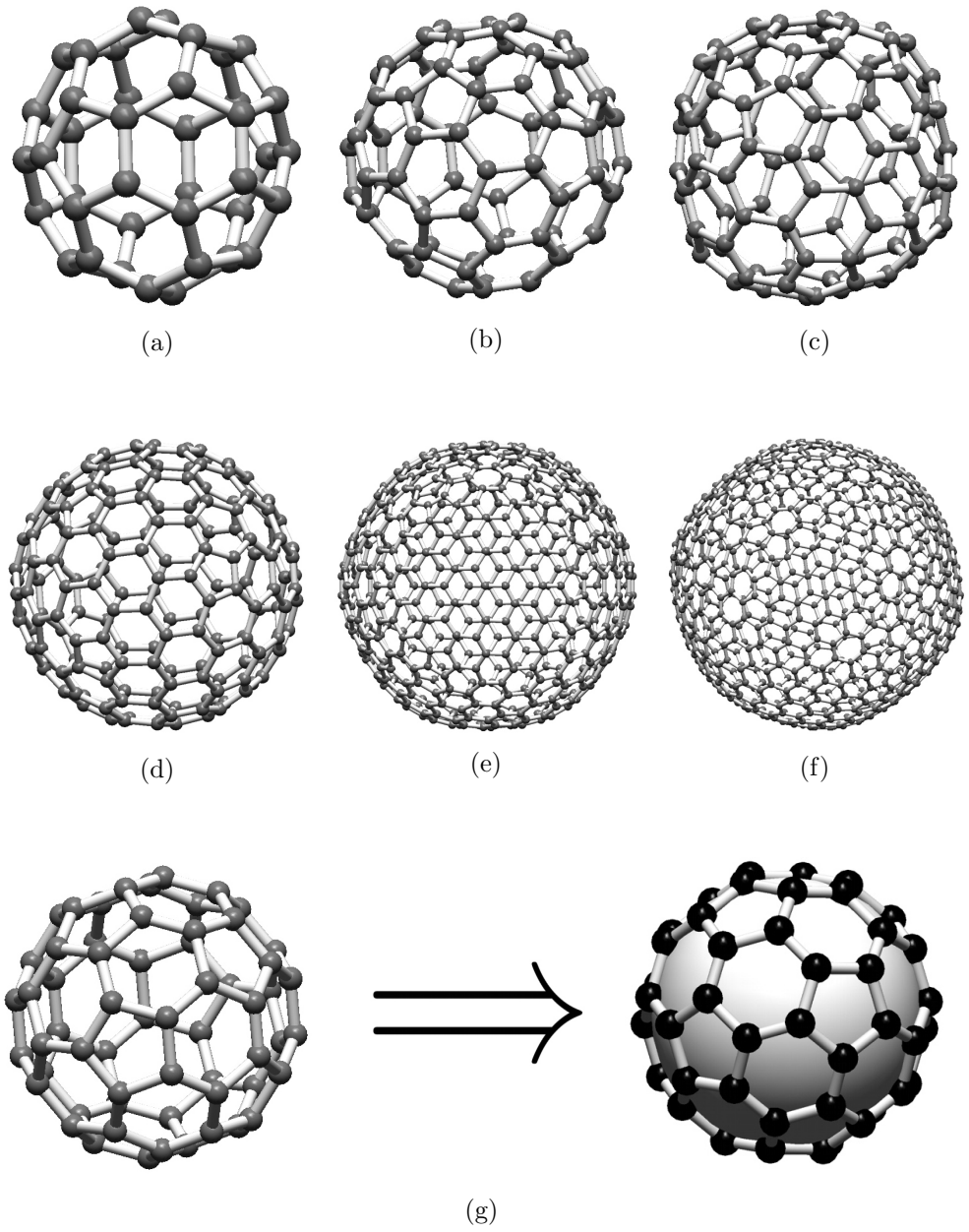

Figure 3.4: The geometry of different fullerene molecules, such as (a) C_{40}, (b) C_{80}, (c) C_{100}, (d) C_{180}, (e) C_{500}, (f) C_{720}, (g) C_{60} accompanied by its representation with the inserted ball [3].

Applying the first-order approximation Eq.(3.13) in the same way as above, the dielectric constant of a fullerene molecule is given in Eq.(3.20). As could be expected, the limiting case (i.e., $\varepsilon_a = 1$) is true in the case of the first-order approximation.

$$\begin{aligned} \varepsilon_f(\vec{r},\vec{r}_0) =& \frac{\tau_1 + 2\tilde{F}_1(\vec{r},\vec{r}_0)}{\tau_1 - \tilde{F}_1(\vec{r},\vec{r}_0)}, \text{ where } \tau_1 = \frac{r_f^3\left(\varepsilon_a+2\right)^2}{r_a^6\left(\varepsilon_a-1\right)^2}, \\ \tilde{F}_1(\vec{r},\vec{r}_0) =& \frac{\sum\limits_{i=1}^{n} \widehat{f}(\vec{r},\vec{r}_i) \times \left[\sum\limits_{j=1}^{n} \widehat{f}(\vec{r}_i,\vec{r}_j) \times \vec{E}_{0j}(\vec{r}_j,\vec{r}_0)\right]}{\widehat{f}(\vec{r},\vec{r}_{cf}) \times \vec{E}_0(\vec{r}_{cf},\vec{r}_0)} \end{aligned} \tag{3.20}$$

3.2.1 Numerical Analysis

For numerical analysis, the dielectric constant ε_a of a carbon atom must first be specified (again, the atom radius $r_a = 0.067$nm [38]). Thanks to the strong force in a carbon atom and its electrically small size, it is safe to assume that electromagnetic waves are not capable of penetrating into the atom and can only excite currents on its surface. In other words, the carbon atom exhibits electromagnetic properties very similar to an ideal metal and should be characterised by a huge conductivity. For the numerical analysis, the permittivity of a carbon atom is thus set here to be equal to $\varepsilon_a = 1 - 1\text{e}10i$. In this respect, the dielectric constant ε_f of a fullerene molecule, which is situated far from both the source and the observation point, can be derived using Eq.(3.19) as follows:

$$\varepsilon_f = \frac{r_f^3/r_a^3 + 2n}{r_f^3/r_a^3 - n}. \tag{3.21}$$

Hence, the permittivity ε_f of the 'distant' fullerene can remarkably be described through its geometric properties. By using the database with the coordinates of fullerene derivatives [3], the variable ε_f is calculated for different fullerenes and presented in Table 3.1. From these computations, it is also observed that a fullerene becomes distant and the approximation in Eq.(3.21) can be applied only when $|\vec{r}_f - \vec{r}_0| \geqslant 20r_f$ and $|\vec{r}_f - \vec{r}| \geqslant 20r_f$. In such a case, the distance between the fullerene centre and the source/receiver is sufficiently larger than the fullerene radius to make the assumption $\widehat{f}(\vec{r},\vec{r}_i) \times \vec{E}_0(\vec{r}_i,\vec{r}_0) = \widehat{f}(\vec{r},\vec{r}_{cf}) \times \vec{E}_0(\vec{r}_{cf},\vec{r}_0)$ stable. The distant fullerene causes no diffraction losses ($\Im(\varepsilon_f) = 0$) and its electromagnetic influence reduces ($\Re(\varepsilon_f) \to 1$) with increasing a number of carbon atoms n in this molecule. The latter is attributable to the fact that the volume density of atoms ρ_n is

the biggest for the smallest fullerene C_{20} and decreases for larger fullerene derivatives (see Table 3.1).

Table 3.1: Dielectric constant ε_f of 'distant' fullerene C_n

n	r_f, [nm]	ε_f	$\rho_n = \frac{n}{4/3 \cdot \pi r_f^3}, \left[\frac{1}{\text{nm}^3}\right]$
20	0.199	10.632	6.053×10^{29}
40	0.297	3.532	1.816×10^{29}
60	0.355	3.041	1.071×10^{29}
80	0.419	2.451	6.470×10^{28}
100	0.486	2.062	4.151×10^{28}
180	0.613	1.922	2.073×10^{28}
260	0.740	1.719	1.181×10^{28}
500	1.039	1.465	4.258×10^{27}
720	1.259	1.365	2.393×10^{27}

Once $|\vec{r}_f - \vec{r}_0|$ and/or $|\vec{r}_f - \vec{r}|$ are of the same order of magnitude as the fullerene size, such a molecule becomes 'adjacent' to the source and/or the receiver and, as a consequence, Eq.(3.20) for the first-order approximation should be employed to estimate its dielectric constant. In this work, by using this equation the complex permittivity ε_f of the adjacent fullerenes C_{20} and C_{60} is computed (see Fig.3.5 and Fig.3.6, respectively). For all these calculations, the observation point is spaced far from the source $|\vec{r} - \vec{r}_0| = 20\lambda$. Fig.3.5a,b and Fig.3.6a,b are obtained by allocating the observation point so that the fullerene centre appears on the source-receiver line of sight. In turn, Fig.3.5c,d and Fig.3.6c,d are drawn assuming that the fullerene molecule is placed close to the source at a nearby distance of $|\vec{r}_f - \vec{r}_0| = 2r_f$, while the observation point moves along the circle in the x0y-plane with varying the azimuthal angle φ. From the simulations, we observe that for a distant fullerene the real part of its permittivity $\Re(\varepsilon_f)$ reaches a maximum as the value $\Re(\varepsilon_f)$ of the adjacent fullerene decreases with reducing the source-fullerene separation $|\vec{r}_f - \vec{r}_0|$. Meanwhile, for any fixed distance $|\vec{r}_f - \vec{r}_0|$ the parameter $\Re(\varepsilon_f)$ is quasi-constant at the optical/ultraviolet frequencies and alters only when the operating frequency belongs to the X-ray band (Fig.3.5a, Fig.3.6a). Also, the $\Re(\varepsilon_f)$ of an adjacent fullerene is influenced by the point-receiver position: in particular, the minimum value $\Re(\varepsilon_f)$ is determined once the point-source, the fullerene centre and the point-receiver are aligned (Fig.3.5c, Fig.3.6c).

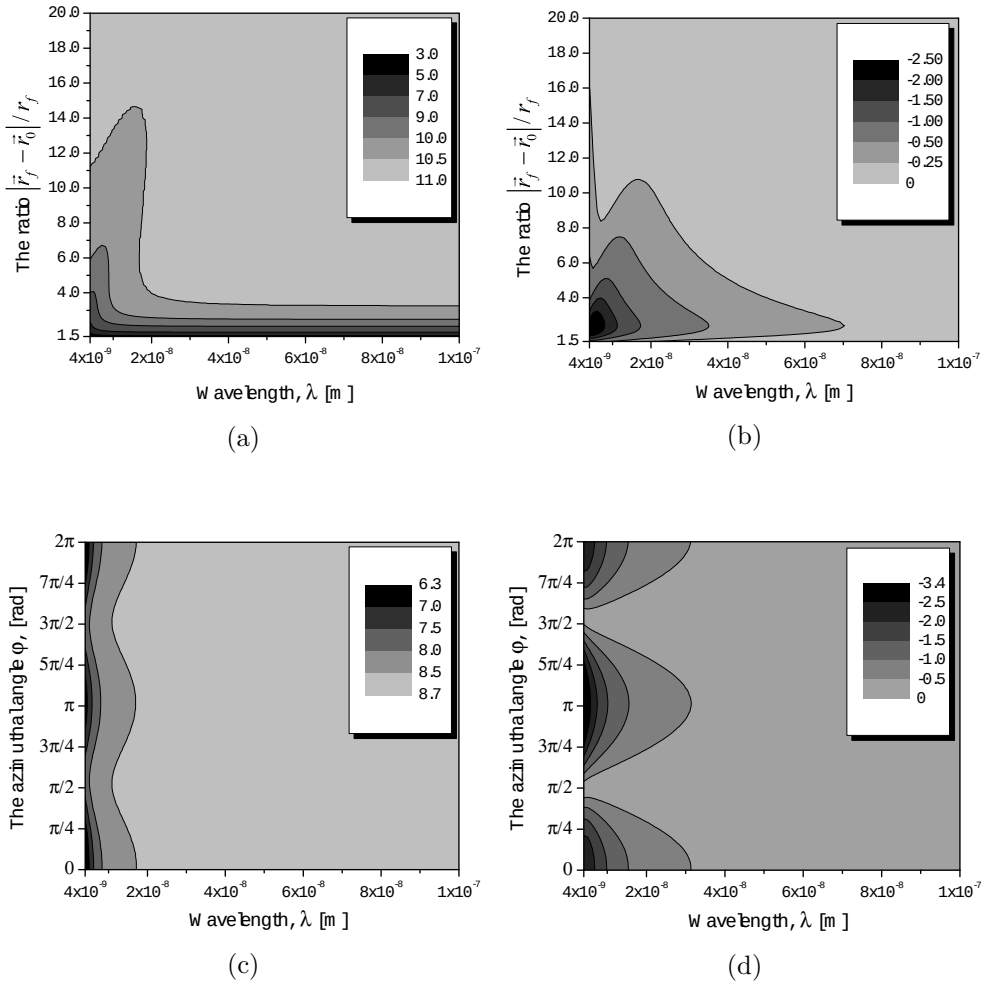

Figure 3.5: The spectral dependence of the dielectric constant ε_f for (a) the fullerene molecule C_{20} and (b) when $|\vec{r}_f - \vec{r}_0| = 2r_f(C_n)$.

Unlike the distant molecule, the adjacent fullerene is characterized by the non-zero imaginary part $\Im(\varepsilon_f)$ (Fig.3.5b, Fig.3.6b). The smaller is the operating wavelength, the larger is the imaginary part. The locations of the fullerene molecule and the observation point affect the variable $\Im(\varepsilon_f)$: e.g. at any given frequency the value $\Im(\varepsilon_f)$ reaches a maximum once the separation $|\vec{r}_f - \vec{r}_0|$ is about of a few fullerene

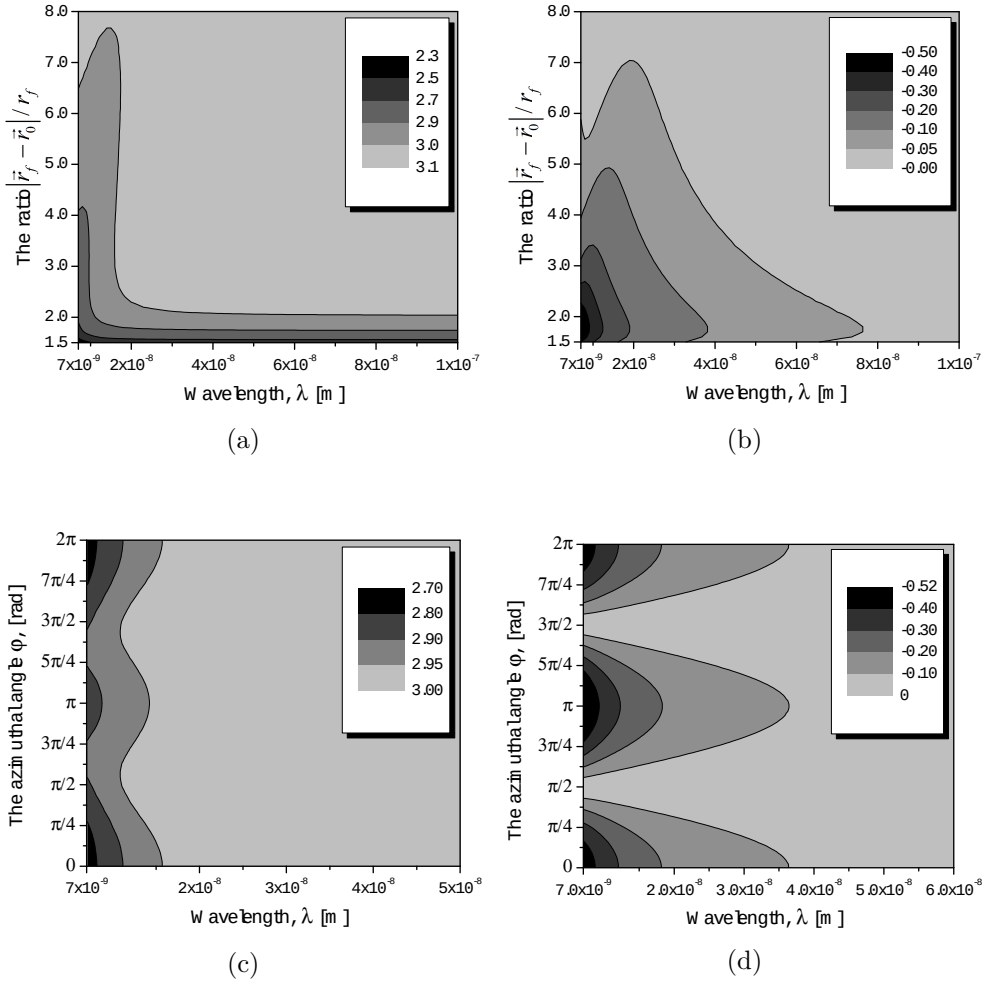

Figure 3.6: The dielectric constant ε_f for (a) the fullerene molecule C_{20} and (b) when $|\vec{r}_f - \vec{r}_0| = 2r_f(C_n)$.

radii and there exists a line through the source, the fullerene centre and the observation point (Fig.3.5d, Fig.3.6d). In conformity with the Lorentz reciprocity theorem, the electromagnetic properties of a fullerene adjacent only to the observation point can be determined by interchanging the source and the receiver and applying directly

the numerical results (Fig.3.5, Fig.3.6) and the respective findings. Once the fullerene is nearby both the source and the observation point, the simulations suggest that the value $\Re(\varepsilon_f)$ reduces even to a greater extent with decreasing the source-fullerene separation $|\vec{r}_f - \vec{r}_0|$. Meanwhile, no relation between such a separation and the variable $\Im(\varepsilon_f)$ is found.

The simulated results can be interpreted in the context of electromagnetic fields. For a distant fullerene, each atom produces an equal diffraction field portion. According to the nice agreement between the results in Table 3.1 and those in Fig.3.5a, Fig.3.6a at relatively large separation $|\vec{r}_f - \vec{r}_0| / r_f = 20$, it can be deduced that the interactions between the atoms of a distant fullerene make no impact on such a diffraction field portion. Hence, as all these field contributions are coherently interfering at the observation point, it therefore results in the strongest diffraction effect, which is implied through the maximum value $\Re(\varepsilon_f)$. For an adjacent fullerene, its atoms yield out-of-phase diffraction field portions. As these contributions add up at the point-receiver with a weaker diffraction impact, the adjacent molecule is therefore characterized by the smaller $\Re(\varepsilon_f)$. In turn, the parameter $\Im(\varepsilon_f)$ stands for 'losses' in a fullerene: it reflects the electromagnetic energy cancelled due to destructive interference between the atom-inspired diffraction fields. In this context, the value $\Im(\varepsilon_f)$ for a distant fullerene must be zero thanks to the coherence of diffraction fields caused by its atoms. Following the same line of reasoning, the imaginary part $\Im(\varepsilon_f)$ of an adjacent fullerene should conversely be non-zero.

Last but not least, with varying the operating wavelength λ or the distance $|\vec{r}_f - \vec{r}_0|$ values $\Re(\varepsilon_f)$ and $\Im(\varepsilon_f)$ for the adjacent fullerene C_{20} changes more substantially than those of the adjacent fullerene C_{60} (see Fig.3.5 and Fig.3.6, respectively). From simulations for other fullerene molecules, it is observed that the larger is a fullerene, the smaller are the change rates of its parameters $\Re(\varepsilon_f)$ and $\Im(\varepsilon_f)$. In this way, we suggest that the dielectric constant of an adjacent fullerene with $n \geq 100$ might reliably be approached through the Table 3.1 due to such quite restrained change rates.

3.3 Fullerene-based Yagi-Uda-type Antenna

For the sake of a deeper insight, the electromagnetic impact of a number of fullerene molecules on the field at the point-receiver is analysed in this chapter. Inspired and motivated by the concept behind the conventional Yagi-Uda antennas [108], we there-

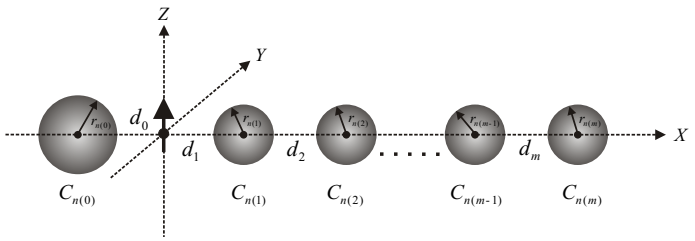

Figure 3.7: The sketch of $(m+1)$ element fullerene-based Yagi-Uda-type antenna indicating the positions of the reflector, the source and directors. Note that each fullerene is illustrated as a sphere.

fore study the directional capabilities of fullerene-based Yagi-Uda-type antenna. Likewise its macro-scale counterpart, this antenna includes the source and the parasitic elements, which are represented by different fullerene molecules (Fig.3.7). Owing to the sub-nm dimension and quite large dielectric constant ε_f of small-atom fullerenes, such a nanoscale Yagi-Uda-type antenna might focus and direct the ultraviolet and X-rays radiation. As this capability is very relevant to a number of biosensing/bioimaging applications, the developed model and its results are employed to determine the radiation performance of the antenna of interest.

The antenna is modelled as shown in Fig.3.7. The point-source is located in the coordinate origin. The reflector fullerene $C_{n(0)}$ is shifted to the left by d_0 along the x-axis, the coordinates of the 1-st director fullerene is $(d_1, 0, 0)$ and the i-th $(2 \leq i \leq m)$ director element is displaced along the x-axis by the distance d_i from the $(i-1)$-th molecule. Each director is described by the fullerene C_{20}, which is the most active in terms of electromagnetic impact. The reflector is given by the molecule C_{24} as it should be barely larger than the director fullerene (i.e., $r_{24(0)}/r_{20(1)} = 1.138$). Following the concept of microwave Yagi-Uda antenna and using the suboptimal optimization, the distances d_0, d_1 and $d_{2\ldots m}$ are respectively set to be equal to 0.35λ, 0.1λ and 0.05λ for the numerical experiments. To fulfil the model's limitation (i.e, the scatterers are much smaller than the operating wavelength), the value $\lambda = 4$nm.

It is well known that the isolated vertically polarised point-source has an isotropic radiation pattern in the H-plane (z = 0). Therefore, as the relative power level against the azimuthal angle φ at the H-plane of the individual source is constant (= 0dB), it is well convenient to study and compare the directional capabilities of nanoscale Yagi-Uda-type antenna by considering such a relation $|F(\varphi)|$. In particular, the relative power level versus the angle φ in z = 0 plane for the fullerene-based

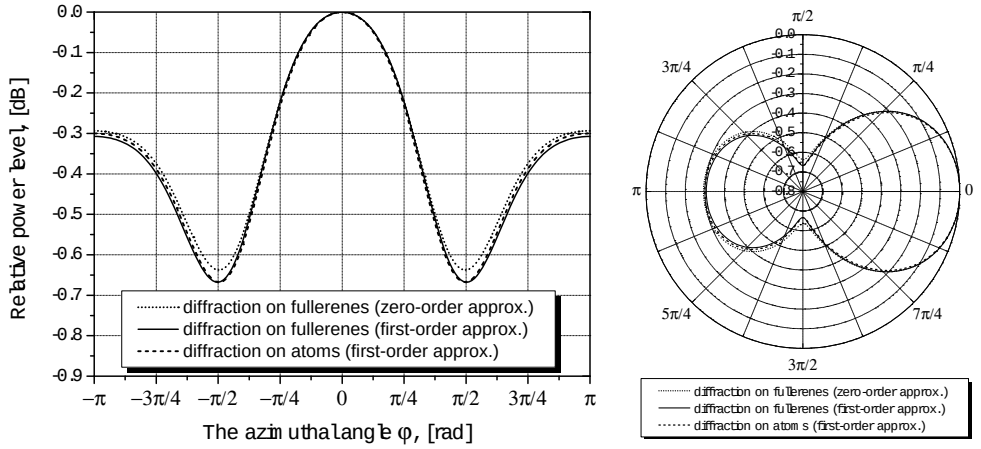

(a)

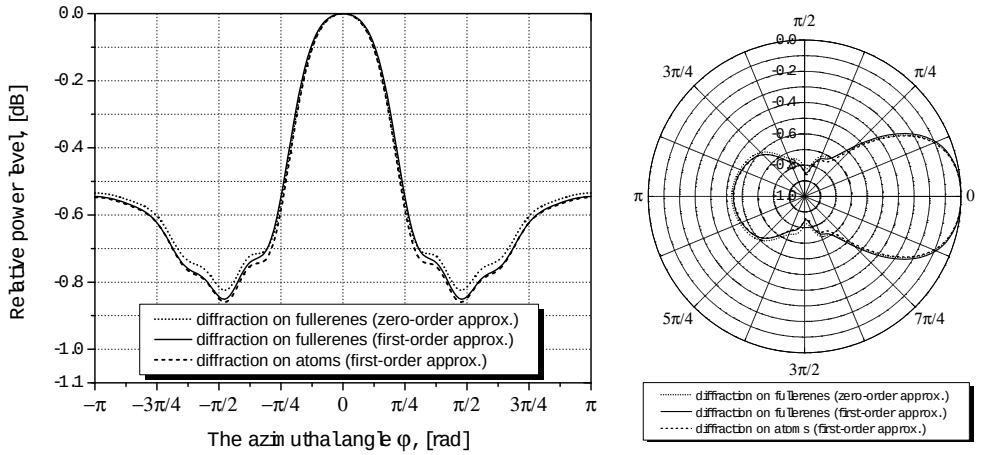

(b)

Figure 3.8: Relative power level as a function of the angle φ in rectangular and polar format at the H-plane of the fullerene-based Yagi-Uda-type antenna with (a) $m = 4$ and (b) $m = 10$.

Yagi-Uda-type antenna with $m = 4$ and $m = 10$ is demonstrated in Fig.3.8a and Fig.3.8b, respectively. The dotted curves in these figures have been evaluated as follows: at first, the permittivity of each fullerene is estimated using Eq.(3.18) for the

zero-order approximation; at second, such an equation is applied to determine the received field as a function of the angle φ and plot $|F(\varphi)|$ after all. The solid lines in Fig.3.8 are obtained in a similar way but employing the first-order approximation Eq.(3.20) instead of Eq.(3.18).

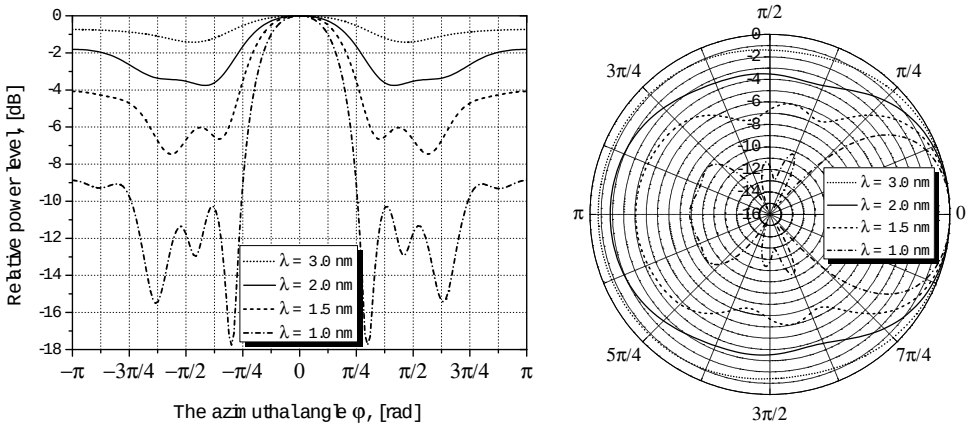

(a)

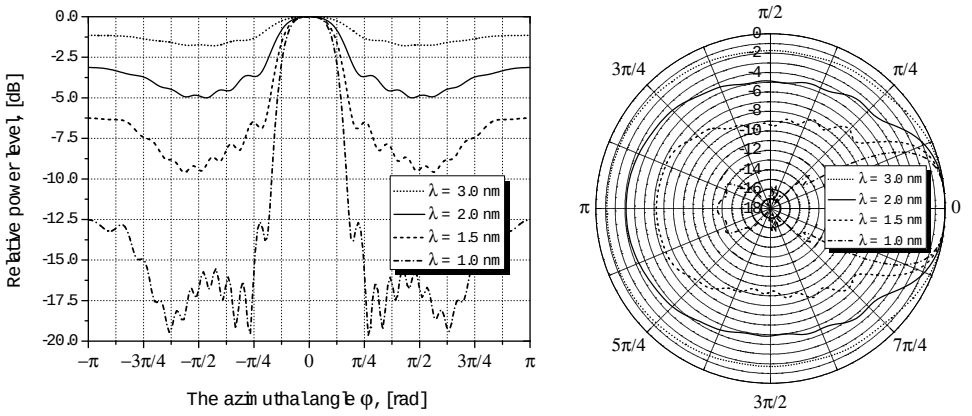

(b)

Figure 3.9: Relative power level as a function of the angle φ in rectangular and polar format in the H-plane of the fullerene-based Yagi-Uda-type antenna with (a) $m = 4$ and (b) $m = 10$ at different frequencies.

For the sake of comparison, the dashed series are assessed by considering each carbon atom in the antenna as a scatterer and using Eq.(3.20) in a straightforward manner. Since the latter series reflect the most accurate results, the good agreement between them and the dotted/solid lines validates the developed model on estimating the relative dielectric constant of fullerene molecules. Meanwhile, the use of the model leads to a significant reduction in computation time and computer load: e.g. the straightforward calculation (from an atomic point of view) of the fullerene-based Yagi-Uda-type antenna with $m = 10$ requires a time larger by two orders of magnitude than that when the model is applied to determine the dielectric properties of fullerene molecules at first.

As expected and shown in Fig.3.8, larger number of director elements results in a better antenna directivity. However, according to the numerical results the directional capabilities of both the considered antennas are quite meager. The key reason behind such a low directivity is that the antenna fullerenes are electrically small in terms of the wavelength $\lambda = 4$nm and thus cause only a modest electromagnetic impact on the point-receiver. In particular, by decreasing the operating wavelength to $\lambda = 1$nm the directivity of the antennas of interest substantially increases in conformity with the data shown in Fig.3.9. These numerical results are estimated by considering the antenna from an atomic point of view and directly applying the Eq.(3.20) for the first-order approximation since $\lambda < 4$nm is beyond the model applicability limits. Note that such an atom-based straightforward calculation is allowable only when $\lambda \geq 1$nm (as the criterion on atom smallness is fulfilled in such case).

3.4 Conclusions

At present, the interactions between electromagnetic waves and nanomaterials have primarily been modelled based on the standard electrodynamics methods, which consider nanoscale particles as continuous objects characterized by a frequency-dependent dielectric constant. The permittivity of a nanoscale object has been determined using the Drude model, which cannot handle extremely small nanoscale particles and is limited to calculate the electromagnetic properties at frequencies up to the visible spectrum. To evaluate the effective dielectric constant of a nanoscale object with a small number of atoms at wavelengths up to 1nm, we have developed a novel model. This model includes the closed-form solution for the field scattered from a small-atom object. Such a field has been derived by considering each atom as a single scatterer

and by using the integral equation formalism. The developed approach nicely complements the Drude model to offer the evaluation of electromagnetic parameters for an object of any size over the very broad frequency spectrum (up to soft X-rays).

Based on the developed model and assuming that a fullerene can be represented as a sphere with a certain 'effective' radius r_f owing to its ball-like atomic constitution, the electromagnetic properties of commonly used fullerene derivatives have been determined for the first time. Once a fullerene is spaced far enough from both the source and receiver (each separation is larger than twenty r_f), it has been found that the molecule causes no diffraction losses and is characterised by the maximum real effective dielectric constant $\Re(\varepsilon_f)$, which is defined through the geometric parameters of the fullerene. The electromagnetic impact of such a C_n fullerene has been found to decay with increasing number n of carbon atoms due to the fact that the volume density of atoms ρ_n is the largest for the smallest fullerene and decreases for larger fullerene derivatives: the permittivity $\Re(\varepsilon_f) = 10.63$ of the fullerene C_{20} decreases to $\Re(\varepsilon_f) = 1.37$ for the molecule C_{720}. Being in the inhomogeneous field of the point-source or/and point-receiver, a fullerene molecule exhibits another electromagnetic behaviour: the value $\Re(\varepsilon_f)$ has been shown to decrease with reducing the distance between the source/receiver and the fullerene, whereas its imaginary dielectric constant $\Im(\varepsilon_f)$ becomes non-zero owing to the destructive interference between the atom-inspired diffraction fields.

Motivated by the concept behind the conventional Yagi-Uda antennas, we have investigated a fullerene-based Yagi-Uda-type antenna: its parasitic elements (reflector and directors) are represented by different fullerenes, which impact is incorporated via their dielectric constants. From the numerical experiments, the fullerene-based Yagi-Uda-type antenna with a few director elements has been demonstrated to generate a high directional radiation only at X-ray frequencies. To achieve high directional capabilities in the optical band, the antenna must include a large number of director fullerenes with their positions approached through an optimization technique (i.e., allocating them in the 3D space so that to maximise the antenna gain). Apparently, such a multiple-element antenna is cumbersome and intractable in terms of the direct calculation from an atomic point of view. Meanwhile, the developed model capable of representing a fullerene as a sphere object with a certain effective dielectric permittivity offers the accurate treatment of a fullerene-based Yagi-Uda-type antenna consisting of a multitude of parasitic fullerenes in a very limited time and thus allows an effective optimization of this antenna.

Chapter 4

Interface Impact on RF Link between Nanomachines

Nanonetworks would often operate close to an interface between two media. Such a observation might attribute to application demands (paintable electronics, smart surfaces, wearing warning systems deployed over different objects and the like) and is inspired by a need to tightly attach nanomachines to the interface: this avoids asbestos-like pathogenic effects on people who might breath in nanoscale sensors [104]. The interface impact on the power budget of RF link between nanomachines might have a substantial impact on the nanonetwork realisation: in particular, the existence of a strong link gain provoked by the interface is demonstrated in [160], where the authors established a connection between microchips due to the surface wave contribution. The existence of a surface wave, excited by a dipole over a lossy underlying half-space, and its properties were formulated and studied by Sommerfeld in his classic pioneering paper [129]. The subsequent publications, e.g [99, 156], expanded the Sommerfeld's pioneering work. It was established that the surface wave amplitude decreases with the distance from the source slower than those of traditional spherical waves due to its cylindrical wave-front. The surface wave amplitude was however shown to decrease exponentially as the separation between the receiver and the surface increases. Due to an electrically large elevation of antennas in macroscale devices above surfaces, they do not excite efficiently the surface wave and consequently the surface impact is ignored in present wireless link models. On the contrary, as minia-

turized devices can be placed very close to the interface, the contribution of the surface wave to the received power might become essential. To the best of our knowledge, the quantitative impact of the half-space, which supports a surface wave, on the wireless link between nanomachines is however not elucidated in the literature. In this chapter, the integrated model, that analyses the impact of a surface-wave supporting substrate on both the wireless propagation link and the characteristics of nanomachine antenna, is formally derived by means of standard electromagnetic methods. The proposed model is employed to demonstrate the significance of such an underlying half-space for nanonetwork design and to suggest its parameters under which the received power is maximised. Compared to the previously-known solutions [11,75,84], the developed model is more comprehensive in the sense that it includes the impact of transmitting and receiving antennas (i.e., current distribution and input impedance, which are influenced by the interface).

Firstly, we analyse a two-layered half-space capable of supporting the surface wave to explore its influence on the wireless link between nanomachines. To rigorously determine this impact, we treat the problem using a full-wave approach. By introducing the surface impedance for the interface between upper and lower half-spaces, we also develop a formal impedance-based model. Unlike the full-wave solution that depends on the geometry of a particular substrate, the latter approach is more general: i.e., the usage of the surface impedance essentially simplifies the solution of the electromagnetic boundary-value problem as there is no need to take care of the fields within the underlying half-space. A good agreement between results obtained through both approaches endorses the impedance-based model, which is derived by applying the approximate impedance boundary conditions. Eventually, numerical analysis is carried out to demonstrate that a substrate, which supports a surface wave, concentrates electromagnetic energy in certain directions and can improve the link gain between two nanomachines due to the surface wave portion. Since this portion is very sensitive to the parameters of the underlying half-space, another point of interest is to formulate the criteria which should be imposed on the surface-wave supporting substrate to maximise the link gain.

Secondly, once a nanoscale antenna is located very close to the underlying half-space, its input impedance might be affected by the interface resulting in mismatch losses between the antenna and transmitter. Evidently, such mismatch influences the power budget of the wireless link between two nanomachines. Therefore, another goal of this work is to analyse such an input impedance as a function of the separation

between the nanoscale antenna and interface. Although this problem has attracted considerable attention in the past, the focus has primarily been either on further theoretical investigations of Sommerfeld's solution or developing approximate methods, which can satisfyingly model changes in the input impedance influenced by the half-space [65, 76, 77, 90, 98, 107, 117, 144, 149]. Moreover, these methods typically addressed the input impedance of an antenna with a length of the order of an operating wavelength. In this chapter, we develop the analytical model capable of determining alterations in the input impedance of a nanoscale antenna as a function of its separation from the interface. Conditions under which mismatch losses between this antenna and transmitter have a negligible impact on the wireless power budget are evaluated through numerical experiments. In the end, by combining these conditions with the calculated impact of the interface on the link gain between two nanomachines, we suggest the requirements on the optimum communication scenario for nanomachines in the presence of a nearby half-space.

This chapter is organized as follows. The system model is described in Section 4.1. In Section 4.2, the analytical model to obtain the received power over the two-layered half-space based on the full-wave formalism is developed, the way to treat it in a numerical fashion is thoroughly discussed and numerical analysis is carried out. In Section 4.3, the model that employs the impedance boundary condition is developed and the numerical analysis is carried out. The impact of the interface on the input impedance of nanoscale antenna is modelled and numerically investigated in Section 4.4. Finally, conclusions are drawn in Section 4.5.

4.1 System Model

The geometry of the problem is depicted in Fig.4.1. The simple half-space, which supports a surface wave, includes an electrically thin dielectric layer coated on an ideal metal. The dielectric layer of thickness d is lossy and characterized by a complex effective dielectric constant ε. The interface is regarded to be perfectly flat due to a short communication distance R. Each nanomachine is anchored to the half-space and equipped with nanoscale antenna, which is minute in terms of the wavelength λ and can thus be modelled as the infinitesimal dipole. Polarization of such an electrically small dipole is supposed to be vertical as it is subject to considerably less attenuation than for horizontally polarised signals. The antenna length is equal to l, while its radius is a. Other payload components are assumed to have no impact on the link

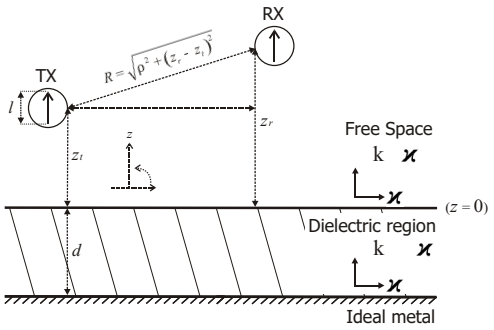

Figure 4.1: Problem geometry.

budget. The cylindrical coordinates and $e^{i\omega t}$ time dependence are used throughout. In particular, the distance between two nodes along the ρ-axis is defined as ρ, whereas the distances between the interface and the center of the transmitting and receiving antenna are z_t and z_r, respectively. To maximise the impact of the surface wave on the wireless propagation link between nanomachines, the heights z_t and z_r are considered to be much smaller than the operating wavelength. The nanomachines are situated in the free space with parameters $\varepsilon_0 = (36\pi)^{-1} \times 10^{-9}$ F/m and $\mu_0 = 4\pi \times 10^{-7}$ H/m. The full-wave analysis involves a detailed treatment of electromagnetic fields within the half-space to obtain the Green's function, which is eventually used to estimate the received power based on the Hertz potential formalism. The derived analytical solution is represented through the Sommerfeld-type integral equation, which can formally be solved by applying the principle of stationary phase. However, this approach is limited to obtain the radiated field in the far field region of the antenna only. As the receiving antenna might be located in the near field region of the transmitting antenna due to severe constraints on the nanomachine energy source, the Sommerfeld-type solution is treated numerically. The technique in which an integration contour is deformed to a steepest descent path [100] is used to estimate the received power for any communication distance between two nanomachines.

For the impedance-based model, the interface is located along the plane $z = 0$ and incorporated in the model through a surface impedance Z_s. This parameter relates the electric $\vec{E}$ and magnetic fields $\vec{H}$ on its surface according to the Leontovich boundary condition $\hat{n} \times \vec{E} = Z_s \cdot \hat{n} \times (\hat{n} \times \vec{H})$, where $\hat{n}$ is the outward unit vector normal to the surface [119]. Such a condition was originally proved to accurately treat any interface only when an incident plane wave comes from the zenith direction (incidence

angle $\theta = 0$). However, the condition's applicability can be expanded to incident plane waves with any incidence angle once the half-space dielectric constant $\varepsilon \gg 1$: only in this case, a charge density on the interface induced by a transmitting antenna is insensitive to its space position [37, 119]. According to [140], the radius of the interface curvature R_i should sufficiently exceed the communication distance R to employ the Leontovich boundary condition in a safe manner. Therefore, to let EM fields at the receiving nanomachine, which are obtained using the impedance boundary condition, approximate accurately the exact fields, the impedance-based model is developed under the assumptions that $\varepsilon \gg 1$ and $R_i \gg R$. The received power is derived based on the Hertz potential formalism: in particular, the Green's function obtained by using Z_s is utilized. The correctness of the impedance-based model is particularly verified by comparing its results for the given two-layered half-space to those calculated using the full-wave approach.

To analyse the input impedance of the nanoscale antenna, the transmitting nanomachine is placed over the interface plane $z = 0$ with a surface impedance Z_s. The separation between the antenna and the interface is equal to z_t. Subsequently, both analytical and numerical treatments are similar to those developed and shown in Section 4.2.

4.2 Surface-Wave Supporting Two-layered Substrate

4.2.1 Analytical Model

As the nanomachine antenna is an electrically small dipole, its current distribution is approximated to be one-dimensional and triangularly distributed along the aperture [77]. The transmitting dipole is excited by a transmitter with frequency f (wavelength λ) and amplitude A. To evaluate the pure interface impact on the RF channel between nanomachines, the transmitter and receiver are considered to be perfectly matched to the antennas. Therefore, using the classical EM approaches [60], a dominant (with respect to the vertical polarization) electric field E_z at the receiving point (ρ, φ, z_r) is derived as follows:

$$E_z(\rho, z_r) = \left(\frac{\partial^2}{\partial z^2} + k^2\right) \Pi_z^e(\rho, \varphi, z_r) = \frac{-15Ali}{k} \left[\left(\frac{\partial^2}{\partial z^2} + k^2\right) G(\rho, z_r, 0, z_t)\right], \quad (4.1)$$

where $k = 2\pi/\lambda$ is the free space wavenumber, and $G(\rho, z_r, 0, z_t)$ corresponds to the Green's function for the vertical Hertz's dipole located above the given two-

layered half-space. As the coordinate φ does not influence the value E_z, the assumption $\varphi = \varphi_0 = 0$ is used without loss of generality and their notations are discarded throughout the rest of the chapter. Based on the full-wave analysis, the function $G(\rho, z_r, 0, z_t)$ is formally derived in Appendix D.1 and has the following form:

$$G(\rho, z_r, 0, z_t) = \int_{-\infty}^{\infty} \frac{\varkappa H_0^{(2)}(\varkappa\rho) \cdot e^{-i\gamma_1(z_r+z_t)}}{i\gamma_1\varepsilon + \gamma_2 \tan(\gamma_2 d)} \mathrm{d}\varkappa, \tag{4.2}$$

where $\varkappa$ is the complex transverse wavenumber (Fig.4.1), while $\gamma_1^2 = k^2 - \varkappa^2$ and $\gamma_2^2 = k^2\varepsilon - \varkappa^2$ are the longitudinal wavenumbers in free space and the dielectric region, respectively. As the current at the receiving antenna obeys the triangular distribution, the received power can thus be expressed mathematically using standard EM theory as:

$$p = \frac{l^2|E_z(\rho, z_r)|^2}{32\Re(Z_a)} = \frac{225A^2l^4}{32k^2\Re(Z_a)} \cdot \left| \left(\int_{-\infty}^{\infty} \frac{\varkappa^3 H_0^{(2)}(\varkappa\rho) \cdot e^{-i\gamma_1(z_r+z_t)}}{i\gamma_1\varepsilon + \gamma_2 \tan(\gamma_2 d)} \mathrm{d}\varkappa \right) \right|^2, \tag{4.3}$$

where l is the length and Z_a the complex impedance of the antenna. Eq.(4.3) contains the Sommerfeld-type integral, which has no formal solution. Such an integral is typically treated using the stationary phase method [75] to produce an approximate analytical solution. The solution's applicability is however limited to cases, where the receiver is in the far field region of the transmitting antenna. To determine the received power at any communication distance, Eq.(4.3) is treated numerically. As it is intractable to evaluate the integral straightforwardly because of its highly oscillatory nature, the steepest descent path method [100] is proposed in Section 4.2.2. This method deforms the integration contour in order to simplify the procedure of obtaining the numerical integral solution.

4.2.2 Sommerfeld-type Integral Treatment

To assure unique specification of the Sommerfeld-type integrand in Eq.(4.3) in the complex $\varkappa$-plane, it is necessary to discuss in detail the properties of the square root $\gamma_1 = \sqrt{k^2 - \varkappa^2}$. For $|\varkappa_i| < k$ the corresponding wave mode propagates along the z-axis and its propagation constant γ_{1i} should be real and positive. When $|\varkappa_i| > k$, to ensure that the radiated field in Eq.(4.3) remains limited with increasing the separation between the nanomachine and the interface as then $|\gamma_{1i}| \cdot |z_t + z_r| \to \infty$, the

imaginary part of γ_{1i} is required to be negative. Eventually, we need to impose the following restrictions:

$$\begin{cases} \gamma_1 > 0, \ when \ |\varkappa| < k; \\ Im(\gamma_1) < 0, \ when \ |\varkappa| > k. \end{cases} \tag{4.4}$$

To facilitate the solution process of the Sommerfeld-type integral, the complex variable ξ is introduced through the transformation $\varkappa = k \cdot \sin\xi$, which changes Eq.(4.3) to Eq.(4.5). The complex $\varkappa$-plane is thus transformed into a single '2π-width' section of the complex ξ-plane due to the periodicity property $\sin(\xi + 2n\pi) = \sin\xi$ for $n = \pm1, \pm2, \ldots \pm \mathbb{N}$. Branch cuts, which are used on the two-sheeted complex Riemann $\varkappa$-plane to set the regulation of passing from one Riemann sheet to another to make the definition of the double-valued function $\gamma_1(\varkappa)$ unique, should be also mapped to the complex ξ-plane. In particular, the deformed integration contour $\overline{C}$ in the ξ-plane (Fig.4.2) is introduced as according to [30] it meets the criteria for γ_1 postulated in Eq.(4.4). The continuous spectrum of eigenvalues $\xi \in \overline{C}$ corresponds to the spectrum of free-space modes with $\gamma_1 > 0$. The set of discrete points $\xi \in [\pi/2, \pi]$ describes surface wave modes [123]. Note that although the poles of leaky wave modes

---

$$p = \frac{225A^2l^4}{32k^2\Re(Z_a)} \times \left| \left(\int\limits_{-\pi-i\infty}^{\pi+i\infty} \frac{k^3 \sin^3(\xi)\cos(\xi) \cdot H_0^{(2)}(k\rho\sin(\xi)) \cdot e^{-ik(z_t+z_r)\cos(\xi)}}{i\varepsilon\cos(\xi) + \sqrt{\varepsilon - \sin^2(\xi)} \cdot \tan\left(kd\sqrt{\varepsilon - \sin^2(\xi)}\right)} \mathrm{d}\xi \right) \right|^2 . \tag{4.5}$$

$$p = \frac{225A^2l^4}{32k^2\Re(Z_a)} \times \left| \left(\int\limits_{\overline{C}} \frac{k^3 \sin^3(\xi)\cos(\xi) \cdot H_0^{(2)}(k\rho\sin(\xi)) \cdot e^{-ik(z_t+z_r)\cos(\xi)}}{i\varepsilon\cos(\xi) + \sqrt{\varepsilon - \sin^2(\xi)} \cdot \tan\left(kd\sqrt{\varepsilon - \sin^2(\xi)}\right)} \mathrm{d}\xi - \right. \right.$$

$$\left. \left. - \sum_{n=1}^{N} \frac{k^3 \sin^2(\xi_p^n)\cos(\xi_p^n) \cdot H_0^{(2)}(k\rho\sin(\xi_p^n)) \cdot e^{-ik(z_t+z_r)\cos(\xi_p^n)}}{i\varepsilon + \cos(\xi_p^n) \left[\dfrac{\cdot \tan\left(kd\sqrt{\varepsilon - \sin^2(\xi_p^n)}\right)}{\sqrt{\varepsilon - \sin^2(\xi_p^n)}} + \dfrac{kd}{\cos^2\left(kd\sqrt{\varepsilon - \sin^2(\xi_p^n)}\right)} \right]} \cdot \right) \right|^2 . \tag{4.6}$$

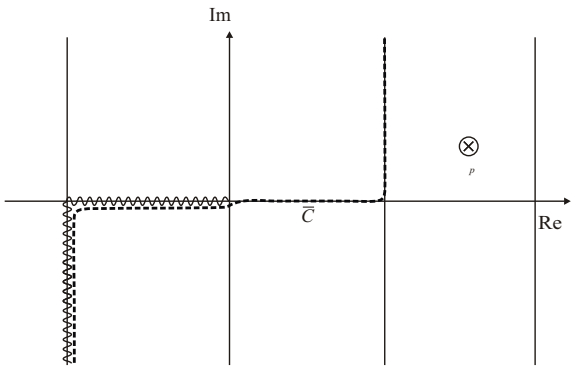

Figure 4.2: The integration contour $\overline{C}$ including the pole ξ_p.

are also determined through the simulations for quite thick dielectric layers, the leaky wave impact is seen to be negligible at the point-receiver (the leaky wave contribution is quite restricted once the heights z_t and z_r are small and decays exponentially along the ρ-axis [30]) and thus are neglected in this chapter. Each surface mode propagates in the subsurface region (i.e., $\gamma_1^2 < 0$ and $\gamma_2^2 > 0$) and its pole ξ_p has to be the root of the dispersive equation, which is basically the denominator of the integrand in Eq.(4.5). Hence, by obtaining the residues of these poles, the received power is decomposed as in Eq.(4.6). The first term in the brackets relates to the contribution of the geometric-optical wave. To determine the amount of received power caused by the portion of the surface wave, the sum in Eq.(4.6) should only be taken into account [123].

4.2.3 Numerical Analysis

By using Eq.(4.6) and following a geometric description of a numerical experiment conducted in [84], the geometric-optical and surface wave field at the point-receiver is calculated. Due to the nice agreement between the obtained results and those shown in Li's publication (see Fig.4.3), the full-wave model is endorsed. Moreover, although there is no straightforward mean to validate this model from a formal perspective, an indirect analytical support can still be provided by means of [86]: the dispersion equation in this chapter is similar to that derived here and being the denominator of the integrand in Eq.(4.5).

The numerical analysis is aimed to demonstrate that the impact of the simple two-

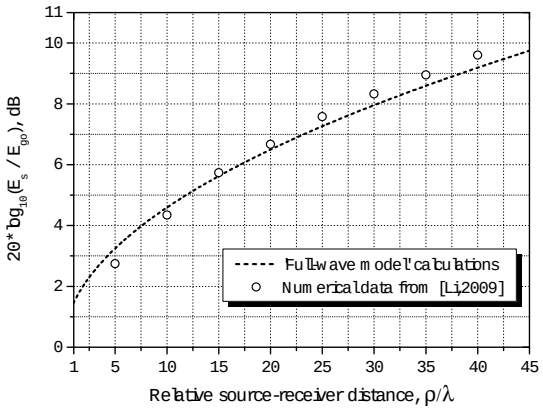

Figure 4.3: By using the full-wave model and following a geometric description of a numerical experiment conducted in [84], the field strength of the surface wave normalized to that of the geometric-optical wave is calculated as a function of the source-receiver distance. The dots correspond to the data shown in Li's paper, Fig 2.11.

layered half-space might substantially improve the link gain of the wireless channel between nanomachines. For numerical experiments, carbon is chosen as a reference dielectric material because it is low-loss and widely used. Its dielectric properties have been characterized in [54] and $\varepsilon = 15 - 8i$ is particularly extracted at frequency $f = 10$ GHz (a higher operating frequency is not selected due to unavailability of the experimental data). Calculations are performed for three different thicknesses: $d_1 = 5 \cdot 10^{-4}$ m, $d_2 = 10^{-3}$ m and $d_3 = 10^{-2}$ m. The heights z_t and z_r are fixed to be equal to $\lambda/10$.

The dispersive equation is solved in a numerical manner as it is transcendent and unable to be analytically treated. In the course of its evaluation for $f = 10$ GHz, the following is concluded: (1) a zero surface mode is always present in the dielectric layer; (2) the higher are the frequency f, the thickness d and the dielectric constant ε, the larger is the total number of surface modes; (3) a multimode regime in the dielectric film occurs when $d > 2 \cdot 10^{-3}$ m. In particular, in Fig.4.4a a single root is estimated once the thickness is equal to d_1 or d_2. To demonstrate the significance of the interface impact, the power contribution of the surface wave p_s is calculated for these thicknesses and normalized to that of the direct wave p_{fs}. Such a field strength is assessed using the free-space Green's function e^{-ikR}/R, where the communication distance R is chosen to be the same as for calculating p_s. The link gain caused by the

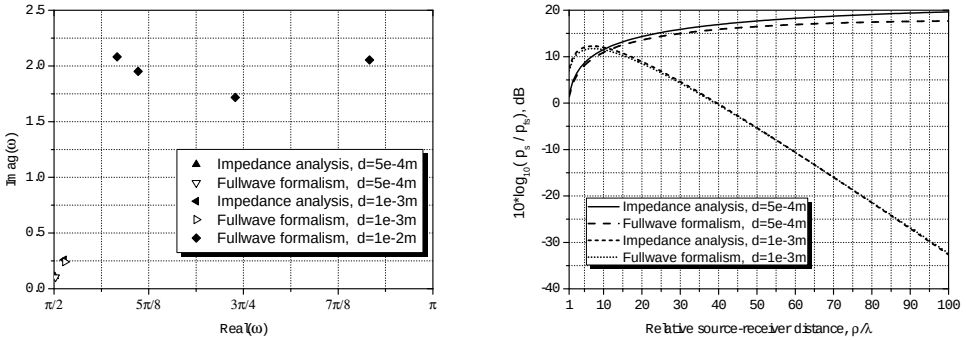

(a) (b)

Figure 4.4: (a) The roots of dispersive equation ξ_p are determined for the given values d. (b) The surface field strength normalized to that in the free space (the communication distance is the same for both scenarios) is demonstrated for the thicknesses d_1 and d_2.

dielectric with thickness d_1 is shown to be larger than 10 dB when $R > 7\lambda$ (Fig.4.4b, dashed line). Meanwhile, the dielectric with thickness d_2 supports the surface wave, which increases the channel gain by more than 10 dB, once $2\lambda < R < 15\lambda$ (Fig.4.4b, short-dashed line). Hence, through the numerical analysis, the interface is shown to have a significant influence on the link gain of RF channel between nanomachines, both at long and short communication ranges.

Now we will investigate the impact of the half-space, which allows multiple surface modes. In particular, the dielectric with thickness d_3 has four surface modes as its dispersive equation includes four different roots (Fig.4.4a). However, all these surface modes (including the zero one) convey a negligible amount of energy to the receiving antenna in free space: i.e., when $R = \lambda$, the ratio $p_s/p_{fs} = -51$ dB and reduces further with increasing the communication range R. The same behaviour is observed for the dielectric, which also supports multiple surface modes but has a different thickness. Therefore, in the multimode scenario the surface wave will only propagate within the dielectric layer and produce negligible impact on the received signal in free space. In other words, the energy coupled into a dielectric slab of electrically large thickness (i.e., described by multiple modes) remains in the slab rather than propagating back to free space.

According to [123], a half-space with a single surface mode can be modelled in terms of its surface impedance. As the impedance-based model is attractive from a fundamental perspective since there is no need to take care of the fields within the

$$G(\rho, z_r, 0, z_t) = \frac{e^{-ik\sqrt{\rho^2+(z_r-z_t)^2}}}{\sqrt{\rho^2+(z_r-z_t)^2}} + \int_{-\infty}^{\infty} \frac{\varkappa H_0^{(2)}(\varkappa\rho)}{\sqrt{\varkappa^2-k^2}} \cdot \frac{\sqrt{k^2-\varkappa^2}-k\overline{Z}_s}{\sqrt{k^2-\varkappa^2}+k\overline{Z}_s} \cdot e^{-i\sqrt{k^2-\varkappa^2}(z_r+z_t)} \mathrm{d}\varkappa. \tag{4.7}$$

$$\begin{aligned} p = \frac{225A^2l^4}{32k^2\Re(Z_a)} \times \Bigg| \Bigg(\left[\frac{\partial^2}{\partial z^2} + k^2\right] \frac{e^{-ik\sqrt{\rho^2+(z_t-z_r)^2}}}{\sqrt{\rho^2+(z_t-z_r)^2}} + \\ + \int_{\overline{C}} k^3 \sin^3(\xi) \cdot H_0^{(2)}(k\rho\sin(\xi)) \cdot \frac{\cos(\xi)-\overline{Z}_s}{\cos(\xi)+\overline{Z}_s} \cdot e^{-ik\cos(\xi)(z_t+z_r)} \mathrm{d}\xi + \\ + \ 4\pi i \cdot k^3 \cdot (1-\overline{Z}_s^2) \cdot H_0^{(2)}\left(k\rho\sqrt{1-\overline{Z}_s^2}\right) \cdot \overline{Z}_s \cdot e^{ik(z_t+z_r)\overline{Z}_s} \Bigg) \Bigg|^2 . \end{aligned} \tag{4.8}$$

underlying half-space, it is developed next.

4.3 Surface Impedance based Approach

4.3.1 Analytical Model

In this section, we study the wireless link between two nanoscale devices over an interface in free space limited at $z = 0$ by the Leontovich boundary condition with surface impedance Z_s. The boundary condition as shown in [119] can be used for modelling dielectric half-spaces with $\varepsilon \gg 1$ and is applicable to arbitrary incident angles. The received field is obtained by applying Eq.(4.1). The Green's function for a vertical electric dipole situated over a flat interface with impedance Z_s is derived from [150] and given by Eq.(4.7). The normalised surface impedance $\overline{Z_s} = Z_s/120\pi$. The first term in Eq.(4.7) corresponds to the free-space Green's function, while the second one represents the interface impact on the field at receiving point (ρ, z_r). As $G(\rho, z_r, 0, z_t)$ contains the Sommerfeld-type integrand, the solution process is similar to that in Section 4.2.2. Thus, the Green's function is revised using the transformation $\varkappa = k \cdot \sin\xi$. Since the restrictions on γ_1 are the same as in Eq.(4.4), the integration contour $\overline{C}$ is applied. Also, the residue of the unique pole $\xi_p = \arccos(-\overline{Z_s})$ needs to be taken into account as it belongs to the proper Riemann sheet. Using Eq.(4.3), the power at the receiving nanomachine is eventually derived as in Eq.(4.8). Note that the power

contribution of the direct, the reflected and the surface wave can respectively be calculated by considering only the first, the second and the third term in the round brackets of this equation.

To validate the impedance-based model, the given two-layered half-space is used and the obtained results are compared to those of the full-wave approach. The normalised surface impedance $\overline{Z}_s$ of the given half-space is derived by taking care of the boundary condition for EM fields on both surfaces of the dielectric layer and adopting the impedance boundary criterion at its upper interface and given by [84]:

$$\overline{Z}_s = i\,(1/\varepsilon)^{1/2} \tan\left(k\sqrt{\varepsilon}d\right). \tag{4.9}$$

Once the dielectric thickness is equal to d_1 and d_2, the normalised impedances of the two-layered half-space are $\overline{Z}_s^1 = 0.0035 + 0.1107i$ and $\overline{Z}_s^2 = 0.0436 + 0.2635i$, respectively. For each thickness, the single root of the dispersive equation is seen in Fig.4.4a to be fairly approximated by $\xi_p = \arccos(-\overline{Z}_s)$, where $\overline{Z}_s$ is estimated using Eq.(4.9). In this way, the power contribution of the surface wave calculated by the impedance-based model for $z_t = z_r = \lambda/10$ is shown to be dominant and in good agreement with those obtained by the full-wave approach (Fig.4.4b). Such a nice match justifies the applicability of the impedance-based model to determine the interface impact on the power budget of wireless channel between nanomachines.

4.3.2 Numerical Results

The impact of the interface is investigated by comparing the total received power p with a reference value p_{fs}, which corresponds to the power delivered through the free-space propagation channel. The power p_{fs} is estimated by taking only into account the first term in the brackets of Eq.(4.8) as it represents the direct wave portion. To better understand the significance of the surface wave, the power contribution of this wave is assessed by solely considering the last term in the brackets of Eq.(4.8) in comparison with p_{fs}. The results, which are obtained for different values of $\overline{Z}_s$ as a function of the separation z_t, z_r, are shown in Fig.4.5. Note that the total power p is calculated under the assumption that the surface wave constructively interferes with the geometric-optical counterpart as a phase shift between these waves is negligibly small due to a short communication range. In particular, the surface velocity has been demonstrated in Appendix D.3 to be large enough to make this assumption. Also, the value of $\overline{Z}_s$ is considered to be limited as it is inversely proportional to the

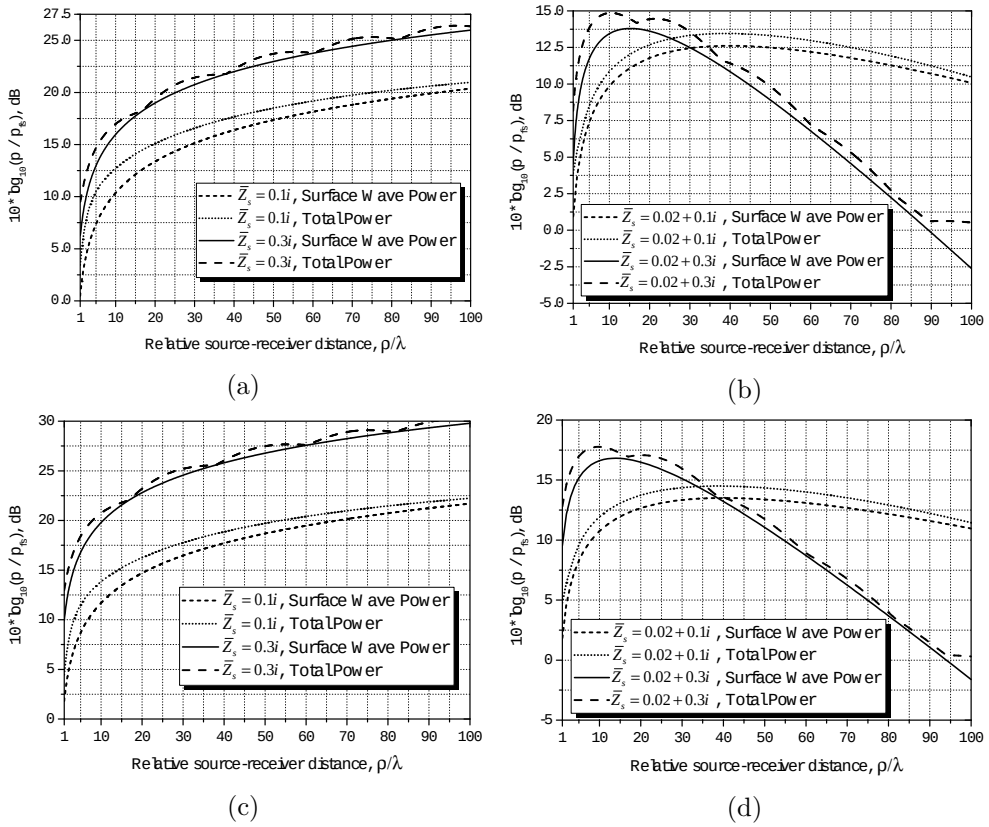

Figure 4.5: The total field power and its surface wave contribution as a function of the distance between the transmitting and receiving antennas. The obtained powers are normalized to the received power p_{fs}, which is related to a free-space wireless channel and calculated under the same conditions. (a) and (b) is plotted when $z_t = z_r = \lambda/10$, (c) and (d) is depicted for $z_t = z_r = \lambda/100$.

square root of the effective dielectric constant ε. Since $\varepsilon > 10$ to satisfy the impedance boundary condition criterion [75], the surface impedance is bounded as $\left|\overline{Z_s}\right| < 0.3$.

As can be seen in Fig.4.5, the interface impact depends significantly on its surface impedance. In particular, the larger is the positive imaginary part of $\overline{Z}_s$, the better are the directive properties of the interface (i.e., no surface wave propagates above the half-space with a zero imaginary part). The losses of the underlying half-space are incorporated in the real part of $\overline{Z}_s$ and thus the constructive impact from the interface is more significant when this real part tends to zero. Eventually, once the half-space is described by a relatively high inductive impedance and nanomachines

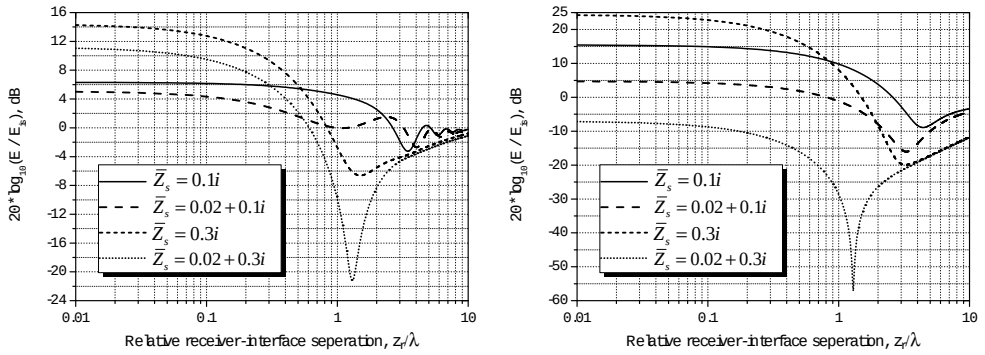

Figure 4.6: The received field strength E influenced by the half-space with the impedance $\overline{Z}_s$ normalized to that E_{is} affected by the perfectly conducting half-space $\overline{Z}_s = 0$ is shown as a function of the receiver-interface separation z_r when (a) $z_t = \lambda/10$, $\rho = 10\lambda$ and (b) $z_t = \lambda/10$, $\rho = 100\lambda$.

are placed very close to it, the received power p can be increased up to an order of magnitude compared to the 'free-space' scenario due to the dominant contribution of the surface wave Fig.4.5(a,c). For example, once $\overline{Z}_s = 0.3i$ and $z_t = z_r = \lambda/100$, the link gain is equal to 20 dB at $R = 10\lambda$ and its value increases with enlarging R. The existence of such a strong power gain may be explained by two facts: first, the surface wave field decays slower than the geometric-optical counterpart ($\sim 1/\sqrt{R}$ instead of $\sim 1/R$); second, a highly inductive half-space redistributes the EM fields by pulling them to the surface. The former is the well-known property of the surface wave coming from its cylindrical nature [140], meanwhile the latter argument needs to be further investigated to prove its reliability. In particular, the EM field strength at the receiving antenna influenced by the half-space with the inductive impedance $\overline{Z}_s$ is compared to that affected by the perfectly conducting half-space ($\overline{Z}_s = 0$) in Fig.4.6. Since a perfectly conducting half-space produces a maximum geometric-optical portion as $R \gg \lambda$ and $z_t \ll \lambda$, such a comparison indicates how the geometric-optical field partly turns into a surface field as well as in dissipation losses. In particular, its transformation into surface wave energy is seen from the trend that the field density increases for $z_r \ll \lambda$, whereas its magnitude decreases for larger z_r (the half-space 'attracts' the EM field to its surface). Meanwhile, for lossless half-spaces the magnitude of the EM field at $z_r \ll \lambda$ weakly decreases with increasing communication distance R due to the slow decay of the surface wave (solid and short-dashed lines

in Fig.4.6). Once the half-space is lossy, despite of such a surface wave effect, the magnitude of the EM field at $z_r \ll \lambda$ may even reduce with increasing R as the EM energy is partly dissipated (dashed and dotted curves in Fig.4.6).

4.4 Antenna Characteristics

The nearby interface influences the input impedance of the nanomachine antenna through changing its current distribution [117]. For the modelling, the electrically small vertically polarised dipole is placed over the plane interface at height z_t. The antenna length is equal to $l \ll \lambda$ and its radius $a \ll l$. The half-space is characterized by the normalised surface impedance $\overline{Z}_s$.

The dipole impedance is analytically derived in Appendix D.2. This impedance can be decomposed as $Z_a = Z_{fs} + \Delta Z$, where Z_{fs} is the input impedance of the antenna in free space and ΔZ is the change due to the presence of the half-space. The free-space antenna impedance Z_{fs} has been determined in [77]. Being the measure of the interface impact, the value ΔZ includes the Sommerfeld-type integrand and is revised using the transformation $\varkappa = k \cdot \sin(\xi)$ and given by Eq.(4.10). This equation is treated in a similar fashion as before and the final form of ΔZ is represented as in Eq.(4.11).

To address ΔZ as a function of the normalised surface impedance $\overline{Z}_s$, the parameters of the radiating dipole are fixed to be $l = 0.01\lambda$ and $a = 0.01l$, where $\lambda = 3 \cdot 10^{-2}$ m. The impedance of such a dipole in free space is estimated to be $Z_{fs} = 0.019 - 11596i$ Ohm. Meanwhile, the complex value ΔZ is shown as a function of the separation z_t in Fig.4.7 for several interfaces characterized by $\overline{Z}_s = 0$,

$$\Delta Z = \frac{15l^2k^2}{2} \int\limits_{-\pi-i\infty}^{\pi+i\infty} \sin^3(\xi) \cdot H_0^{(2)}(k\rho\sin(\xi)) \cdot \frac{\cos(\xi) - \overline{Z}_s}{\cos(\xi) + \overline{Z}_s} \cdot e^{-2ikz_t\cos(\xi)} \mathrm{d}\varkappa. \quad (4.10)$$

$$\begin{aligned} \Delta Z = \frac{15l^2k^2}{2} \Bigg[& \int\limits_{\overline{C}} \sin^3(\xi) \cdot H_0^{(2)}(k\rho\sin(\xi)) \cdot \frac{\cos(\xi) - \overline{Z}_s}{\cos(\xi) + \overline{Z}_s} \cdot e^{-2ikz_t\cos(\xi)} \mathrm{d}\varkappa + \\ & + 4\pi i \cdot (1 - \overline{Z}_s^2) \cdot H_0^{(2)}\left(k\rho\sqrt{1 - \overline{Z}_s^2}\right) \cdot \overline{Z}_s \cdot e^{2ikz_t\overline{Z}_s} \Bigg]. \end{aligned} \quad (4.11)$$

$\overline{Z}_s = 0.1i$ and $\overline{Z}_s = 0.25i$, respectively. It can be seen that the obtained results match those calculated using the electromagnetic solver [1], which are shown as markers. The latter could be assessed in the following way. First, the dipole antenna in free space is modelled in FEKO as an one-dimensional wire element with the feed point at the middle and its impedance Z_{fs} is straightforwardly determined via simulations. Second, the antenna impedance Z_a is directly estimated by considering the dipole antenna as previously, whilst the interface impact is introduced through a 'planar multilayer substrate' tool available in FEKO. To provide the interface with the required impedance $\overline{Z}_s$, by using Eq.(4.9) the constitution and layer thickness of the two-layered half-space discussed above is respectively adapted (except for the interface characterized by $\overline{Z}_s = 0$, which stands for the half-space made of a perfectly conducting metal). In the end, for each set of input parameters the complex value ΔZ is evaluated by correspondingly subtracting Z_{fs} from Z_a.

As a transmitter can typically adapt the real part of its impedance to avoid a mismatch with the antenna, the attention is primarily paid to the imaginary part of Z_a. It can be concluded from Fig.4.7 that the rate of increase of the imaginary part $\Im(\Delta Z)$ grows with lowering the value $\overline{Z}_s$. This finding is explained by the fact that with decreasing $\overline{Z}_s$ the interface tends to behave as a perfect conductor, which is known to strongly affect only the imaginary part of a vertically polarised antenna. Meanwhile, the starting point of increasing $\Im(\Delta Z)$ is independent from the properties of an underlying half-space. While modelling the transmitting antenna of a different length and radius, it appears that such a starting point is mainly related to the ratio z_t/l. From a physical perspective, it can be explained that the separation between the antenna and interface z_t has to be increased in order to not induce a perturbation of currents on the aperture of a larger antenna. Our results suggest that the value $\Im(\Delta Z)$ can be considered insignificant once $z_t/l \geqslant 1$ for any kind of half-space and antenna radius $a \leqslant 0.1l$. Hence, once the separation z_t exceeds the dipole length l, the interface will cause a negligible mismatch between the antenna and transmitter as it does not affect the imaginary part of Z_a. Moreover, the real part $\Re(\Delta Z)$, which is directly associated with the amount of energy radiated from the antenna, can even be enhanced by means of the nearby interface (Fig.4.7a,c,e).

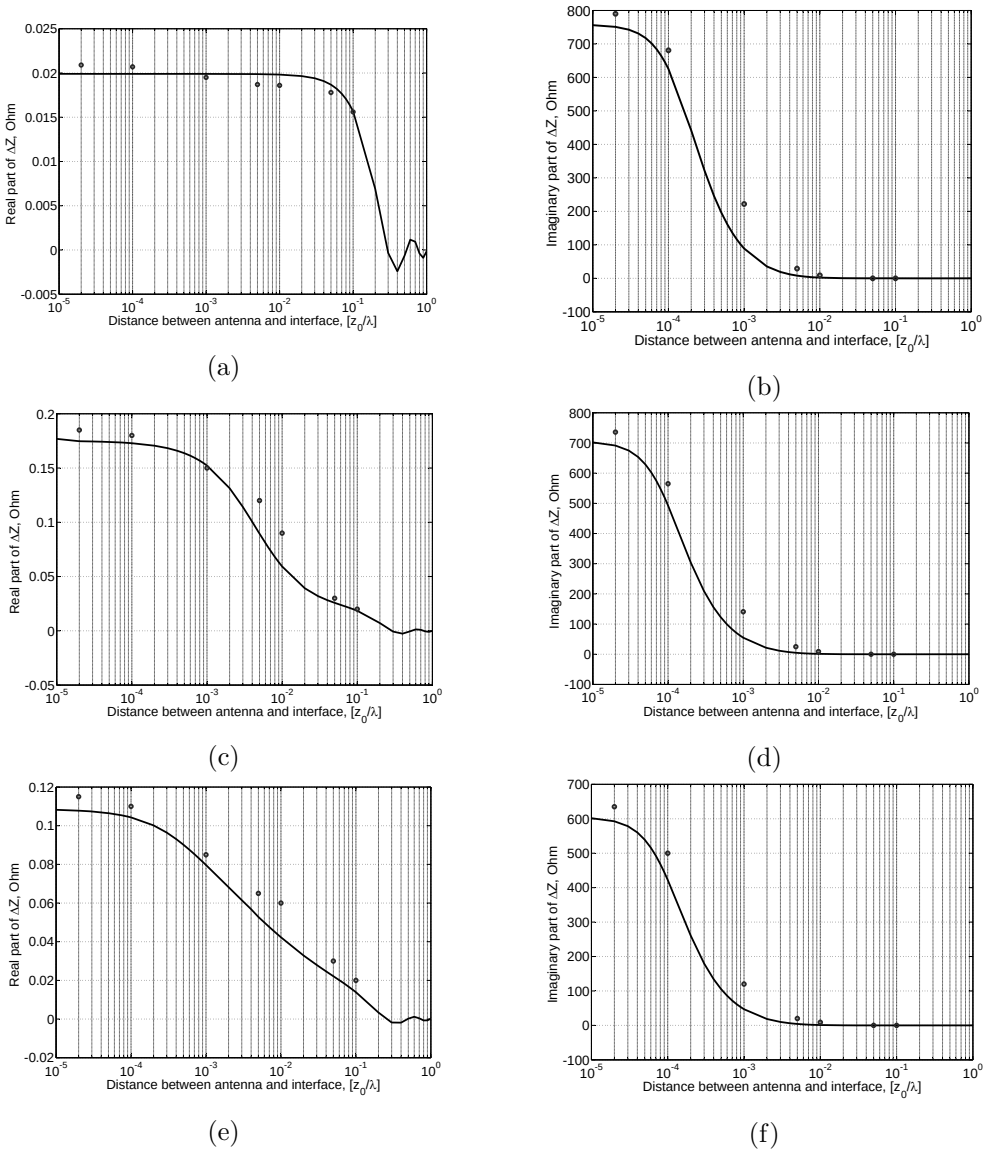

Figure 4.7: The value of ΔR for different types of half-space: (a) and (b) for $Z_s = 0$; (c) and (d) for $Z_s = 0.1i$; (e) and (f) for $Z_s = 0.25i$. The results obtained are shown in solid line, whilst those simulated in FEKO are depicted by markers.

4.5 Conclusions

To analyse the impact of a media interface on the wireless link between nanomachines in RF smart-dust-like networks, we have developed an integrated model, which involves the formal treatment of the interface impact both on the propagation path and RF antennas, and respectively performed the numerical analysis. We assumed that both transmitting and receiving nanomachine are equipped with an electrically small vertically polarised linear dipole and respectively placed over the half-space at the height z_t and z_r, which is much smaller than the operating wavelength.

Firstly, the influence of a surface wave on the wireless link between nanomachines in a two-layered half-space has been modelled using the full-wave formalism. The good agreement between the results obtained via this proposed model and those recognized in the literature endorses the model's correctness. Through numerical experiments, it has been shown that particular realisations of the two-layered half-space might cause a constructive and significant impact on the power budget of the propagation channel between nanomachines: once the communication distance $R > 2\lambda$ and $z_t = z_r = \lambda/10$, the link gain is increased by more than 10 dB due to the contribution of the surface wave. Secondly, by using the surface impedance concept another model has been formally developed to describe the interface impact on the wireless link (the latter approach is more attractive from a fundamental perspective as there is no need to take care of the fields within the half-space). The usage of the impedance-based model has been verified by comparing its output with available full-wave simulation results in particular cases and observing a good match between them. Inspired by the impedance-based approach, the subsequent numerical analysis demonstrates that a half-space with a highly inductive impedance substantially improves the power budget of a wireless link between nanomachines: i.e., the link gain increase is more than 20 dB when $R > 10\lambda$ and $z_t = z_r = \lambda/100$. The existence of such a large gain is explained by two facts: 1. the surface wave field decays slower than the geometric-optical counterpart ($\sim 1/\sqrt{R}$ instead of $\sim 1/R$); 2. a highly inductive half-space redistributes the EM fields by pulling them to the surface. From the nanomachine design point of view, this finding suggests developing antennas which will mainly transfer transmitting power in a surface wave rather than in space (volumetric) wave.

Thirdly, the influence of the nearby half-space on the antenna impedance has been analytically studied since the half-space might cause a mismatch between the nanomachine antenna and transmitter. The developed model has been validated through the

comparison analysis of the antenna impedances from the calculated results and those simulated in FEKO electromagnetic solver. Numerical experiments have indicated that the half-space negligibly affects the antenna input impedance once the separation z_t between antenna and interface exceeds the dipole length l. In this respect, the scenario when a highly inductive impedance significantly and constructively affects the wireless path gain between nanomachines without bringing extra mismatch of their antennas (the criteria $\lambda \gg z_t > l$, $\lambda \gg z_r > l$ can simply be fulfilled due to nanoscale antenna dimensions) is realisable in practice. This novel finding is essential as it offers an opportunity to communicate between nanomachines: i.e., thanks to the strong link gain provoked by such an interface, the wireless channel between devices with electrically small antenna is realizable and thus a functional wireless sensor nanonetwork might be implemented. Unlike the perfectly conducting half-space which merely supports the geometric-optical wave (it is formed as an interference of direct and reflected waves and thus its magnitude is subject to substantial alterations with varying source-receiver distance), the interface with a highly inductive surface impedance is moreover capable of maintaining the wireless link over a wide and continuous range of communication distances due to the significant contribution of the surface wave.

Chapter 5

Towards Connectivity and Source Positioning in Nanonetworks

At present, environmental sensing using electromagnetic waves can be performed using two different approaches. The first approach implies the use of devices, that sense an environment remotely (e.g., radars or lidars). Another approach requires a number of sensor nodes, which are distributed in an application area, perform sensing directly inside the phenomenon and wirelessly communicate with each other and with the external reference nodes. The locally collected data are then transmitted through such a wireless sensor network towards an end-user in a multihop fashion. The ability to operate and monitor in harsh, complex and inaccessible environments makes the latter approach more promising and ensures a wide range of applications for wireless sensor networks. In particular, there already exist low-end sensor-network-based solutions aiming to detect a sniper location [81], monitor volcano activity [154], detect a forest fire [50], control water waste in homes [74] and the like [2]. All these existing sensor networks consist of a small number of macro-scale nodes with their positions carefully engineered or pre-determined and capable of coarse-grained sensing. In turn, the nanonetwork is foreseen as a swarm of densely deployed nanoscale nodes within an application area: thanks to the high node density, the network can still support a long-distance transmission using a multihop communication paradigm. The simple functionality of the nanomachines implies that the nanonetwork topology cannot be retrieved (a node has no energy to reconnoitre its surroundings). A large number of

these nodes also entails that a random scattering over the area to be monitored is the most convenient or perhaps the only option to deploy them. All these features make nanonetworks very distinguishable from the existing sensor systems. Therefore, novel solutions and paradigms at the networking level are needed to transfer and extract information gathered by the nanonetworks.

The nanonetwork is speculated to be a massive decentralized communication system with nodes merely deployed in a random manner due to a lack of tools capable of manipulating nanomachines. Moreover, the topology of this network would be highly dynamic because of the wavering of node power levels, nanomachine failures and emerging of new added devices. Hence, the first challenge to be addressed is to determine the optimal density of nanomachines that provides and maintains connectivity so that sensed data originated from any network device could reach an end-user terminal (the so-called sink node).

Secondly, the delay performance and throughput of the nanonetworks are well shown to be heavily dependent on hop counts in multihop transmissions: e.g. the degradation of network capacity on increasing the number of hops was particularly demonstrated in the literature. Furthermore, the hop count also influences the source localization cost in the network. Because of a necessity to consider a sheer number of nodes, the graph and probability theory, widely used to study ad-hoc and mesh wireless sensor networks with a moderate number of entities, can be hardly implemented in the analysis of large-scale randomly distributed nanonetworks. Since, as far as our knowledge goes, there is no thought-out approach on how to determine the number of hops for packet forwarding in a nanonetwork, another challenge to be studied here is the development of a reliable framework suitable to estimate the hop count between source and sink node in a nanonetwork. Based on the developed approach, we could propose a model capable of estimating the probability $P(r,t)$ of successful reception of the message by a sink node spaced at distance r from a source in a given time t.

Thirdly, an efficient method capable of localising a source node in nanonetwork is required. The use of GPS on all nanoscale nodes is unacceptable in terms of energy resources, node dimensions and its inability to operate indoor, so other techniques have to be considered. At present, there are two such major GPS-free techniques for positioning in multihop environments: centralised and distributed localisation. In the first approach, all ranges between all nodes in the network are measured, marked by unique node numbers and are transmitted to a global central unit, which processes and computes the location of each node in the network [27, 36, 120]. Evidently, the

centralised approach is not good candidate for the nanonetwork since it requires a very large communication overhead. Distributed localisation algorithms [49, 80, 88, 109] require communication and ranging only with direct neighboring nodes and are in general more robust and energy efficient than centralised schemes. With distributed localisation, each node in the network is capable of processing and computing to remove a lack of reliance on a single point of possible failure and is provided with an optimum load balancing. Both approaches mentioned above require a large amount of energy to perform the prerequisite self-organization stage since the nodes must reconnoitre their surroundings to form a network topology. Due to modest processing capabilities and very limited energy resources of the nodes, the distributed localisation however becomes unaffordable and impracticable for the nanonetwork. In view of this, we propose a pioneering approach to estimate the location of a source node in the nanonetwork with arbitrary positions of nodes without consuming extra energy on the self-organization step. This approach employs the analysis of hop progress in such a network and uses time differences of last arriving signals to its borders to position a source (initially transmitting) node.

All the key findings of this chapter are formulated and obtained through exploiting the concepts and principles of percolation theory. Thus, principles of percolation theory and the system modelling from the percolation perspective is discussed in Section 5.1. By using these principles, a way to solve the connectivity problem of the large-scale nanonetwork, a technique to determine the hop count of the source-to-sink channel and the validation of the probability $P(r, t)$ through a numerical experiment is demonstrated in the Section 5.2. The source-positioning method for the nanonetwork is introduced and discussed in Section 5.3. Eventually, the chapter concludes with Section 5.4.

5.1 Modelling from Percolation Perspective

In physics, chemistry and materials science, percolation typically refers to the movement and filtering of fluids through porous materials. In mathematics, percolation theory describes the behavior of connected clusters in a system. The percolation theory originated in the 1950s as a mathematical model to address the flow of liquid through a porous medium. The connectivity problem in a sensor network was firstly explored from the percolation perspective in a series of papers starting in the 1970s. In particular, using the principles of continuum percolation, the connectivity

and hop count of a 2-dimensional large-scale network has been modelled and analysed for sensor nodes distributed in a plane according to a Poisson point process. Intents of solving the connectivity enigma of a 3-dimensional nanonetwork by applying the continuum percolation has recently gained reasonable attention as well. However, due to the complexity and the unknown locations of sensor nodes, determination of the hop count in the source-to-sink path of the nanonetwork is intractable with these solutions based on statistical laws (e.g. the Poisson distribution). Models available in the literature on the probabilistic analysis of the hop count in a large-scale and decentralized system are currently limited to two-dimensional (2D) networks. In particular, the probability of establishing a connection of a given length through a planar network with uniformly distributed nodes with a given number of hops has been investigated in [20]. There it was shown that node density does not greatly affect the hop count but has a huge effect on whether a connection can be made at all. In turn, the distribution of euclidean distances to the n-th node in a Poisson process is studied in [41]. For homogeneous sensor networks, the connectivity probability in one or two hops is derived and the connectivity in multiple hops is examined with analytical bounds in [13]. In [142], the distribution of the hop distance and its expected value in uniformly distributed networks are analysed by means of numerical simulations. The results indicate that directional nodes might substantially decrease the hop count compared to omnidirectional ones, although the connectivity of a large-scale sensor system will degrade. Hence, as there are merely solutions suitable to determine the hop count in specific 2D nanonetwork structure, which require heavy computational resources to treat large-scale networks, a different model capable of analysing the source-to-sink multihop path in a 2D/3D nanonetwork and obtaining its hop count in a low-cost manner is developed here.

In the proposed model, the nanonetwork topology is mapped to a regular lattice, where each lattice site is occupied by a sensor node with certain occupation probability. In this network, the sensed data spreads through the flooding protocol (i.e., a node transmits a signal either when it is triggered by its sensor or when a signal is received from neighbouring nodes [40]) as it is the most suitable way for a network with unknown node topology. To minimize interference overhead, a node is regarded not to broadcast the same message twice if it comes from different transmitting nodes with a delay in time. Each node is assumed to radiate omni-directionally with a coverage distance b_d, meanwhile the region covered by the nanonetwork is represented by a regular lattice structure with a given lattice spacing a_d (in the following, the

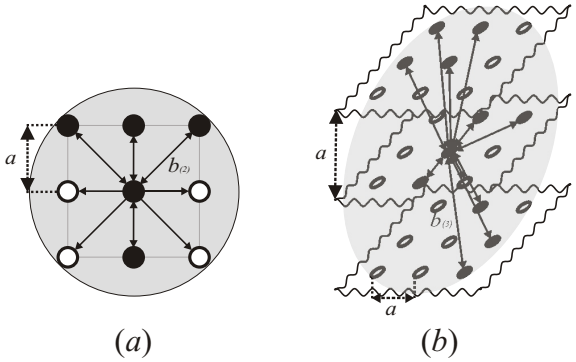

Figure 5.1: Node coverage is mapped to a regular lattice at (a) 2D surface and (b) 3D space. Occupied sites are indicated in black, whereas empty ones are drawn in white.

suffix d indicates the dimension). In this chapter, the 2D area of interest is discretized in a regular square lattice with $a_2 = b_2/\sqrt{2}$ and thus the amount of sites to be reached through an one-hop link (i.e., adjacent) is limited by the node degree number $m_2 = 8$ (Fig.5.1a). In turn, the 3D application space is simplified to a regular cubic lattice with $a_3 = b_3/\sqrt{3}$ and, consequently, the number of adjacent sites is limited to $m_3 = 26$ (Fig.5.1b). Both selected structures are chosen so to be conceptual since any square/cubic lattice with lattice spacing $a_2 < b_2/\sqrt{2}$ ($a_3 < b_3/\sqrt{3}$) can be converted to such a corresponding structure using the position-space renormalization group technique and be subsequently resolved [158].

Due to the regularity, the probability that a site of this lattice is occupied by a node is uniform and can be obtained as $p_{occ} = \rho \cdot (a_d)^d$, where ρ is the given node density $\left[\mathrm{m}^{-\mathrm{d}}\right]$ and $(a_d)^d$ indicates the d-dimensional space occupied by a single site. Two occupied sites are interconnected only if either there exists a one-hop link or both of them share such links with another occupied site. The one-hop link exists solely when the sites are spaced at a distance less than b_d, while occupied sites separated by a large range (i.e., $\gg b_d$) can still establish a connection through a multihop channel. The occupied sites form clusters in the lattice. When the occupation probability p_{occ} is small, there is a sparse population of occupied sites, and clusters composed of small numbers of these sites predominate. However, by increasing p_{occ} more occupied sites become interconnected and thus become part of the same cluster. Eventually, for p_{occ} large enough the lattice experiences a critical phase transition: i.e., once p_{occ} reaches the percolation threshold p_c, an infinitely large percolating cluster of interconnected

sensor sites emerges for the first time [132]. For a finite-sized lattice this cluster is bounded by the lattice edges, thus also called the spanning cluster [8]. The percolation threshold value p_c depends merely on the lattice geometry and the 'lattice' node coverage: the number and organization of sites which are interconnected through a one-hop link. Note that due to an exceedingly complex structure of the percolating cluster in higher dimensions, it is cumbersome to determine the percolation threshold analytically except for the 1D and a few 2D lattices [56]. In this respect, the value p_c is typically estimated via a numerical experiment.

When $p_{occ} < p_c$, the nanonetwork is basically fragmented, i.e., composed of many disjoint clusters. Therefore, due to the finite size of a cluster, in which the source node is located, the probability to receive sensed data abruptly goes to zero with increasing source-to-sink separation. In this way, such a sensor network is unreliable and its modelling will not be treated in this chapter. Once $p_{occ} > p_c$, the nanonetwork becomes a dependable system since at any source-to-sink distance there always exists a multi-hop channel between two arbitrary chosen occupied sites when they belong to the percolating cluster. Hence, the probability $P(r,t)$ that a node at euclidean distance r from a source receives a message in a time interval t can be decomposed as:

$$P(r,t) = p(r,t) \cdot p_{cl}^2, \tag{5.1}$$

where p_{cl} is the probability a site belongs to the percolating cluster (the power of two is due to the fact that both source and sink nodes must be part of this cluster), whereas $p(r,t)$ is the probability a signal conveyed through such a cluster is received within the time interval t by the sink node at distance r from the source.

The probability $p(r,t)$ is determined based on the diffusion process defined on the sites of a percolating cluster. In particular, the time variable t is considered discrete. Note that the time unit is determined by the processing delay time in a sensor node Δt as it is much larger in general than the propagation time. In other words, at each time unit Δt a message is regarded to hop from its current positions to adjacent occupied sites, i.e., the signal propagates in a flooding manner. Hence, in time interval t the sensed signal propagating in a wave-front manner performs $h = \lfloor t/\Delta t \rfloor$ hops and the occupied nodes, which are eventually reached, form an aggregation. For the sake of understanding, such a particular aggregation for $h = 20$ hops in the 2D lattice of interest with $p_{occ} = 0.5$ is demonstrated in Fig.5.2. Since any aggregation is obviously inscribed by a circle (or a sphere for 3D) with its center coincided with a source site

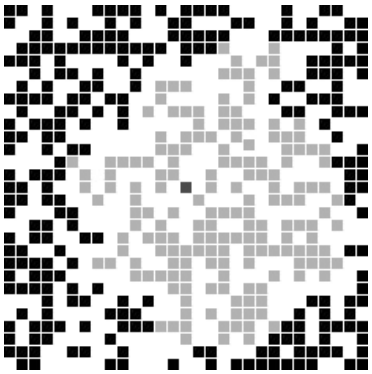

Figure 5.2: Aggregation of the occupied nodes for $h = 20$ in the 2D lattice characterized by $p_{occ} = 0.5$. The blank sites are drawn in white, the occupied sites are shown in black. The sites, which belong to the aggregation, are depicted in light grey, whilst the origin node is displayed in dark grey.

and radius of $h \cdot b$, the probability $p(r, t)$ is a non-zero value only when the number of hops h in time interval t exceeds the minimum hop count $n = \lceil r/b \rceil$ required to cover a distance r. To reach a sink node spaced at r in the minimum number of hops $h = n$ with probability 1, it is required to have no empty sites in a lattice (i.e., $p_{occ} = 1$) in order to transmit a signal between sites which are merely located along the source-to-sink direction; thus, the resulting multihop path is a straight line and its fractal degree is equal to 1. For a lattice with $p_{occ} < 1$, the presence of blank sites implies that the fractal degree of the source-to-sink multihop path exceeds 1 and, as a consequence, $h > n$ hops are needed to cover the distance r. Evidently, in the worst case scenario the probability $p(r, t)$ has to be related to the multihop path with the highest fractal degree, which demands the largest number of hops h for reaching the sink at distance r. Since such a 'longest' path is composed of the sites situated on the hull of a percolating cluster, statistical parameters of the source-to-sink path can directly be associated with the fractal properties of this cluster hull. As shown in [29, 148], the hop count of a path through a cluster hull is typically distributed according to the Gaussian law. Therefore, the multihop path of interest can be defined in terms of its mean and variance and the probability $p(r, t)$, regarded as the cumulative distribution function of its hop count, is expressed as:

$$p(r,t) = \frac{1}{\sigma\sqrt{2\pi}} \int_{n}^{h} \exp\left[\frac{(u-\mu)^2}{2\sigma^2}\right] du, \; h > n. \tag{5.2}$$

where μ and σ are the mean and variance corresponding to the hop count in the 'hull' multihop path. The parameter h is the actual number of hops made in time t, while the minimum number of hops needed to cover the source-to-sink distance r is equal to n. Hence, the probability $p(r,t)$ increases monotonically from zero ($h < n$) to 1 ($h \gg \mu$), where μ formally corresponds to the average number of hops to be made to reach the sink node through a 'hull' multihop path.

Since the hull of a percolating cluster does possess fractal properties [29], fractal principles demand that the parameters μ and σ, which describe the multihop path composed of sites appertaining to the cluster hull, are expressed via n as follows (this conclusion is also supported through calculations in [103]):

$$\begin{cases} \mu = c_\mu \cdot n^{d_\mu}, \\ \sigma = c_\sigma \cdot n^{d_\sigma}, \end{cases} \tag{5.3}$$

where c and d are respectively the effective amplitude and the fractal (or Hausdorff) dimension of the Gaussian parameters μ and σ. Hence, Eq.(5.2) for $p(r,t)$ can be rewritten using Eq.(5.3) as:

$$\begin{aligned} p(r,t) = {} & \frac{1}{c_\sigma n^{d_\sigma}\sqrt{2\pi}} \times \\ & \times \int_n^h \exp\left[\frac{\left(u - c_\mu n^{d_\mu}\right)^2}{2c_\sigma^2 n^{2d_\sigma}}\right] du, \ h > n. \end{aligned} \tag{5.4}$$

As can be seen in Eq.(5.4), the probability $p(r,t)$ can be determined once the effective amplitudes c_μ, c_σ and the fractal dimensions d_μ, d_σ are known. Such fractal parameters merely depend on the lattice geometry and are estimated by means of numerical experiments (the modelling is simple and shown below). It is also notable that once these parameters are known, the probability $p(r,t)$ can be assessed for any distance r without extra numerical simulations as the fractal parameters are independent of the source-to-sink separation. This is an essential advantage of the proposed model since, unlike other simulation solutions, it can treat a very large-scale sensor network in a simple way.

5.2 Connectivity and Hop Count in Nanonetworks

The percolation threshold p_c and the size of a percolating cluster are numerically explored as both coefficients are of particular interest: the value p_c distinguishes per-

colating from fragmented systems, while its size is directly related to the probability p_{cl} that an occupied site belongs to the percolating cluster. To determine the fractal parameters related to the cluster hull, the hop count of a multihop path only composed of sites belonging to the hull is investigated as well.

Percolation thresholds of 2-dimensional and 3-dimensional lattices of interest ($p_{c(2)}$ and $p_{c(3)}$, respectively) can be initially predicted by using a Bethe lattice, also known as a Cayley tree. For the Bethe lattice, there is a central/origin site with m bonds. Each bond ends in another site from which m bonds stretch out again in ways that $m-1$ bonds lead to new sites whereas one bond is in connection with the source site. The same stretching algorithm is continued repeatedly until we reach up to the surface of the lattice. In this manner, starting from any interior site of the Bethe lattice one can forward to $m-1$ other directions besides each starting direction. As the branching process has stopped at the surface of the lattice, only one bond connects the surface site with an interior one. The Bethe structure has no closed loops or cycles: never stepping back we might move in new directions solely. Therefore, in order to provide a connection between the sites spaced by a distance of l, all the $(l-1)$ intermediate sites also have to be occupied by sensor nodes. Since the probability of a site to be occupied is p_{occ} and the l - layer of the Bethe lattice contains $m(m-1)^{l-1}$ sites, the correlation length for such a lattice is expressed as follows: $g(l) = m((m-1)p_{occ})^l/(m-1)$ [56]. For $l \to \infty$ this function exponentially converges to zero when $p_{occ}(m-1) < 1$ and diverges otherwise. Consequently, the percolation threshold of the Bethe lattice is $p_c = 1/(m-1)$ as an infinite cluster may appear in such a structure only when $p_{occ} \geq 1/(m-1)$. Since this expression is derived for the structure without closed loops, it gives a smaller value of percolation threshold than is obtained in case of a real lattice, the structure of which has loops. Thereby, we can state that the percolation threshold of a 2-dimensional lattice exceeds the value of $p_{c(2)} > 1/(8-1) \approx 0,143$, whereas the percolation threshold of the the 3-dimensional regular structure has to overcome the value of $p_{c(3)} > 1/(27-1) \approx 0,04$.

In order to determine upper limits of the percolation thresholds $p_{c(2)}$ and $p_{c(3)}$, we use the position-space renormalization group technique: i.e., a small cell of lattice sites is replaced by a single super-site with a certain rule governing whether the new super-site would be active or not. It is known that only at the percolation threshold, when scale invariance is viable, the occupation probability of super-sites in the new renormalized super-lattice p'_{occ} is equal to the occupation probability of sites in the original lattice p_{occ} (i.e., $p_c = p_{occ} = p'_{occ}$). In other words, for the lattice being

exactly at the percolation threshold it will be impossible to detect modifications in the system appearance as the lattice scale is changed. In turn, for a lattice structure with sites occupied with the probability $p_{occ} \neq p_c$ its properties will move with varying the lattice dimension N: the trajectory produced by the repeated renormalization to such a system will lead to 0 when $p_{occ} \leq p_c$, whereas for $p_{occ} \geq p_c$ this trajectory will move to 1. Based on the latter fact, by clustering sites of the 2-dimensional lattice in basic cells of 5×5 sites, we have derived and determined the upper bound for percolation threshold $p_{c(2)}$ to be equal to $p_{c(2)}^{upper} = 0,471$. In perfect analogy, by grouping sites of the 3-dimensional lattice into $2 \times 2 \times 2$ cells (with 8 sites in each cell), the solution for the upper limit of the percolation threshold $p_{c(3)}$ is found to be $p_{c(3)}^{upper} = 0,228$. Finally, the rigorously obtained intervals for the percolation thresholds of both the selected lattices ($0,143 < p_{c(2)} < 0,471$ and $0,04 < p_{c(3)} < 0,228$) are further used for verification of numerically computed results.

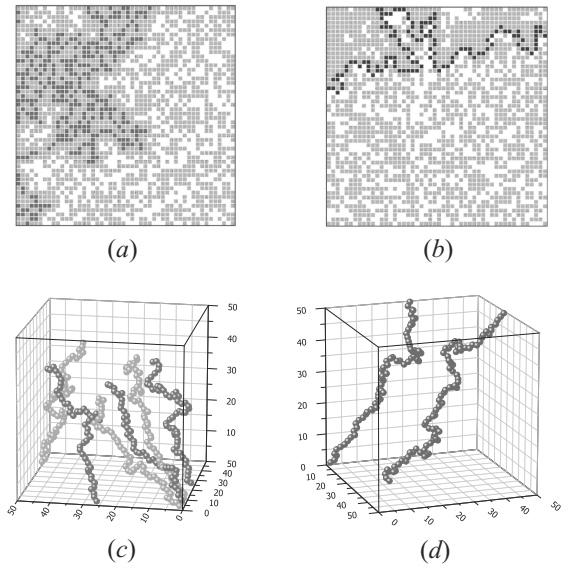

Figure 5.3: Different phases of the percolation process: (a) the non-connected planar network: $P_{ooc} < P_{c(2)}$, (b) the 2-dimensional network is connected: $P_{ooc} > P_{c(2)}$, (c) the disconnected system in the 3-D space: $P_{ooc} < P_{c(3)}$, (d) the 3-dimensional network carries the connectivity: $P_{ooc} > P_{c(3)}$.

To estimate these parameters p_c and p_{cl}, a set of Monte-Carlo simulations are carried out. Due to computer limitations, the largest source-to-sink distance of a 2D lattice being analysed is 2000 sites, whereas that of a 3D system is bounded by 500

sites. To get accurate results, each set of numerical experiments requires $Q = 3000$ iterations. Per simulation a signal is only transmitted to the adjacent occupied sites, which are found based on the left-hand maze rule in order to keep its propagation along the cluster hull (by keeping the left hand in contact with one wall of a maze the player is guaranteed not to get lost and will reach a different exit if there is one). Once there exists a multihop path between the source site and sink spaced at distance n, the outcome is assumed to be successful and the hop count h of this path is stored. After applying this procedure Q times, the value p_c is determined as the ratio between the number of successful outcomes and the total number of iterations, while the mean value μ and the standard deviation σ are eventually determined through using their common representations. For example, the connected and non-connected lattices of dimension $N = 50$ in both 2-dimensional and 3-dimensional environments are demonstrated in Fig.5.3.

The percolation threshold of a 2D structure is equal to $p_{c(2)} = 0.4073 \pm 0.0007$. This result is in agreement with the data presented in [122]. The percolation threshold of a 3D lattice is significantly less than $p_{c(2)}$ and determined to be $p_{c(3)} = 0.0977 \pm 0008$. The further estimations are performed under the assumption that the occupation probability p_{occ} exceeds the percolation threshold to ensure that a percolating cluster arises.

The probability p_{cl} that a site belongs to the percolating cluster directly corresponds to the ratio of the number of sites in this cluster and the total number of occupied sites. The size of a percolating cluster is determined from numerical simulations on a square and cubic lattice, whereas the amount of occupied sites is consequently expressed as $p_{occ} \cdot n^d$, where d is the lattice dimension. To understand the behaviour of the probability p_{cl}, the size of a percolating cluster is in particular analysed for different values of p_{occ} and lattice dimensions. For a 2D and 3D structure, the probability that the starting node belongs to the percolating cluster is found to be reasonably less than 1 in the vicinity of the percolation threshold p_c (Fig.5.5). Nonetheless, for both lattices of interest, the value of p_{cl} rapidly tends to 1 once the occupation probability p_{occ} increases. In other words, with raising p_{occ} the level of disjoint clustering in a lattice considerably decreases as more and more occupied sites become part of the percolating cluster. Hence, although p_{cl} never strictly equals 1 as long as some randomness occurs in a nanonetwork ($p_{occ} < 1$), for practical applications the probability p_{cl} can be supposed to be about 1 since a node density would be chosen such that p_{occ} is reasonably larger than the respective p_c for ensuring network

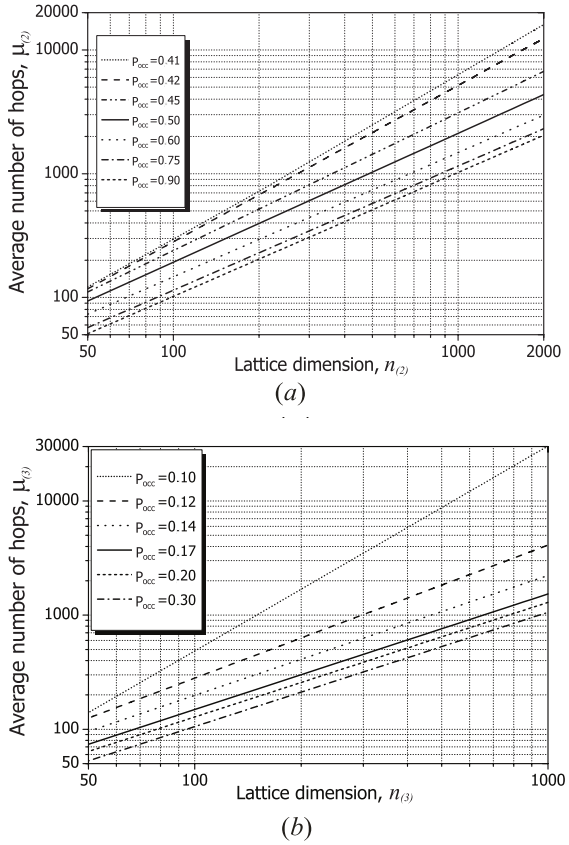

Figure 5.4: The dependence of the average hop count μ on the lattice dimension under different p_{occ} for the (a) 2D and (b) 3D structures.

connectivity. Note that we however rely on the actual values of p_{cl} to obtain accurate results here.

For any lattice, the fractal dimensions d_μ and d_σ are found to reach their maxima when the probability p_{occ} is near the percolation threshold p_c and become minimum when p_{occ} tends to 1. The reason for such a behaviour is that by increasing the probability p_{occ}, we decrease the degree of randomness in a network and, consequently, the mean number of hops μ moves to n as well as the value of σ decreases to zero. To demonstrate that the fractal dimension is the prime characteristic which affects the rate of increase of μ and σ with increasing the value n, the fractal parameters for both 2D and 3D lattices are obtained by fitting the mean and variance of the hop count

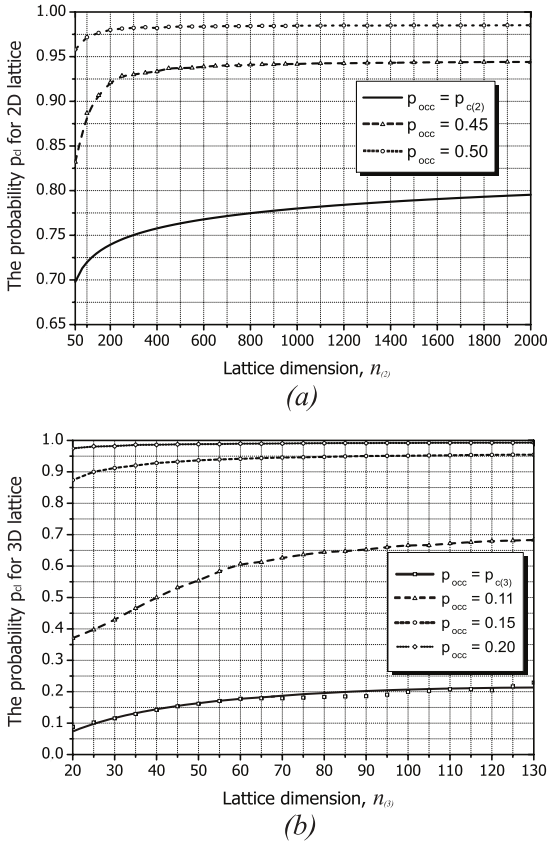

Figure 5.5: The probability that a site belongs to the percolating cluster for different p_{occ} for the (a) 2D and (b) 3D lattices of interest.

h calculated for different n to Eq.(5.3). These results are shown in Fig.5.4 (only for μ), whereas the estimated parameters are indicated in Table 5.1. Also note that such a fractal behaviour is not seen for small hop distances n since the percolation theory requires a great number of entities to become applicable. In particular, according to the numerical experiments it is suggested to keep n larger than 50 to be able to use this approach.

The Kolmogorov-Smirnov criterion is applied to test the suitability of the Gaussian distribution to the random distributions of the hop counts h_2 and h_3 for the 2D and 3D systems, respectively. For the sake of curiosity, other major statistical hypotheses are considered as well. In particular, the lognormal distribution fits best both the

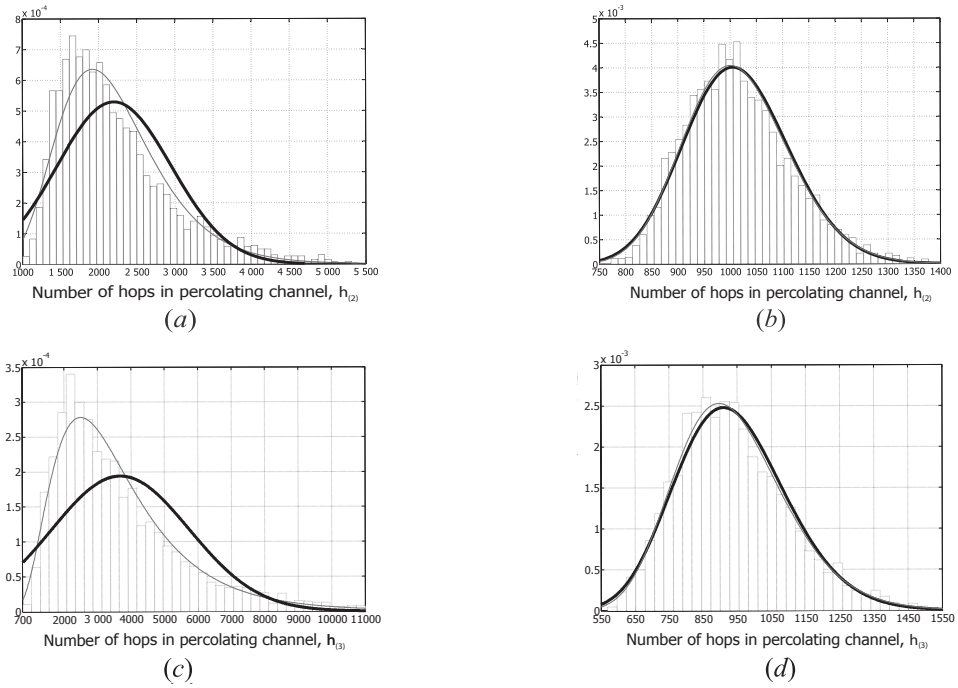

Figure 5.6: The random distribution histograms are plotted for the 2D lattice of dimension $N = 500$ and occupation probabilities (a) $p_{occ(2)} = 0,42$ and (b) $p_{occ(2)} = 0,50$ as well as for the 3D lattice of dimension $N = 300$ and the occupation probabilities (c) $p_{occ(3)} = 0,10$ and (d) $p_{occ(3)} = 0,14$. A Gaussian distribution approximation is depicted in bold whereas a line following a lognormal distribution is of standard thickness.

random distributions of the hop counts. Meanwhile, it has been found that the normal distribution fits well to the calculated random data sets and can fairly well describe the arbitrary behaviour of the hop counts h_2 and h_3 only if p_{occ} is more than 0.5 and 0.14, respectively (Fig.5.6). Nonetheless, the assumption of normally distributed parameter $p(r, t)$ in Eq.5.4 is valid and thus the model still furnishes proper results for the very broad spectrum of p_{occ}.

To better understand the actual impact of randomness on the nanonetwork, a 'tortuosity' level of the multihop path along the hull of the percolating cluster is introduced as $\Delta = \mu/n$ and analysed as a function of the probability p_{occ} and the hop distance n (Fig.5.7). As can be seen, the larger the distance n and the smaller the probability p_{occ}, the more convoluted is the hop count of the path between a source and sink node. Meanwhile, for large values of p_{occ}, the randomness impact significantly

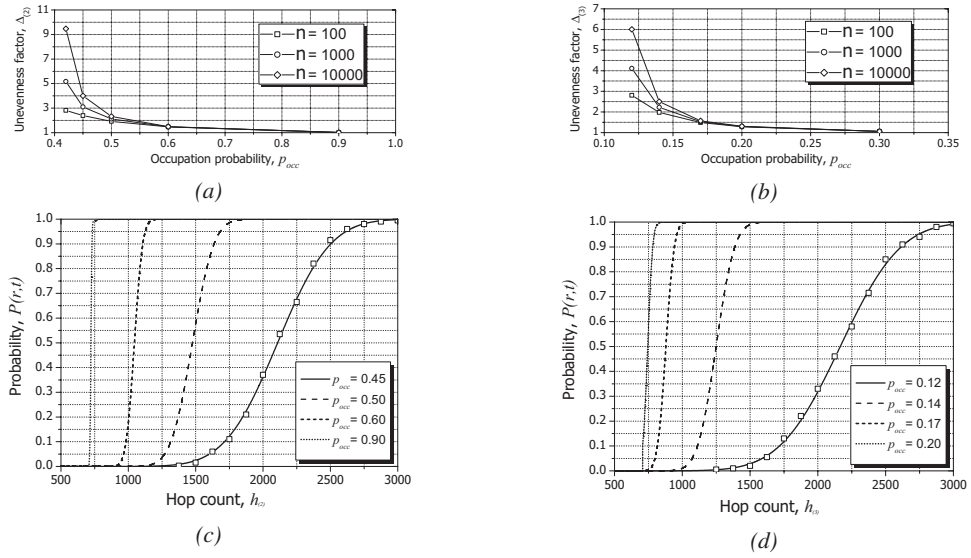

Figure 5.7: The tortuosity parameter Δ and the probability $P(r,t)$ for 2D *(a,c)* and 3D *(b,d)* lattices. For figures *(c,d)*, the source-to-sink separation is $n = 700$.

decreases as Δ is close to 1 and only slightly varies with changing the source-to-sink distance n. In other words, when p_{occ} is in the vicinity of the percolation threshold, the probability $P(r,t)$ becomes negligible since (a) the value of p_{cl} is small and (b) for a large source-to-sink separation r, the probability $p(r,t)$ is also small due to the high

Table 5.1: Fractal characteristics of 2D and 3D lattice structures

$p_{occ(2)}$	0,41	0,42	0,45	0,50	0,60	0,90
$c_{\mu(2)}$	0,5736	0,8393	1,4337	1,5947	1,4389	1,0169
$d_{\mu(2)}$	1,3469	1,2631	1,1116	1,0410	1,0041	1,0007
$c_{\sigma(2)}$	0,1252	0,2560	1,1821	1,9558	1,6301	0,2291
$d_{\sigma(2)}$	1,3921	1,2470	0,8479	0,6343	0,5178	0,5022

$p_{occ(3)}$	0,10	0,12	0,14	0,17	0,20	0,30
$c_{\mu(3)}$	0,1245	1,3137	1,5666	1,4140	1,2569	1,0556
$d_{\mu(3)}$	1,7956	1,1650	1,0508	1,0116	1,0041	1,0004
$c_{\sigma(3)}$	0,0153	1,7925	2,7176	1,9873	1,1938	0,3684
$d_{\sigma(3)}$	2,0603	0,8296	0,5788	0,5038	0,5033	0,5025

'tortuosity' of the multihop path of interest. Hence, a nanonetwork with p_{occ} being about p_c seems to be out of interest from a practical perspective. Once p_{occ} reasonably exceeds the percolation threshold, the probability $P(r,t)$ is mainly determined by the parameter $p(r,t)$ since the value p_{cl} is close to 1. For 2D and 3D lattices, the probability $P(r,t)$ is calculated and shown in Fig.5.7c and Fig.5.7d. As can be seen, the initial value of p_{occ} considerably affects such a probability: in particular, the value of $P(r,t)$ increases pretty fast by slightly increasing p_{occ}. From this point it follows that to meet a common criterion of nanonetwork-based applications, i.e., to receive a signal with a high probability, it is better to add extra sensors and increase the value p_{occ} rather than expand the time interval t. Another fact to be emphasised is that the dimensionality significantly affects the characteristics of a percolating cluster: e.g., $d_{\mu(3)}$ decreases much faster than $d_{\mu(2)}$ with increasing the occupational probability due to having an extra degree of freedom in 3D networks. Note also that the Gaussian distribution of multihop path, which is derived from the results of Monte-Carlo simulations, is depicted in markers in Fig.5.7c and Fig.5.7d and correspond to $p_{occ(2)} = 0,45$ and $p_{occ(3)} = 0,12$, respectively.

Eventually, once the parameters r and t are specified, the lowest density of nodes (i.e., the minimum value of p_{occ}) needed to keep the probability $P(r,t)$ above a given threshold can be determined by using the proposed model. Alternatively, for a given node density and time interval t, the distance r in the network can be obtained so that the probability $P(r,t)$ still exceeds some specified level. Since the probability $P(r,t)$ can basically be considered as a good indicator for the performance of a large-scale sensor network, the proposed model is relevant for handling such a system. The source-to-sink path with the maximum number of hops, which can be rigorously defined through the fractal characteristics of the hull of the percolating cluster, is also important from a communication perspective as its modelling helps to avoid inter-message interference in the nanonetwork (i.e., the source node must send more than one message to complete its report). However, the proposed model is not limited to such predictions on communication properties of a nanonetwork but also can be used to effectively position a source node in this network.

5.3 Source-positioning Method

Once a source node in the nanonetwork triggers, its position is assumed to be detectable only when this node is located at one of the network borders (i.e., an end-user

can only get access and treat such 'outward' sensor nodes). If a message originates from one of the 'inward' nodes, there is no direct way to localise this node as it is inaccessible from an end-user point of view. Nonetheless, if such an 'inward' source belongs to the percolating cluster, the originating message spreads throughout the nanonetwork and is only terminated by the lattice borders. By using the data collected at these borders and applying the developed model of hop progress in the nanonetwork, the position of the 'inward' source node can be reliably estimated.

The positioning algorithm is in particular described for the 3D nanonetwork. For the sake of simplicity, it is assumed that this area can be represented by a regular lattice of $N_i \times N_j \times N_k$. Once the 'inward' source node with coordinates (i, j, k) belongs to the percolating cluster, a signal originating from it and spreading within this cluster reaches all the lattice borders after all (Fig.5.8). Hereinafter, let us focus on the determination of parameter i as the values of j and k can be estimated in a similar manner. Evidently, the absolute times of last arriving signals at the left and right borders, denoted as t_l and t_r, are simply measured (without loss of generality, we may also suppose that $t_l \geqslant t_r$). As discussed, these time values reflect the product of Δt and the hop count of the corresponding peripheral path. In this way, since hop counts h_l and h_r are normally distributed parameters, the delay time difference $\Delta t_i = t_l - t_r$ is also distributed by the Gaussian law and thus its mean value $\mu(\Delta t_i)$

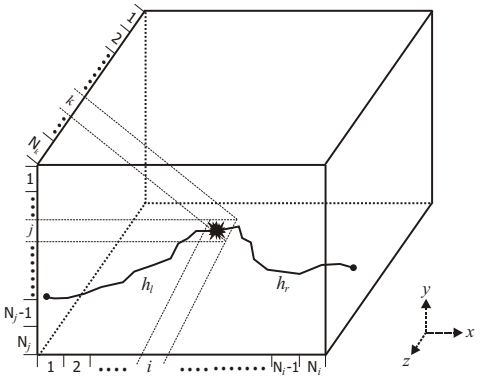

Figure 5.8: The sketch of 'hull' multihop paths to the left and right (opposite) borders in a 3D nanonetwork. The network is simplified by a lattice of dimension $N_i \times N_j \times N_k$ and a source node is situated at the (i, j, k) site, respectively.

and the standard deviation $\sigma(\Delta t_i)$ can be expressed as follows:

$$\begin{aligned}\mu(\Delta t_i) = \ & \mu(t_l) - \mu(t_r) = \Delta t[\mu(h_l) - \mu(h_r)] = \\ & = \Delta t \cdot c_{\mu(3)}[i^{d_{\mu(3)}} - (N_i - i)^{d_{\mu(3)}}];\end{aligned} \tag{5.5}$$

$$\begin{aligned}\sigma(\Delta t_i) = & \sqrt{\sigma(t_l)^2 + \sigma(t_r)^2} = \\ & = \Delta t \cdot c_{\sigma(3)} \sqrt{i^{2d_{\sigma(3)}} + (N_i - i)^{2d_{\sigma(3)}}},\end{aligned} \tag{5.6}$$

where effective amplitudes $c_{\mu(3)}$,$c_{\sigma(3)}$ and the fractal dimensions $d_{\mu(3)}$,$d_{\sigma(3)}$ are obtained as described in Section 5.2. In this context, the coordinate i of the source node can be calculated by measuring the delay times t_l and t_r and solving Eq.(5.5) with $\mu(\Delta t_i) = t_l - t_r$. Other coordinates j and k can be determined in a similar fashion by assessing the delay times Δt_j and Δt_k between the respective lattice boundaries.

From Eq.5.6 by taking $\partial\{\sigma(\Delta t_i)\}/\partial i = 0$, it follows that the maximum standard deviation *in sites* for the relative time Δt_i is given as follows (this derivation is thoroughly discussed in [103]):

$$\sigma_{max}(\Delta t_i) = \frac{c_{\sigma(3)} \cdot N_i^{d_{\sigma(3)}}}{c_{\mu(3)} \cdot N_i^{d_{\mu(3)}}} \cdot N_i. \tag{5.7}$$

The maximum standard deviation for Δt_j and Δt_k are obtained using the same equation but substituting N_i with N_j and N_k, respectively. In this regard, the accuracy of the proposed positioning method can be numerically tested by comparing a confidence region of signal origin to the entire lattice area. The confidence region is estimated by using the maximum standard deviation of each of three parameters Δt_i, Δt_j, Δt_k and the normal distribution quantile function (as all these parameters have the Gaussian distribution) and described as:

$$\begin{aligned}CR_{(3)} = & Z_p^3 \cdot \frac{c_{\sigma(3)} \cdot N_i^{d_{\sigma(3)}}}{c_{\mu(3)} \cdot N_i^{d_{\mu(3)}}} \cdot \frac{c_{\sigma(3)} \cdot N_j^{d_{\sigma(3)}}}{c_{\mu(3)} \cdot N_j^{d_{\mu(3)}}} \times \\ & \times \frac{c_{\sigma(3)} \cdot N_k^{d_{\sigma(3)}}}{c_{\mu(3)} \cdot N_k^{d_{\mu(3)}}} \cdot N_i \cdot N_j \cdot N_k,\end{aligned} \tag{5.8}$$

where Z_p is the normal distribution quantile for a known confidence level p. Since the total number of sites in the lattice is $N_i \cdot N_j \cdot N_k$, the ratio between the confidence region and the entire lattice area is simplified from Eq.5.8 as follows:

$$\Delta_{(3)} = Z_p^3 \cdot \frac{c_{\sigma(3)} \cdot N_i^{d_{\sigma(3)}}}{c_{\mu(3)} \cdot N_i^{d_{\mu(3)}}} \cdot \frac{c_{\sigma(3)} \cdot N_j^{d_{\sigma(3)}}}{c_{\mu(3)} \cdot N_j^{d_{\mu(3)}}} \cdot \frac{c_{\sigma(3)} \cdot N_k^{d_{\sigma(3)}}}{c_{\mu(3)} \cdot N_k^{d_{\mu(3)}}}. \tag{5.9}$$

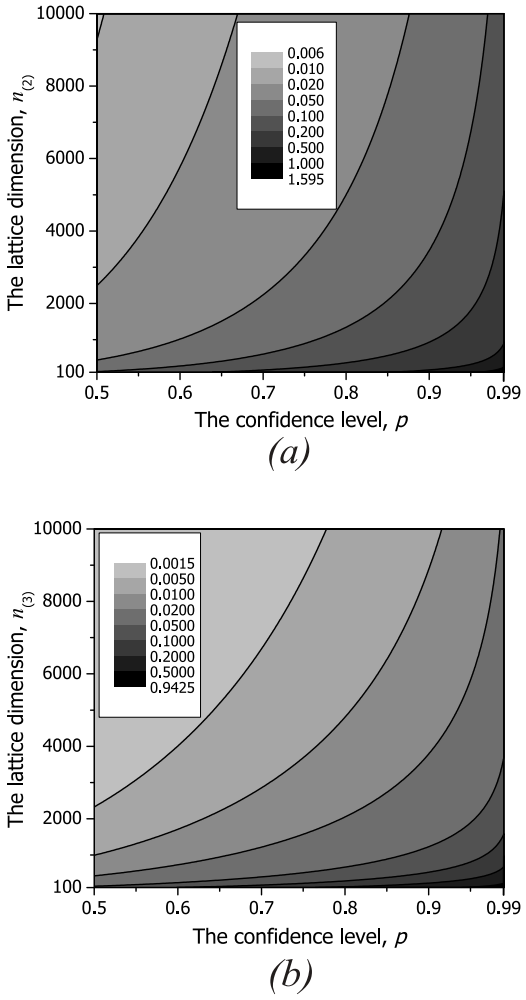

Figure 5.9: The accuracy of source localization (i.e., the ratio between the confidence area and the entire lattice area) as a function of the lattice dimension $n_{(2)}$ and the confidence level p when *(a)* $p_{occ(2)} = 0.45$ and *(b)* $p_{occ(2)} = 0.5$ from [102].

Evidently, the accuracy of the positioning method for a 2D nanonetwork can be treated in the same way as above. The ratio $\Delta_{(2)}$ is thus reduced from Eq.5.9 and has the squared Z_p and no term containing N_k due to $d = 2$.

The analysis of the results suggests that the proposed positioning method is limited to cases when the fractal dimension $d_{\sigma(2,3)}$ is smaller than the value of $d_{\mu(2,3)}$.

Otherwise, the algorithm becomes inaccurate and unstable as the value of $\Delta_{(2,3)}$ would diverge with increasing lattice sizes. This requirement puts a limit on the occupation probability, such as according to Table 5.1 for the lattices of interest $p_{occ(2)} > 0.42$ and $p_{occ(3)} > 0.11$. Note that due to the fast decrease of $d_{\sigma(2)}$ with increasing occupational probability, the algorithm accuracy noticeably improves once $p_{occ(2)}$ is moderately larger than the percolation threshold (see Fig.5.9). For 3D nanonetworks, this accuracy refinement is even more substantial due to an extra dimensionality.

5.4 Conclusions

Two fundamental problems, connectivity and data transfer, of random nanonetworks have been addressed from the discrete percolation perspective. Firstly, the total number of sensor nodes which have to be deployed within a certain area so that the nanonetwork will be physically connected with a probability greater or equal to some prespecified value has been estimated. In this respect, after analysing both the selected lattice structures analytically the percolation thresholds $p_{c(2)}$ and $p_{c(3)}$ are precisely obtained through exhaustive numerical Monte Carlo simulations: the critical percolation probability of a 2-dimensional lattice structure is $p_{c(2)} = 0,40725 \pm 0,0003$, whereas the percolation threshold of a lattice in the 3-dimensional space is equal to $p_{c(3)} = 0,097 \pm 0,0008$.

Secondly, we propose a novel method to obtain in a simple manner the worst case number of hops of the source-to-sink path in a very large-scale network with an arbitrary network complexity and unknown locations of the wireless nodes. The model assumes that the network topology can be represented by a regular lattice, where each lattice site is occupied by a sensor node with occupation probability p_{occ}. The value p_{occ} should exceed the percolation threshold p_c for the emergence of a percolating cluster. Then, by relating statistical parameters (such as mean and variance) of the hop count of the source-to-sink path to the fractal parameters of the percolating cluster, the probability $P(r,t)$ indicating a successful arrival of the sensed signal to a sink node spaced at distance r from a source within a specified time t, has been mathematically expressed. The simple approach to estimate fractal parameters of the percolating cluster based on the left-hand maze rule has been used.

The numerical analysis has been performed for 2D and 3D conceptual lattices to better understand the impact of randomness on a large-scale network. It has been shown that the network with p_{occ} being close to p_c is an unreliable system from an

application perspective. Meanwhile, it has also been demonstrated that the occupational probability p_{occ} greatly affects the level of randomness in the network: i.e., the value $P(r,t)$ increases pretty fast by slightly increasing p_{occ} beyond p_c. From this, the practical conclusion can be drawn that it is more effective to increase $P(r,t)$ through adding extra sensors rather than by raising the time t. Increasing $P(r,t)$ by increasing the number of sensors is much faster in a 3D network than that in a 2D network due to having an extra degree of freedom. The inverse problem, i.e., the determination of the occupational probability needed to maintain a required $P(r,t)$, can also be solved using the developed model. Note that although the model's applicability is currently limited by nodes radiating omnidirectionally, the approach shown in the chapter implies that the model can be expanded to nodes with directional coverage once the fractal parameters in the respective lattice structure are estimated.

An effective source-positioning method, which can localise a source node in a large-scale network with arbitrary positions of nodes and without retrieving the network topology, has been proposed based on the developed connectivity model. This localization method, which can be applied in very large scale networks, exploits the fractal nature of the percolating cluster. The accuracy analysis of the method has demonstrated its high performance for the very broad spectrum of values of the occupation probability p_{occ}. As the counterpart approaches are impartially restricted to positioning in very large-scale networks, this method is the first of its kind to localise a source in these networks and thus is useful for the design of such networks in the near future.

Chapter 6

Conclusions

6.1 Major Results and Novelties

In this thesis, the research challenges described in the Introduction chapter have been considered and solved:

[1] *Feasibility analysis on the RF link between nano-scale devices.* To predict the energy level available in the nanomachine, we have completed a survey on promising battery-driven solutions and potential power scavenging technologies. Based on the developed integrated model, which includes the fundamental principles of the electromagnetic and communication theories and statistics, we have computed a minimum output power, which is required to enable the connection between two nanoscale devices by means of far-field RF waves. By relating these calculated results with the capabilities of up-to-date power sources, the minimum device size (around a few tens of microns), under which RF communication could be established with the current state-of-the-art in power accumulation, has been determined. The resulting output stipulates us to develop both antenna-based and channel-based solutions to bridge the gap between the communication demands of a nanomachine and its energy budget provided by a promising power source and, as a consequence, enable the wireless link between truly nanoscale devices.

The results are published in:

D. Penkin, G. Janssen, and A. Yarovoy. "Feasibility analysis of peer-to-

peer microwave communications between self-powered miniature electronic devices." In Antennas and Propagation (EUCAP), Proceedings of the 5th European Conference on, pp. 122-125. IEEE, 2011.

[2] *Electromagnetic modelling of nano-scale objects from an atomic perspective.* We have developed and implemented a novel model capable of evaluating equivalent electromagnetic properties of small-atom particles at wavelengths up to 1 nm. This approach includes a closed-form solution which is derived by considering each atom as a single scatterer and by using the integral equation formalism. Based on the developed model and assuming that a fullerene is represented as a sphere with a certain 'effective' radius r_f owing to its ball-like atomic constitution, we have determined the electromagnetic properties of commonly used fullerene derivatives which has never been done before. Furthermore, by using the developed model, we have studied the directional capabilities of a fullerene-based Yagi-Uda-type antenna (i.e., the parasitic elements are represented by different fullerenes) and demonstrated that such an antenna with a few director elements generates a highly directional radiation only at X-ray frequencies. As the fullerenes are the smallest particles that can be handled by current technology, the obtained result provides a fundamental understanding on the maximum frequency for which it is still possible to propose a directional antenna concept.

The results are submitted to:

D. Penkin, G. Janssen, and A. Yarovoy. "Electromagnetic properties of fullerene derivatives." Nanoscale Research Letters, 2015.

D. Penkin, G. Janssen, and A. Yarovoy. "Investigation of a Fullerene-based Yagi-Uda-type Antenna." IEEE Antennas and Wireless Propagation Letters, 2015.

[3] *Impact of a surface-wave supporting interface.* We have developed a novel approach to describe the impact of a plain, surface-wave supporting substrate on (1) the wireless propagation link between nanomachines as well as (2) the performance of their electrically small antennas. The employment of the surface impedance concept in the developed approach expands the applicability spectrum to different media on the one hand and leads to computational simplicity on the another hand. A fair agreement between the results obtained via this approach and those acquired through the full-wave analysis in limiting cases has endorsed the model's formalism. Using the developed model, the impact

of the plain interface between free space and a medium with a highly inductive impedance has been analysed. Our simulations demonstrated that this interface could significantly raise the link budget due to the fact that the electrically small devices benefit from the strong surface wave contribution, while the interface brings no extra mismatch of the nanomachine's antenna. The outcome of the performed analysis is essential from a practical perspective as it offers new opportunities in RF-based communication between electrically small devices: i.e., more functional nanonetworks might be implemented thanks to the strong link gain provoked by a surface-wave supporting interface.

The results are published in:

D. Penkin, G. Janssen, and A. Yarovoy. "Impact of a half-space interface on the wireless link between tiny sensor nodes." Radio Science, 49(9), pp.798-811, 2014.

D. Penkin, G. Janssen, and A. Yarovoy. "Surface impedance model for nano-scale device communications over an interface." In Communications and Vehicular Technology in the Benelux (SCVT), 19th Symposium on, pp. 1-5. IEEE, 2012.

[4] *Signal propagation throughout a nanonetwork.* As existing solutions for macro-scale sensor networks are not applicable to nanonetworks, a pioneering model describing the message propagation in a dense, large-scale network with an arbitrary node distribution has been developed in this thesis. Firstly, based on the percolation theory and by simplifying the nanonetwork topology to a regular lattice, an approach has been formulated in order to determine the minimal node density required to ensure a sufficient nanonetwork connectivity. Secondly, once the nanonetwork has appropriately been connected (i.e., a percolating cluster emerges), we have determined the probability $P(r, t)$ of successful reception of the message by a sink node spaced at distance r from a source within a given time t, for the first time. By means of the proposed model, we have furthermore developed a novel source-positioning method, which can localise a source node in the nanonetwork without retrieving its topology (i.e., no energy is consumed to perform the prerequisite self-organization stage at which sensor nodes scout their surroundings). By relying on the fractal nature of the percolating cluster, this method has been demonstrated through numerical calculations to exhibit an effective localisation of a source node in very large-scale networks. Since al-

ternative positioning algorithms are impartially restricted in localising an origin in the nanonetwork, this method is the first of its kind to pinpoint a source node in such a large-scale system in a reliable manner.

The results are published in:

D. Penkin, G. Janssen, and A. Yarovoy. "Source positioning in a large-scale tiny-sensor network of arbitrary topology." EURASIP Journal on Advances in Signal Processing, no. 1, pp. 1-11, 2014.

D. Penkin, G. Janssen, and A. Yarovoy. "Source node location estimation in large-scale wireless sensor networks." In Microwave Conference (EuMC), 42nd European, pp. 333-336. IEEE, 2012.

D. Penkin, G. Janssen, and A. Yarovoy. "A study on communication aspects of two-dimensional large-scale wireless sensor networks using percolation principles." In Communications and Vehicular Technology in the Benelux (SCVT), 17th Symposium on, pp. 1-6. IEEE, 2010.

In edition to the major challenges, the following extra problem directly related to the communication between nanoscale devices has been studied:

- *Antenna concept for RF nanomachine.* In Appendix A, we have proposed and demonstrated a novel, high-efficiency and electrically small antenna design (with a physical size equal to one hundredth of the wavelength) in order to relax power consumption demands of nanomachines (i.e., the antenna exhibits a power gain of 0 dB, which is close to the maximum gain of the half-wave resonant dipole). The developed antenna has a dipole-like structure and represents itself as a metal rod coated with a thin highly magnetic layer. Such an 'encapsulated antenna' concept possesses a number of benefits, such as the simple architecture, low directivity radiation pattern and small operational bandwidth (thus, the antenna could operate as a filter circuit). Unlike other antenna alternatives, the proposed antenna moreover has a sufficiently large interior hollow space usable to house other delicate payload components and preserve them by its metal body.

  The results are published in:

  D. Penkin, G. Janssen, and A. Yarovoy. "The effective electrically small encapsulated antenna applied for communication between self-powered miniature devices." In Antennas and Propagation (EUCAP), Proceedings of the 5th European Conference on, pp. 3801-3803. IEEE, 2011.

6.2 Recommendations for Future Work

The work presented in this thesis can be continued in the direction of further improvement of the wireless link between nanomachines as well as the networking-level communication aspects:

- The proposed design of an encapsulated antenna, in its present form, is characterised by a large Q-factor. In this respect, the communication with such miniature antennas will be greatly affected by the tolerance and temperature stability. The approaches with the aim to reduce the antenna sensitivity against these factors could contribute to the practicability of the proposed antenna concept.

- The formal model, which has been developed and used to determine the complex permittivity of fullerene derivatives, can also be employed to explore the dielectric properties of more complex nanoscale objects, such as different graphene-based structures and single-wall and multi-wall carbon nanotubes.

- The directional capabilities of the fullerene-based Yagi-Uda-type antenna with several director elements are shown to be constrained at X-ray frequencies. Extended studies and new optimisation techniques might help to develop a high directional antenna operating at the optical band by either considering larger nanoscale objects as directors or increasing the number of fullerene directors (this is very attractive and useful from an application perspective).

- The developed nanochannel propagation model, suitable to calculate the impact of surface-wave supporting interface on the communication link between nanomachines, contains the Sommerfeld-type integral equation which has an analytical solution only if the receiver is in the far-field region of the transmitting antenna. As this substantially reduces computational time and resources, it is relevant to develop the mathematical framework, which can formally treat the Sommerfeld-type integral even when the receiving antenna is placed in the near field region of the transmitting one. Moreover, the model can be broadened by exploring the influence of this interface when both antennas possess random orientation/polarisation (i.e., modelling an arbitrary distribution of nodes in the nanonetwork).

- The model to determine signal propagation in a nanonetwork has been devel-

oped under the assumptions that the nodes possess omnidirectional coverage and the network topology can be mapped to a very large-scale lattice structure (i.e., the influence of system borders is neglected). Firstly, the proposed model can be expanded to nodes with a certain directional coverage by estimating the fractal parameters of the respective lattice structure by means of numerical simulations. Secondly, the model's applicability can be broadened by investigating the impact of actual borders on signal spreading within the percolating cluster in medium-scale and finite-sized lattices. Since these borders can exhibit reflection or absorption properties, it is also of interest to model each of these influences.

- The cooperative routing effect, which comes from an arbitrary set of synchronized nanomachines and which offers larger/irregular hops within the nanonetwork [73], may potentially take place and affect the hop count of signal propagation. Consideration of such a routing effect and its influence can add further weight to the developed networking-level model.

6.3 Research Impact

The results obtained in this thesis cover fundamental problems of nanonetworks at both the physical layer and the networking layer. They demonstrate the potential and feasibility of nanonetworking concepts and thus represent an important step forward in the development of nanonetworks with superior fine-grained sensing capabilities. The research presented in this thesis resulted in 2 accepted journal articles (Radio Science and EURASIP), 2 prepared and submitted journal papers (NRL-Springer and IEEE AWPL) and 6 papers in the proceedings of the several major conferences (EuMC, EuCAP, ISMICT and IEEE SCVT).

Appendix A

Antenna Candidate for Nanomachines

As shown in Chapter 2, the high power consumption of the communication component is mainly due to the fact that canonical antennas, scaled down to the nanoscale, convert an electric power into RF waves in an extremely inefficient manner. Typically, most antennas in the microwave band are designed such that their dimensions are comparable to the operating wavelength λ. In such a case, the antenna impedance is real and, as a consequence, the antenna is easy compatible with a transceiver to which it is connected. Antennas sized this way are called resonant-length. When the largest dimension of the antenna is at or under $\lambda/10$ (there is no significant phase shift over the electrical path length), it is regarded to be electrically small. Once traditional antennas operate at frequencies for which they are electrically small, a mismatch between them and a transmitter/receiver circuit is large. Since the actual communication channel at very high frequencies (e.g., the terahertz range and higher) is shown to experience high levels of both propagation loss and absorption attenuation caused by the molecules and other small particles [66], it is essential to develop a concept of an efficient ESA, which can be integrated in the nanomachine in an appropriate/friendly fashion as its usage would offer a substantial decrease in the power consumption level of the device's wireless component.

The remainder of this appendix is organized as follows. The technical background on ESAs, which leads to better understanding of their modes of action, is given in

Section A.1. Subsequently, the novel concept of ESA, which has a number of privileges compared to other ESA designs, is proposed and discussed in Section A.2. Eventually, the performance of such an antenna is numerically investigated in Section A.3.

A.1 Design Principles of ESAs

The electrical size of an antenna, i.e., its physical size with respect to the operating wavelength, predominantly determines the antenna characteristics. To perform the efficient transformation of a guided wave into radiated wave (and vice versa), the antenna dimensions should, as is known, be of the order of the wavelength. Smaller antennas can be deployed at the expense of its power gain and/or operational bandwidth. Therefore, antenna miniaturisation is the art of compromise: by considering the best trade-off between efficiency, volume and bandwidth, one can design the smallest possible antenna, which meets the requirements of a specific application. Since nanomachines would operate on a frugal budget, our objective is in particular to develop an electrically small antenna with high radiation capabilities. Several primary principles, which aim to make an antenna smaller than resonant size while keeping its resonant properties, are reviewed as their usage might help to design a suitable antenna to be integrated in a nanomachine.

Since an electrically small antenna is always characterised by a strong reactive terminal impedance, the most straightforward way to realise an ESA with a high radiation performance is to compensate its impedance through an appropriate loading [34]. For example, to match an electrically small loop-based antenna, a capacitor loading is often used. Also, the loading is accomplished by adding lumped elements or some conductive parts. Once the loading is applied, it maintains the antenna efficiency at the cost of reducing its operational bandwidth [28, 141].

An alternative idea, put forward by Wheeler [155], is that a small antenna would operate in a better manner once it makes better use of the volume it occupies: by twisting the antenna structure, the current over its aperture is forced to serpentine and, as a consequence, the antenna seems electrically larger than it really is. A fair example of this concept is the inverted-L antenna, which was built from the classical monopole through its bending. Another example is a microstrip patch antenna with cut slots in its geometry: these slots would urge the surface currents to meander, thus increasing the antenna's electrical length without modifying its physical dimensions. This idea also offers the development of volume-loading-based antennas and folded-

spherical-helix-based antennas. In the former design [91], a thick wire framework is used as the end-loading body and this maximises the capacitance in the space allocated for the antenna and thus permits the antenna to exhibit resonance properties at frequencies at which it is electrically small. Due to the particular geometry of the latter antenna [12], it possesses both internal inductance and capacitance and resonates at a lower frequency than a standard antenna of the same size. Meanwhile, the described technique is very frequency selective and, as a consequence, the bandwidth of the antennas is reduced compared to that of classical antennas.

To develop an efficient ESA, the approach that includes the coating of the conducting antenna elements with a layer of dielectric or magnetic material has been proposed half a century ago [9]. Due to the phenomenon that the wavelength is shorter in a high-permittivity material, the antenna with resonant properties becomes smaller when embedded in such a substance. The size reduction would depend on the permittivity and the shape of dielectric/magnetic covering. Again, the usage of this loading reduces the bandwidth of the resulting antenna by enhancing its quality factor. This is due to the concentration of the electric field in the high-permittivity regions, which makes the adaptive launching of a guided wave into free space radiation more difficult [62].

A.2 Encapsulated ESA Concept

The first two approaches shown in Section A.1 are not well suited for the design of nanoscale efficient antenna: the former requires additional physical space to allocate a capacitor loading, whilst the latter assumes complex-shaped antennas which would be cumbersome to realise due to a lack of manipulation tools at nano-level. Unlike these approaches, the use of a dielectric/magnetic coating attracts considerable attention as this concept offers the implementation of efficient, quite simple and durable antennas in a smaller scale and is commonly employed in the development of antennas for portable and handy gadgets. In particular, by using a metal enclosure covered with dielectric material, Schantz in [118] has designed a new antenna, which might be exploited in miniaturized electronic sensor devices. The fact, that other payload components (e.g. sensors/actuators, processing unit, energy-supply element and the like) might be placed inside the antenna hollow to approach a space-saving geometry as well as to provide such delicate components with the protection from environmental phenomena, makes the proposed antenna very advantageous against other ESA solu-

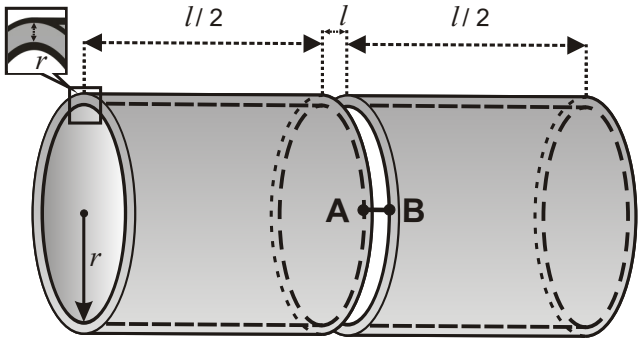

Figure A.1: The geometry of the encapsulated antenna. The magnetic coating is depicted in grey.

tions. Nonetheless, in the Schantz's antenna the dielectric coating occupies a large volume (i.e., 88% of the entire antenna space) and this shortcoming is essential in terms of the implementation and usability of this antenna in nanomachines. To overcome this limitation, the concept of a new encapsulated dipole antenna is therefore developed here. The design of such an antenna includes a metal enclosure covered with a thin magnetic layer and its radiation properties are similar to those of the dielectric-coating-based antenna in [118]. The resulting volume gain can meanwhile be used to locate other payload components of the nanomachine in a more effective way.

The proposed antenna is dipole-like: it is composed of two metal cylinders which are closely spaced (the separation between such 'dipole arms' Δl is much smaller than the antenna length) and connected through the feeding line AB (Fig.A.1). The length of each cylinder is equal to $l/2$, while r stands for its radius. The metal enclosure is covered with a magnetic layer of the thickness Δr and magnetic constant μ.

The Maxwell's equations should generally be used to carry out a full-wave analysis of the proposed dipole-like antenna. At first, the electromagnetic field strengths are formally expressed in two different spatial volumes, such as the magnetodielectric layer and an infinite external medium. At second, by adopting the boundary conditions at the two interfaces and taking into consideration the source properties, a 3D electromagnetic problem can be formulated. Although this problem can be reduced to a 2D boundary-value problem thanks to the symmetry in the antenna geometry, there is no way to derive its analytic solution without introducing severe approxima-

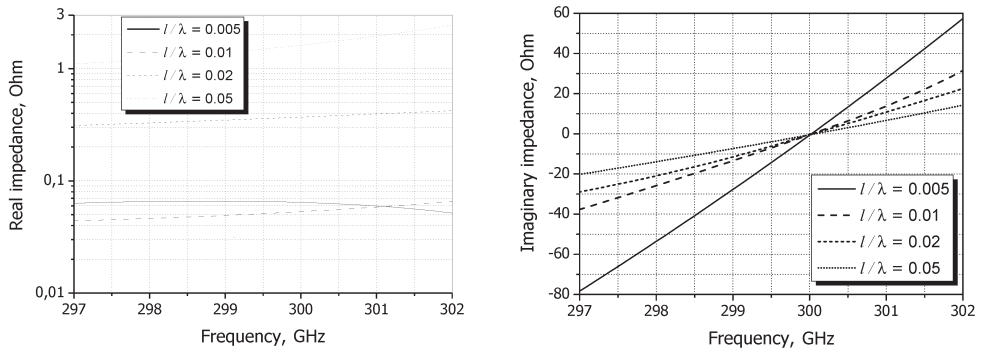

(a) (b)

Figure A.2: (a) The real and (b) imaginary part of the input impedance of the dipole-like encapsulated antenna at 300 GHz .

tions. In this way, the concept of the surface impedance [119] is employed here to describe the physics behind using a magnetic layer and the operating principles of the developed antenna. In particular, a first approximation for the surface impedance $\overline{Z}_s$ of a thin magnetodielectric cylindrical layer has been derived in [97] as follows:

$$\overline{Z}_s = ikr\mu\mu_0 \cdot ln\left(r_e/r_i\right), \tag{A.1}$$

where i is the imaginary unit, $k = 2\pi/\lambda$ stands for the free-space wavenumber, r_e and r_i are respectively the external and internal radii of the cylindrical layer, whilst μ and μ_0 indicate the relative magnetic constant and the free-space permeability. As seen in Eq.(A.1), not the relative dielectric constant ε but its relative permeability μ plays the dominant role in affecting the surface impedance and thus the electromagnetic properties of a thin magnetodielectric layer. Note that a similar conclusion has been drawn in [57], where the authors investigate the radiation properties of an infinite cylindrical wire covered with a thin magnetodielectric layer. In this respect, a thin magnetic film characterized by $(\varepsilon = 1, \mu > 1)$ should impact on a metal antenna quite as much as a thick dielectric layer with the parameters $(\varepsilon > 1, \mu = 1)$. This idea straightforwardly offers the realisation of smaller-scale antennas and is thus behind the proposed dipole-like antenna concept.

A.3 Numerical Results

Since the formal analysis of the developed antenna is cumbersome (see Section A.2), its properties are determined through numerical simulations by means of the electromagnetic solver [1]. The computational engine of this software and the numerical techniques used are discussed in details in Appendix B. For the simulations, the magnetic ring model [92] is employed to excite the proposed dipole-like antenna as well as the magnetic layer is discretised into tetrahedrons with a mesh length less than $\lambda/20$ to calculate the antenna characteristics in an accurate manner. The ratio between the external and internal radius is kept constant and equal to $r_0/r_i = (r + \Delta r)/r = 0.9$ to allow the hollow/usable volume occupies 81% of the total antenna size. Also, the ratio between the antenna diameter and its length $2r_0/(2l + \Delta l)$ is set to be 1 as this leads to a more realistic design of the nanoscale antenna. The separation between the two antenna parts $\Delta l = 0.01l$. The dipole-like antenna is excited with a voltage point-source, which operates at 300 GHz (i.e., the wavelength $\lambda = 1$ mm) and exhibits a zero reactive impedance to be feasible.

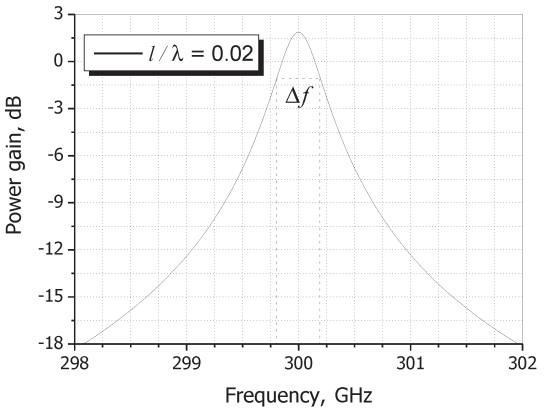

Figure A.3: The total power gain of the resonant encapsulated dipole-like antenna with $l = 0.02\lambda$.

The electrically small antennas of standard design are known to possess a high reactive impedance and cannot thus be matched with the point-source of interest. The covering made of a thin magnetic layer might decrease the antenna reactance and provide it with resonance properties. In particular, the proposed dipole-like antenna with its length equal to 0.005λ, 0.01λ, 0.02λ and 0.05λ is shown through numerical experiments in FEKO to be resonant, i.e., having no reactive impedance,

once the relative magnetic constant of the top layer μ is respectively 30520, 7540, 1905 and 290 (the complex input impedance of these antennas as a function of the operating frequency is illustrated in Fig.A.2). As the current technology offers the realisation of a material with a very high magnetic constant (e.g. [139]), this allows to develop the resonant encapsulated dipole-like antenna with the length $l \ll \lambda$ in practice. Note that the real part of such an antenna impedance would decrease with reducing its length.

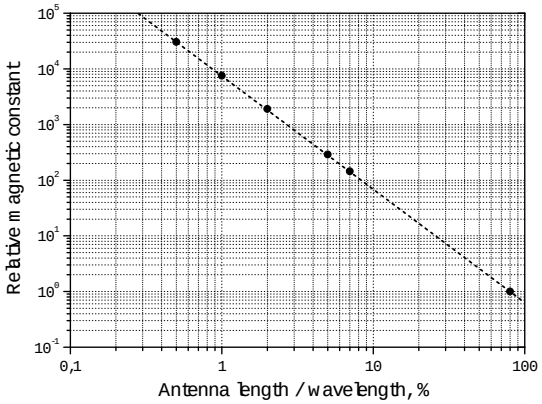

Figure A.4: The asymptotic dependence for the relative magnetic permeability μ required to provide the encapsulated antenna of a certain length with the resonance properties.

The direction capabilities of the proposed dipole-like ESA are similar to those of a Hertzian dipole: i.e., the direction pattern of the encapsulated antenna with $l = 0.005\lambda$ is determined to be torus-shaped with a maximum gain of 1.77 dBi (compared to 1.76 dBi for the elementary doublet [9]). The power gain of the encapsulated antenna with $l = 0.02\lambda$ and $\mu = 1905$, which exhibits the resonance properties at 300 GHz and is fed at this frequency by a perfectly matched source (such a generator should have a zero reactive impedance and can thus be simply implemented), is calculated via FEKO and depicted in Fig.A.3. As shown in this figure, the power gain, as expected, approaches maximum at 300 GHz as well as the high performance of such a dipole-like antenna is achieved at the cost of reducing its operational bandwidth. In particular, the Q-factor of the considered antenna ($Q = f/\Delta f$, where Δf is the 3dB fractional bandwidth) is estimated to be ~ 750, which is sufficiently larger than that of the half-wavelength dipole ($\sim 10 \ldots 20$). Through numerical simulations, the Q-factors of the other resonant encapsulated antennas with $l = 0.005\lambda$, $l = 0.01\lambda$ and

$l = 0.05\lambda$ are also determined and equal to 2500, 1600 and 690, respectively. From this it is concluded that the encapsulated antenna of a smaller length becomes more frequency selective (i.e., its operational bandwidth is reduced) to keep its resonance properties.

Last but not least, since calculations on the relative magnetic constant μ needed to make the encapsulated antenna resonant are challenging and time-consuming, the discovered asymptotic dependence between the magnetic permeability and the 'antenna length/wavelength' ratio (see Fig.A.4) is essential and of importance for the antenna engineering community. Meanwhile, note that for the resonant encapsulated antenna the permeability μ can be lowered by increasing the thickness of magnetic layer Δr. The latter however results in the smaller usable/hollow space within antenna and is hence out of consideration here.

Appendix B

Electromagnetic Simulation Software FEKO

The numerical experiments of different electromagnetic problems addressed throughout this thesis has been performed via the FEKO solver [1]. The program FEKO is a commercial simulator, which primarily uses the MoM to treat such problems. The MoM is the fundamental numerical method, which is achieved widespread acceptance by the engineering community due its ability to accurately analyse antennas and scatterers [47].

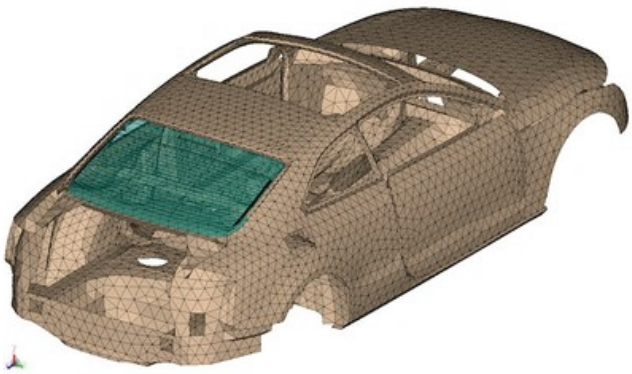

Figure B.1: Computational model of the car in FEKO with courtesy of `https://www.feko.info/`.

The idea behind the MoM is as follows. The radiating and scattering structures are simplified by wire segments, surface patches and/or tetrahedrals (for inhomogeneous dielectric bodies). Each of these elements is in turn replaced by equivalent surface or volumetric current (Fig.B.1). In FEKO, linear and triangular (the so-called Rao-Wilton-Glisson) basis functions are particularly implemented for current approximation. The relevant boundary condition is then applied to all the interactions between elements and external environment: in particular, the boundary conditions on a metal surface are verified so that to hold in several points within the limits of each element (strictly, these conditions should be carried out in all the element points). Subsequently, by taking into consideration the impact of every element, a system of linear equations with respect to a magnitude of the basis function is derived using the Green's function of the problem. When these magnitudes are determined, the approximate current per each element can straightforwardly be calculated as a linear combination of them and the known basis functions. Once the current distribution over an entire body is known, all the relevant parameters, such as near/far electric fields, scattering parameters, directivity, input impedance and the like, could be obtained by using standard electromagnetic methods. The typical dimensions of the resulting matrix range from a few hundreds for simple antenna problems to several thousands for complex electromagnetic problems. Thus, the suitability of MoM to solve an electromagnetic problem is often related to computational capabilities and/or acceptable runtime. More detailed description can be found in the manual available at the official FEKO website.

Appendix C

Components of the Tensor $\widehat{f}(\vec{r}, \vec{r_i})$

Using Eq.3.5 and making the necessary mathematical transformations, we eventually arrive at the following components of 3x3 tensor $\widehat{f}(\vec{r}, \vec{r_i})$:

$$f_{xx}(\vec{r}, \vec{r_i}) = \frac{e^{-ikR}}{R}\left[k^2 - \frac{ik}{R} - \frac{1}{R^2} + \frac{(x-x_i)^2}{R^4}\left(-k^2R^2 + 3ikR + 3\right)\right],$$

$$f_{xy}(\vec{r}, \vec{r_i}) = (x-x_i)(y-y_i)\frac{e^{-ikR}}{R^5}\left[-k^2R^2 + 3ikR + 3\right],$$

$$f_{xz}(\vec{r}, \vec{r_i}) = (x-x_i)(z-z_i)\frac{e^{-ikR}}{R^5}\left[-k^2R^2 + 3ikR + 3\right],$$

$$f_{yx}(\vec{r}, \vec{r_i}) = (x-x_i)(y-y_i)\frac{e^{-ikR}}{R^5}\left[-k^2R^2 + 3ikR + 3\right],$$

$$f_{yy}(\vec{r}, \vec{r_i}) = \frac{e^{-ikR}}{R}\left[k^2 - \frac{ik}{R} - \frac{1}{R^2} + \frac{(y-y_i)^2}{R^4}\left(-k^2R^2 + 3ikR + 3\right)\right],$$

$$f_{yz}(\vec{r}, \vec{r_i}) = (y-y_i)(z-z_i)\frac{e^{-ikR}}{R^5}\left[-k^2R^2 + 3ikR + 3\right],$$

$$f_{zx}(\vec{r},\vec{r_i}) = (x-x_i)\,(z-z_i)\,\frac{e^{-ikR}}{R^5}\left[-k^2R^2+3ikR+3\right],$$

$$f_{zy}(\vec{r},\vec{r_i}) = (y-y_i)\,(z-z_i)\,\frac{e^{-ikR}}{R^5}\left[-k^2R^2+3ikR+3\right],$$

$$f_{zz}(\vec{r},\vec{r_i}) = \frac{e^{-ikR}}{R}\left[k^2-\frac{ik}{R}-\frac{1}{R^2}+\frac{(z-z_i)^2}{R^4}\left(-k^2R^2+3ikR+3\right)\right],$$

where $R=|\vec{r}-\vec{r_i}|=\sqrt{(x-x_i)^2+(y-y_i)^2+(z-z_i)^2}$ is the distance between the considered points.

Appendix D

Modelling on Interface Impact

D.1 The Green's Function of a Vertical Dipole located over Two-layered Half-space

Here, the Green's function of a vertically polarised elemental dipole located over the given two-layered half-space is derived. As shown in Fig.4.1, the dipole is placed in the point $(0, 0, z_t)$. The general representation of the Green's function $G(\rho, z_r, 0, z_t)$ for a vertical elemental antenna located over an interface is known to be written as [30]

$$G(\rho, z_r, 0, z_t) = \frac{1}{4\pi} \int_{-\infty}^{\infty} \varkappa H_0^{(2)}(\varkappa\rho) g(z_r, z_t) \mathrm{d}\varkappa, \tag{D.1}$$

where $\varkappa$ is the complex transverse wavenumber, $H_0^{(2)}$ stands for the Hankel function of the second kind and zero order and the function $g(z_r, z_t)$ is the one-dimensional modal Green's function. The function $g(z_r, z_t)$ depends generally on the nature of z stratification. For the given half-space, $g(z_r, z_t)$ is derived by adopting the rigorous boundary conditions (e.g. the tangential components of the electric field are continuous across the interface) on both surfaces of the dielectric layer and by using the wave equations for free space and the dielectric medium. This results in a system of four linear equations with four unknown parameters. By solving it, the representation of $g(z_r, z_t)$ is expressed as:

$$g(z_r, z_t) = \frac{4\pi \cdot e^{-i\gamma_1(z_r+z_t)}}{i\gamma_1\varepsilon + \gamma_2 \tan(\gamma_2 d)}, \tag{D.2}$$

where $\gamma_1^2 = k^2 - \varkappa^2$ and $\gamma_2^2 = k^2\varepsilon - \varkappa^2$ are the longitudinal wavenumbers in free space and the dielectric region, respectively. In this way, the final form of the Green's function $G(\rho, z_r, 0, z_t)$ is given by:

$$G(\rho, z_r, 0, z_t) = \int_{-\infty}^{\infty} \frac{\varkappa H_0^{(2)}(\varkappa\rho) \cdot e^{-i\gamma_1(z_r+z_t)}}{i\gamma_1\varepsilon + \gamma_2 \tan(\gamma_2 d)} \mathrm{d}\varkappa. \tag{D.3}$$

D.2 Input Impedance of a Vertical Dipole placed over an Impedance Half-space

Here, the input impedance of a vertical dipole located over the impedance interface at height z_t is derived. The dipole length is equal to $l \ll \lambda$, while $a \ll l$ stands for its radius. The interface is characterized by the normalised surface impedance $\overline{Z}_s$.

The antenna can fairly be modelled to be fed through a delta voltage generator located at its center. In this way, the dipole excitation is described as follows:

$$E_z(a, z) = -V_0 \cdot \delta(z - z_t), \tag{D.4}$$

where V_0 is the amplitude [V]. By taking into account that $V_0 = Z_a \cdot j(z_r)$, and using Eq.(4.1), Eq.(4.7) and standard mathematical methods, the above expression can be written as Eq.(D.5). The first term in the square brackets corresponds to the free-space Green's function, while the second term includes the interface impact. Therefore, the antenna impedance Z_a can be decomposed as $Z_a = Z_{fs} + \Delta Z$, where Z_{fs} is the impedance of the dipole in free space and ΔZ is the portion due to the presence of the half-space. Through simple algebra, the value of ΔZ is determined as in Eq.(D.6).

D.3 Analysis on a Surface Wave Velocity

According to [140], the group velocity of the surface wave ν_c is given by:

$$\nu_c = \nu \cdot \Re(\varkappa_p), \tag{D.7}$$

where ν is the wave propagation velocity in the dielectric, whereas $\varkappa_p$ is the transverse wavenumber of the surface wave. The wave propagation velocity is known to be expressed as:

$$\nu = \frac{c}{\sqrt{\Re(\varepsilon)}}, \tag{D.8}$$

$$Z_a = \frac{30i}{k} \cdot \int_{z_t-l/2}^{z_t+l/2} \left(1 - \frac{|z-z_t|}{l/2}\right) \cdot \left[\frac{\partial^2}{\partial z^2} + k^2\right] \int_{z_t-l/2}^{z_t+l/2} \left(1 - \frac{|z'-z_t|}{l/2}\right) \left[\frac{e^{-ik\sqrt{\rho^2+(z-z')^2}}}{\sqrt{\rho^2+(z-z')^2}} + \right.$$
$$\left. + \int_{-\infty}^{\infty} \frac{\varkappa H_0^{(2)}(\varkappa\rho)}{i\sqrt{k^2-\varkappa^2}} \cdot \frac{\sqrt{k^2-\varkappa^2} - k\overline{Z}_s}{\sqrt{k^2-\varkappa^2} + k\overline{Z}_s} \cdot e^{-i\sqrt{k^2-\varkappa^2}(z+z')} \mathrm{d}\varkappa \right] \mathrm{d}z' \, \mathrm{d}z. \tag{D.5}$$

$$\Delta Z = \frac{15l^2}{2k} \int_{-\infty}^{\infty} \frac{\varkappa^3 H_0^{(2)}(\varkappa\rho)}{\sqrt{k^2-\varkappa^2}} \cdot \frac{\sqrt{k^2-\varkappa^2} - k\overline{Z}_s}{\sqrt{k^2-\varkappa^2} + k\overline{Z}_s} \cdot e^{-2iz_t\sqrt{k^2-\varkappa^2}} \mathrm{d}\varkappa. \tag{D.6}$$

where c is the speed of light, and ε is the dielectric constant of the upper half-space layer. The transverse wavenumber can be derived through the surface impedance as $\varkappa_p = \sqrt{1-\overline{Z}_s^{\,2}}$. Hence, using Eq.(D.7) and Eq.(D.8), the ratio $\Delta\nu_c = \nu_c/c$ can be given as:

$$\Delta\nu_c = \frac{\Re\left(\sqrt{1-\overline{Z}_s^{\,2}}\right)}{\sqrt{\Re(\varepsilon)}}. \tag{D.9}$$

For the given two-layered half-space, the ratio $\Delta\nu_c = \nu_c/c$ is plotted in Fig.D.1 as a function of the thickness d at the wavelength $\lambda = 0.03$m. Note that the dielectric constant ε is selected both actual and hypothetical to better understand its influence

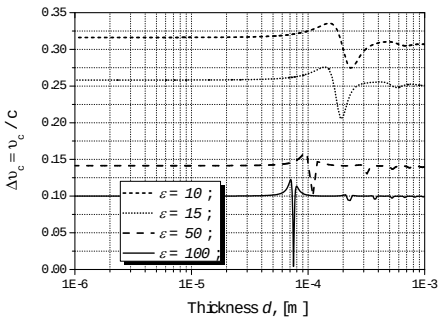

Figure D.1: The value $\Delta\nu_c = \dfrac{\nu_c}{c}$ as a function of thickness d for various types of the two- layered half-spaces (ν_c is the group velocity of the surface wave).

on the group velocity ν_c. The numerical results indicate that $\nu_c \ll c$ only when $\Re(\varepsilon) \geqslant 100$. However, the most constructive impact on the power budget of the node-to-node channel is expected once the half-space has a high inductive impedance and is thus characterized by a low value of $\Re(\varepsilon)$. Hence, due to $\nu_c \sim c$ and the small communication distance, the assumption that there is no phase shift between the surface and the geometric-optical waves is valid.

Bibliography

[1] "Electromagnetic Simulation Software FEKO," http://www.feko.info/, accessed: 25-Jun-2014.

[2] "Sensor Platform Provider," http://www.libelium.com/, accessed: 25-Jun-2014.

[3] "Yoshida's Fullerene Library," http://www.jcrystal.com/products/wincnt/, accessed: 25-Jun-2014.

[4] I. F. Akyildiz, F. Brunetti, and C. Blázquez, "Nanonetworks: a new communication paradigm," *Computer Networks*, vol. 52, no. 12, pp. 2260–2279, 2008.

[5] I. F. Akyildiz and J. M. Jornet, "Electromagnetic wireless nanosensor networks," *Nano Communication Networks*, vol. 1, no. 1, pp. 3–19, 2010.

[6] I. F. Akyildiz and X. Wang, "A survey on wireless mesh networks," *Communications Magazine, IEEE*, vol. 43, no. 9, pp. S23–S30, 2005.

[7] N. W. Ashcroft, N. D. Mermin, and R. Smoluchowski, "Solid state physics," *Physics Today*, vol. 30, p. 61, 1977.

[8] D. Avraham and S. Havlin, *Diffusion and Reactions in Fractals and Disordered Systems*, 2000.

[9] C. A. Balanis, *Antenna theory: analysis and design*. John Wiley & Sons, 2012.

[10] F. Balestra, *Nanoscale CMOS: innovative materials, modeling and characterization*. John Wiley & Sons, 2013.

[11] A. Baños, *Dipole Radiation in the Presence of a Conducting Half-space*, ser. International Series of monographs in electromagnetic waves. Pergamon Press, 1966.

[12] S. R. Best, "The radiation properties of electrically small folded spherical helix antennas," *Antennas and Propagation, IEEE Transactions on*, vol. 52, no. 4, pp. 953–960, 2004.

[13] C. Bettstetter and J. Eberspacher, "Hop distances in homogeneous ad hoc networks," in *Vehicular Technology Conference, 2003. VTC 2003-Spring. The 57th IEEE Semiannual*, vol. 4. IEEE, 2003, pp. 2286–2290.

[14] P. Bharadwaj, B. Deutsch, and L. Novotny, "Optical antennas," *Advances in Optics and Photonics*, vol. 1, no. 3, pp. 438–483, 2009.

[15] P. Bondavalli, P. Legagneux, and D. Pribat, "Carbon nanotubes based transistors as gas sensors: state of the art and critical review," *Sensors and Actuators B: Chemical*, vol. 140, no. 1, pp. 304–318, 2009.

[16] H. Boulaiz, P. J. Alvarez, A. Ramirez, J. A. Marchal, J. Prados, F. Rodríguez-Serrano, M. Perán, C. Melguizo, and A. Aranega, "Nanomedicine: application areas and development prospects," *International journal of molecular sciences*, vol. 12, no. 5, pp. 3303–3321, 2011.

[17] P. Burke and C. Rutherglen, "Towards a single-chip, implantable RFID system: is a single-cell radio possible?" *Biomedical microdevices*, vol. 12, no. 4, pp. 589–596, 2010.

[18] P. J. Burke, S. Li, and Z. Yu, "Quantitative theory of nanowire and nanotube antenna performance," *Nanotechnology, IEEE Transactions on*, vol. 5, no. 4, pp. 314–334, 2006.

[19] S. F. Bush, *Nanoscale Communication Networks*. Artech House, 2010.

[20] S. Chandler, "Calculation of number of relay hops required in randomly located radio network," *Electronics Letters*, vol. 25, no. 24, pp. 1669 –1671, 1989.

[21] S.-W. Chang and S. L. Chuang, "Fundamental formulation for plasmonic nanolasers," *Quantum Electronics, IEEE Journal of*, vol. 45, no. 8, pp. 1014–1023, 2009.

[22] S. Choi and K. Sarabandi, "Performance assessment of bundled carbon nanotube for antenna applications at terahertz frequencies and higher," *Antennas and Propagation, IEEE Transactions on*, vol. 59, no. 3, pp. 802–809, 2011.

[23] J. W. Chon and K. Iniewski, *Nanoplasmonics: Advanced Device Applications*. CRC Press, 2013.

[24] S. Datta, *Electronic transport in mesoscopic systems*. Cambridge university press, 1997.

[25] M. Diallo, A. Street, R. Sustich, J. Duncan, and N. Savage, *Nanotechnology Applications for Clean Water: Solutions for Improving Water Quality*. William Andrew, 2009.

[26] T. Dinadayalane and J. Leszczynski, "Remarkable diversity of carbon–carbon bonds: structures and properties of fullerenes, carbon nanotubes, and graphene," *Structural Chemistry*, vol. 21, no. 6, pp. 1155–1169, 2010.

[27] L. Doherty, L. El Ghaoui *et al.*, "Convex position estimation in wireless sensor networks," in *INFOCOM 2001. Twentieth Annual Joint Conference of the IEEE Computer and Communications Societies. Proceedings. IEEE*, vol. 3. IEEE, 2001, pp. 1655–1663.

[28] R. M. Fano, "Theoretical limitations on the broadband matching of arbitrary impedances," *Journal of the Franklin Institute*, vol. 249, no. 1, pp. 57–83, 1950.

[29] J. Feder, *Fractals*, ser. Physics of solids and liquids, 1988.

[30] L. Felsen and N. Marcuvitz, *Radiation and Scattering of Waves*, ser. IEEE Press Series on Electromagnetic Wave Theory. Wiley, 1994.

[31] R. P. Feynman, "There's plenty of room at the bottom," *Engineering and Science*, vol. 23, no. 5, pp. 22–36, 1960.

[32] R. A. Freitas, *Nanomedicine, volume I: basic capabilities*. Landes Bioscience Georgetown, TX, 1999.

[33] H. T. Friis, "A note on a simple transmission formula," *proc. IRE*, vol. 34, no. 5, pp. 254–256, 1946.

[34] K. Fujimoto, *Small antennas*. Wiley Online Library, 1987.

[35] L. Genzel and U. Kreibig, "Dielectric function and infrared absorption of small metal particles," *Zeitschrift für Physik B Condensed Matter*, vol. 37, no. 2, pp. 93–101, 1980.

[36] G. Giorgetti, S. K. Gupta, and G. Manes, "Wireless localization using self-organizing maps," in *Proceedings of the 6th international conference on Information processing in sensor networks*. ACM, 2007, pp. 293–302.

[37] Z. Godziński, "The surface impedance concept and the structure of radio waves over real earth," *Proceedings of the IEE-Part C: Monographs*, vol. 108, no. 14, pp. 362–373, 1961.

[38] I. S. Grigoriev and Meĭ, *Handbook of physical quantities*.

[39] A. Gupta, A. Arora, A. Menakshi, A. Sehgal, and R. Sehgal, "Nanotechnology and its applications in drug delivery: A review," 2012.

[40] Z. J. Haas, J. Y. Halpern, and L. Li, "Gossip-based ad hoc routing," *IEEE/ACM Trans. Netw.*, vol. 14, no. 3, pp. 479–491, Jun. 2006.

[41] M. Haenggi, "On distances in uniformly random networks," *Information Theory, IEEE Transactions on*, vol. 51, no. 10, pp. 3584–3586, 2005.

[42] G. W. Hanson, "Fundamental transmitting properties of carbon nanotube antennas," *Antennas and Propagation, IEEE Transactions on*, vol. 53, no. 11, pp. 3426–3435, 2005.

[43] ——, "Current on an infinitely-long carbon nanotube antenna excited by a gap generator," *Antennas and Propagation, IEEE Transactions on*, vol. 54, no. 1, pp. 76–81, 2006.

[44] ——, "Dyadic Greens functions and guided surface waves for a surface conductivity model of graphene," *Journal of Applied Physics*, vol. 103, no. 6, p. 064302, 2008.

[45] ——, "Radiation efficiency of nano-radius dipole antennas in the microwave and far-infrared regimes," *Antennas and Propagation Magazine, IEEE*, vol. 50, no. 3, pp. 66–77, 2008.

[46] J. Hao and G. W. Hanson, "Infrared and optical properties of carbon nanotube dipole antennas," *Nanotechnology, IEEE Transactions on*, vol. 5, no. 6, pp. 766–775, 2006.

[47] R. F. Harrington and J. L. Harrington, *Field computation by moment methods*. Oxford University Press, 1996.

[48] O. Hayden, R. Agarwal, and C. M. Lieber, "Nanoscale avalanche photodiodes for highly sensitive and spatially resolved photon detection," *Nature materials*, vol. 5, no. 5, pp. 352–356, 2006.

[49] T. He, C. Huang, B. M. Blum, J. A. Stankovic, and T. Abdelzaher, "Range-free localization schemes for large scale sensor networks," in *Proceedings of the 9th annual international conference on Mobile computing and networking*, 2003, pp. 81–95.

[50] M. Hefeeda and M. Bagheri, "Wireless sensor networks for early detection of forest fires," in *Mobile Adhoc and Sensor Systems, 2007. MASS 2007. IEEE Internatonal Conference on*, 2007, pp. 1–6.

[51] J. L. Hill and D. E. Culler, "MICA: A wireless platform for deeply embedded networks," *Micro, IEEE*, vol. 22, no. 6, pp. 12–24, 2002.

[52] M. T. Hill, Y.-S. Oei, B. Smalbrugge, Y. Zhu, T. De Vries, P. J. Van Veldhoven, F. W. Van Otten, T. J. Eijkemans, J. P. Turkiewicz, H. De Waardt *et al.*, "Lasing in metallic-coated nanocavities," *Nature Photonics*, vol. 1, no. 10, pp. 589–594, 2007.

[53] N. A. Hizhnyak, *Integral equations of macroscopic electrodynamics (in RUS)*. Navukova Dumka, 1986.

[54] M. Hotta, M. Hayashi, M. T. Lanagan, D. K. Agrawal, and K. Nagata, "Complex permittivity of graphite, carbon black and coal powders in the ranges of X-band frequencies (8.2 to 12.4 GHz) and between 1 and 10 GHz," *ISIJ international*, vol. 51, no. 11, pp. 1766–1772, 2011.

[55] Y. Huang, X. Duan, Q. Wei, and C. M. Lieber, "Directed assembly of one-dimensional nanostructures into functional networks," *Science*, vol. 291, no. 5504, pp. 630–633, 2001.

[56] A. Hunt and R. Ewing, "Percolation theory: Topology and structure," in *Percolation Theory for Flow in Porous Media*. Springer Berlin / Heidelberg, 2009, pp. 1–36.

[57] P. M. Ikonen, K. N. Rozanov, A. V. Osipov, P. Alitalo, and S. A. Tretyakov, "Magnetodielectric substrates in antenna miniaturization: Potential and limitations," *Antennas and Propagation, IEEE Transactions on*, vol. 54, no. 11, pp. 3391–3399, 2006.

[58] M. Ilyas and I. Mahgoub, *Smart Dust: Sensor Network Applications, Architecture and Design*, 2006.

[59] K. Iniewski, *Wireless technologies: circuits, systems, and devices*. CRC press, 2007.

[60] J. D. Jackson, *Classical Electrodynamics*. Wiley India Pvt. Limited, 2007.

[61] S. Jain, K. Khomane, A. K Jain, and P. Dani, "Nanocarriers for transmucosal vaccine delivery," *Current Nanoscience*, vol. 7, no. 2, pp. 160–177, 2011.

[62] J. James and A. Henderson, "Electrically short monopole antennas with dielectric or ferrite coatings," in *Proceedings of the Institution of Electrical Engineers*, vol. 125, no. 9. IET, 1978, pp. 793–803.

[63] X. Jiao and S. Blair, "Optical antenna design for fluorescence enhancement in the ultraviolet," *Optics express*, vol. 20, no. 28, pp. 29 909–29 922, 2012.

[64] P. B. Johnson and R.-W. Christy, "Optical constants of the noble metals," *Physical Review B*, vol. 6, no. 12, p. 4370, 1972.

[65] W. Johnson and D. Dudley, "Real axis integration of Sommerfeld integrals: source and observation points in air," *Radio science*, vol. 18, no. 2, pp. 175–186, 1983.

[66] J. M. Jornet and I. F. Akyildiz, "Channel capacity of electromagnetic nanonetworks in the terahertz band," in *Communications (ICC), 2010 IEEE International Conference on*. IEEE, 2010, pp. 1–6.

[67] ——, "Graphene-based nano-antennas for electromagnetic nanocommunications in the terahertz band," in *Antennas and Propagation (EuCAP), 2010 Proceedings of the Fourth European Conference on*. IEEE, 2010, pp. 1–5.

[68] T. Joseph and M. Morrison, *Nanotechnology in agriculture and food: a nanoforum report*. Nanoforum. org, 2006.

[69] L. Kaounides, H. Yu, and T. Harper, "Nanotechnology innovation and applications in textiles industry: current markets and future growth trends," *Materials Science and Technology*, vol. 22, no. 4, pp. 209–237, 2007.

[70] R. Kappeler, D. Erni, C. Xudong, and L. Novotny, "Field computations of optical antennas," *Journal of Computational and Theoretical Nanoscience*, vol. 4, no. 3, pp. 686–691, 2007.

[71] S. D. Keller and A. I. Zaghloul, "Lightweight, durable army antennas using carbon nanotube technology," DTIC Document, Tech. Rep., 2013.

[72] K. Kempa, J. Rybczynski, Z. Huang, K. Gregorczyk, A. Vidan, B. Kimball, J. Carlson, G. Benham, Y. Wang, A. Herczynski *et al.*, "Carbon nanotubes as optical antennae," *Advanced Materials*, vol. 19, no. 3, pp. 421–426, 2007.

[73] A. E. Khandani, E. Modiano, J. Abounadi, and L. Zheng, "Cooperative routing in wireless networks," in *Advances in Pervasive Computing and Networking*. Springer, 2005, pp. 97–117.

[74] Y. Kim, T. Schmid, Z. M. Charbiwala, J. Friedman, and M. B. Srivastava, "NAWMS: nonintrusive autonomous water monitoring system," in *Proceedings of the 6th ACM conference on Embedded network sensor systems*, ser. SenSys '08, 2008, pp. 309–322.

[75] R. King, "Electromagnetic wave propagation over a constant impedance plane," *Radio Science*, vol. 4, no. 3, pp. 255–268, 1969.

[76] R. W. P. King, M. Owens, and T. T. Wu, *Lateral electromagnetic waves: Theory and applications to communications, geophysical exploration, and remote sensing*, ser. Graduate texts in contemporary physics. Springer, 1992.

[77] R. King and G. Smith, "Antennas in matter: fundamentals, theory and application," 1981.

[78] A. Knoll, D. Grogg, M. Despont, and U. Duerig, "Fundamental scaling properties of electro-mechanical switches," *New Journal of Physics*, vol. 14, no. 12, p. 123007, 2012.

[79] L. D. Landau, E. M. Lifšic, J. B. Sykes, J. S. Bell, M. Kearsley, and L. P. Pitaevskii, *Electrodynamics of continuous media*. Pergamon press Oxford, 1960, vol. 364.

[80] K. Langendoen and N. Reijers, "Distributed localization in wireless sensor networks: a quantitative comparison," *Computer Networks*, vol. 43, no. 4, pp. 499–518, 2003.

[81] A. Lédeczi and et al, "Countersniper system for urban warfare," *ACM Trans. Sen. Netw.*, vol. 1, no. 2, pp. 153–177, 2005.

[82] A. Lerer, "The radio-transmitting properties of a carbon nanotube vibrator located on the boundary of a dielectric," *Moscow University Physics Bulletin*, vol. 65, no. 5, pp. 378–385, 2010.

[83] F. L. Lewis, "Wireless sensor networks," *Smart environments: technologies, protocols, and applications*, pp. 11–46, 2004.

[84] K. Li, *Electromagnetic fields in stratified media*, ser. Advanced topics in science and technology in China. Springer, 2009.

[85] L. Li, S. F. Lim, A. A. Puretzky, R. Riehn, and H. Hallen, "Near-field enhanced ultraviolet resonance raman spectroscopy using aluminum bow-tie nanoantenna," *Applied physics letters*, vol. 101, no. 11, p. 113116, 2012.

[86] R. Ling, J. Scholler, and P. Y. Ufimtsev, "The propagation and excitation of surface waves in an absorbing layer," *Progress In Electromagnetics Research*, vol. 19, pp. 49–91, 1998.

[87] B. Liu, K. Y. Kim, Y. Lai, X. Li, F. Ou, and S.-T. Ho, "Near-field nanoimaging by nanoscale photodetector array," *Optics letters*, vol. 34, no. 21, pp. 3367–3369, 2009.

[88] G. Mao, B. Fidan, and B. D. Anderson, "Wireless sensor network localization techniques," *Computer Networks*, vol. 51, pp. 2529 – 2553, 2007.

[89] K. Matthews, B. Carey, K. Evans, and P. Moloney, "NASA's relationship with nanothechnology: Past, present and future challenges," Baker Institute Policy Report, Tech. Rep., 2012.

[90] K. Michalski, "On the efficient evaluation of integral arising in the sommerfeld halfspace problem," in *Microwaves, Antennas and Propagation, IEE Proceedings H*, vol. 132, no. 5. IET, 1985, pp. 312–318.

[91] D. B. Miron, "Volume-loaded short dipole antenna," Nov. 16 1999, uS Patent 5,986,610.

[92] R. Mittra, "A vector form of compensation theorem and its application to boundary-value problems," *Applied Scientific Research, Section B*, vol. 11, no. 1-2, pp. 26–42, 1964.

[93] M. Moore, A. Enomoto, T. Nakano, R. Egashira, T. Suda, A. Kayasuga, H. Kojima, H. Sakakibara, and K. Oiwa, "A design of a molecular communication system for nanomachines using molecular motors," in *Pervasive Computing and Communications Workshops, 2006. PerCom Workshops 2006. Fourth Annual IEEE International Conference on.* IEEE, 2006, pp. 6–pp.

[94] Y. Moritani, S. Hiyama, and T. Suda, "Molecular communication for health care applications," in *Pervasive computing and communications workshops, 2006. PerCom Workshops 2006. Fourth Annual IEEE International Conference on.* IEEE, 2006, pp. 5–pp.

[95] T. Nakano, A. W. Eckford, and T. Haraguchi, *Molecular communication.* Cambridge University Press, 2013.

[96] T. Nakano, T. Suda, M. Moore, R. Egashira, A. Enomoto, and K. Arima, "Molecular communication for nanomachines using intercellular calcium signaling," in *Fifth IEEE Conference on Nanotechnology*, vol. 2, 2005, pp. 478–481.

[97] M. Nesterenko and V. Katrich, "Thin vibrators with arbitrary surface impedance as a handset antennas," in *IEE conference publication.* Institution of Electrical Engineers, 2003, pp. 16–20.

[98] J. L. Nicol and P. V. Ridd, "Antenna input impedance: experimental confirmation and geological application," *Canadian journal of physics*, vol. 66, no. 9, pp. 818–823, 1988.

[99] K. A. Norton, "The propagation of radio waves over the surface of the earth and in the upper atmosphere," *Radio Engineers, Proceedings of the Institute of*, vol. 25, no. 9, pp. 1203–1236, 1937.

[100] P. Parhami, Y. Rahmat-Samii, and R. Mittra, "An efficient approach for evaluating Sommerfeld integrals encountered in the problem of a current element radiating over lossy ground," *Antennas and Propagation, IEEE Transactions on*, vol. 28, no. 1, pp. 100–104, 1980.

[101] Q.-H. Park, "Optical antennas and plasmonics," *Contemporary physics*, vol. 50, no. 2, pp. 407–423, 2009.

[102] D. Penkin, G. Janssen, and A. Yarovoy, "Source node location estimation in large-scale wireless sensor networks," in *Microwave Conference (EuMC), 2012 42nd European*, 2012, pp. 333–336.

[103] D. Penkin, A. Yarovoy, and G. Janssen, "A study on communication aspects of two-dimensional large-scale wireless sensor networks using percolation principles," in *Communications and Vehicular Technology in the Benelux (SCVT), 2010 17th IEEE Symposium on.* IEEE, 2010, pp. 1–6.

[104] C. A. Poland, R. Duffin, I. Kinloch, A. Maynard, W. A. Wallace, A. Seaton, V. Stone, S. Brown, W. MacNee, and K. Donaldson, "Carbon nanotubes introduced into the abdominal cavity of mice show asbestos-like pathogenicity in a pilot study," *Nature nanotechnology*, vol. 3, no. 7, pp. 423–428, 2008.

[105] J. Polo, T. Mackay, and A. Lakhtakia, *Electromagnetic Surface Waves: A Modern Perspective.* Newnes, 2013.

[106] L. Ponomarenko, F. Schedin, M. Katsnelson, R. Yang, E. Hill, K. Novoselov, and A. Geim, "Chaotic dirac billiard in graphene quantum dots," *Science*, vol. 320, no. 5874, pp. 356–358, 2008.

[107] B. Popovic and D. Djurdjevic, "Entire-domain analysis of thin-wire antennas near or in lossy ground," *IEE Proceedings-Microwaves, Antennas and Propagation*, vol. 142, no. 3, pp. 213–219, 1995.

[108] D. M. Pozar, "Beam transmission of ultra short waves: an introduction to the classic paper by H. Yagi," *Proceedings of the IEEE*, vol. 85, no. 11, pp. 1857–1863, 1997.

[109] C. S. J. Rabaey and K. Langendoen, "Robust positioning algorithms for distributed ad-hoc wireless sensor networks," in *USENIX technical annual conference*, 2002.

[110] R. Ramanathan and J. Redi, "A brief overview of ad hoc networks: challenges and directions," *IEEE communications Magazine*, vol. 40, no. 5, pp. 20–22, 2002.

[111] A. G. Ramm, *Wave scattering by small bodies of arbitrary shapes*. Springer, 2005.

[112] P. Ramm and A. Klumpp, "Through-silicon via technologies for extreme miniaturized 3D integrated wireless sensor systems (e-CUBES)," in *Interconnect Technology Conference, 2008. IITC 2008. International*. IEEE, 2008, pp. 7–9.

[113] D. Rickerby and A. Carbone, "Nanosystems for water quality monitoring and purification," *Presentation at Nanotech Northern Europe Copenhagen*, pp. 23–25, 2008.

[114] N. Rikhtegar and M. Keshtgary, "A brief survey on molecular and electromagnetic communications in nano-networks." *International Journal of Computer Applications*, vol. 79, 2013.

[115] S. Roundy, B. P. Otis, Y.-H. Chee, J. M. Rabaey, and P. Wright, "A 1.9 GHz RF transmit beacon using environmentally scavenged energy," *optimization*, vol. 4, no. 2, p. 4, 2003.

[116] S. Roundy, D. Steingart, L. Frechette, P. Wright, and J. Rabaey, "Power sources for wireless sensor networks," in *Wireless sensor networks*. Springer, 2004, pp. 1–17.

[117] A. Rudge, "Input impedance of a dipole antenna above a conducting half space," *Antennas and Propagation, IEEE Transactions on*, vol. 20, no. 1, pp. 86–89, 1972.

[118] H. Schantz, "Nanoantennas: A concept for efficient electrically small UWB devices," in *IEEE International Conference ICU*, 2005, pp. 264–268.

[119] T. B. Senior and J. L. Volakis, *Approximate boundary conditions in electromagnetics*. Iet, 1995, no. 41.

[120] Y. Shang, W. Ruml, Y. Zhang, and M. P. Fromherz, "Localization from mere connectivity," in *Proceedings of the 4th ACM international symposium on Mobile ad hoc networking & computing*. ACM, 2003, pp. 201–212.

[121] E. Sheka, *Fullerenes: nanochemistry, nanomagnetism, nanomedicine, nanophotonics*. CRC Press, 2011.

[122] C.-C. Shen, Z. Huang, and C. Jaikaeo, "Directional broadcast for mobile ad hoc networks with percolation theory," *Mobile Computing, IEEE Transactions on*, vol. 5, no. 4, pp. 317–332, 2006.

[123] V. V. Shevchenko and V. V. Shevchenko, *Continuous transitions in open waveguides: introduction to the theory*, ser. The Golem series in electromagnetics. Golem Press, 1971.

[124] M. Shuba, G. Y. Slepyan, S. Maksimenko, C. Thomsen, and A. Lakhtakia, "Theory of multiwall carbon nanotubes as waveguides and antennas in the infrared and the visible regimes," *Physical Review B*, vol. 79, no. 15, p. 155403, 2009.

[125] F. Simonis and S. Schilthuizen, *Nanotechnology: Innovation Opportunities for Tomorrow's Defence*. TNO Science and Industry, 2006.

[126] G. Y. Slepyan, M. Shuba, S. Maksimenko, and A. Lakhtakia, "Theory of optical scattering by achiral carbon nanotubes and their potential as optical nanoantennas," *Physical Review B*, vol. 73, no. 19, p. 195416, 2006.

[127] G. Y. Slepyan, M. Shuba, S. Maksimenko, C. Thomsen, and A. Lakhtakia, "Terahertz conductivity peak in composite materials containing carbon nanotubes: Theory and interpretation of experiment," *Physical Review B*, vol. 81, no. 20, p. 205423, 2010.

[128] E. A. Soliman, "Circularly polarized nanoring antenna for uniform overheating applications," *Microwave and Optical Technology Letters*, vol. 54, no. 9, pp. 2209–2214, 2012.

[129] A. Sommerfeld, "Über die ausbreitung der wellen in der drahtlosen telegraphie [On the propagation of waves for the wireless telegraphy]," *Ann.Phys.Leipzig*, vol. 28, pp. 665–737, 1909.

[130] N. Sozer and J. L. Kokini, "Nanotechnology and its applications in the food sector," *Trends in biotechnology*, vol. 27, no. 2, pp. 82–89, 2009.

[131] C. Stampfer, T. Helbling, D. Obergfell, B. Schöberle, M. Tripp, A. Jungen, S. Roth, V. Bright, and C. Hierold, "Fabrication of single-walled carbon-nanotube-based pressure sensors," *Nano Letters*, vol. 6, no. 2, pp. 233–237, 2006.

[132] D. Stauffer and A. Aharony, *Introduction to percolation theory.* Taylor and Francis, 1991.

[133] M. D. Stoller, S. Park, Y. Zhu, J. An, and R. S. Ruoff, "Graphene-based ultracapacitors," *Nano letters*, vol. 8, no. 10, pp. 3498–3502, 2008.

[134] T. Suda, M. Moore, T. Nakano, R. Egashira, A. Enomoto, S. Hiyama, and Y. Moritani, "Exploratory research on molecular communication between nanomachines," in *Genetic and Evolutionary Computation Conference (GECCO), Late Breaking Papers*, 2005, pp. 25–29.

[135] P. Sudeep, B. I. Ipe, K. G. Thomas, M. George, S. Barazzouk, S. Hotchandani, and P. V. Kamat, "Fullerene-functionalized gold nanoparticles. a self-assembled photoactive antenna-metal nanocore assembly," *Nano Letters*, vol. 2, no. 1, pp. 29–35, 2002.

[136] I. E. Tamm, *Fundamentals of the Theory of Electricity.* Mir, 1979.

[137] G. Thoonen, E. Lopelli, J. van der Tang, and A. van Roermund, "System level considerations for ultra-low power transmitter-only wireless networks in the indoor environment," *ProRisc*, 2004.

[138] R. Tomellini, U. Faure, and O. Panzer, "European technology platform on nanomedicine: Nanotechnology for health," *Office for Official Publications of the European Communities: European Commission, Belgium*, 2005.

[139] M. Tsay, M. Tung, C. Chen, and T. Liu, "The manufacture of high permeability Mn-Zn ferrites by atmospherical protect," *Le Journal de Physique IV*, vol. 7, no. C1, pp. C1–71, 1997.

[140] L. A. Vaynshteyn, *Open resonators and open waveguides.* Golem Press, 1969.

[141] G. D. Vendelin, "Design of amplifiers and oscillators by the S-parameter method," *New York, Wiley-Interscience, 1982. 200 p.*, vol. 1, 1982.

[142] R. Vilzmann, C. Bettstetter, D. Medina, and C. Hartmann, "Hop distances and flooding in wireless multihop networks with randomized beamforming," in *Proceedings of the 8th ACM international symposium on Modeling, analysis and simulation of wireless and mobile systems*. ACM, 2005, pp. 20–27.

[143] T. Vo-Dinh, B. M. Cullum, and D. L. Stokes, "Nanosensors and biochips: frontiers in biomolecular diagnostics," *Sensors and Actuators B: Chemical*, vol. 74, no. 1, pp. 2–11, 2001.

[144] L. E. Vogler and J. L. Noble, *Curves of input impedance change due to ground for dipole antennas*, ser. Monograph (United States). US Department of Commerce, National Bureau of Standards, 1964, no. 72-79.

[145] J. L. Volakis, C.-C. Chen, and K. Fujimoto, *Small antennas: miniaturization techniques & applications*. McGraw-Hill New York, NY, 2010.

[146] R. Vullers, R. van Schaijk, I. Doms, C. Van Hoof, and R. Mertens, "Micropower energy harvesting," *Solid-State Electronics*, vol. 53, no. 7, pp. 684–693, 2009.

[147] F. Vullum, D. Teeters, A. Nytén, and J. Thomas, "Characterization of lithium nanobatteries and lithium battery nanoelectrode arrays that benefit from nanostructure and molecular self-assembly," *Solid State Ionics*, vol. 177, no. 26, pp. 2833–2838, 2006.

[148] S. Vural and E. Ekici, "Analysis of hop-distance relationship in spatially random sensor networks," in *Proceedings of the 6thinternational symposium on Mobile ad-hoc networking and computing*, 2005, pp. 320–331.

[149] J. Wait, *Electromagnetic waves in stratified media*, ser. The IEEE/OUP Series on Electromagnetic Wave Theory / Donald G. Dudley. Institute of Electrical and Electronic Engineers, 1996.

[150] J. Wait and G. Schlak, "New asymptotic solution for the electromagnetic fields of a dipole over a stratified medium," *Electronics Letters*, vol. 3, no. 9, pp. 421–422, 1967.

[151] Z. L. Wang, "Energy harvesting for self-powered nanosystems," *Nano Research*, vol. 1, no. 1, pp. 1–8, 2008.

[152] ——, "Towards self-powered nanosystems: From nanogenerators to nanopiezotronics," *Advanced Functional Materials*, vol. 18, no. 22, pp. 3553–3567, 2008.

[153] J. Weldon, K. Jensen, and A. Zettl, "Nanomechanical radio transmitter," *physica status solidi (b)*, vol. 245, no. 10, pp. 2323–2325, 2008.

[154] G. Werner-Allen and et al, "Deploying a wireless sensor network on an active volcano," *Internet Computing, IEEE*, 2006.

[155] H. A. Wheeler, "Fundamental limitations of small antennas," *Proceedings of the IRE*, vol. 35, no. 12, pp. 1479–1484, 1947.

[156] W. H. Wise, "The grounded condenser antenna radiation formula," *Radio Engineers, Proceedings of the Institute of*, vol. 19, no. 9, pp. 1684–1689, 1931.

[157] C. R. Yonzon, D. A. Stuart, X. Zhang, A. D. McFarland, C. L. Haynes, and R. P. Van Duyne, "Towards advanced chemical and biological nanosensorsan overview," *Talanta*, vol. 67, no. 3, pp. 438–448, 2005.

[158] Y. Yuge, "A renormalisation group approach for two-dimensional site percolating system," *Journal of Physics A: Mathematical and General*, vol. 11, no. 4, p. L83, 1978.

[159] G. Zaragoza-Galán, J. Ortíz-Palacios, B. X. Valderrama, A. A. Camacho-Dávila, D. Chávez-Flores, V. H. Ramos-Sánchez, and E. Rivera, "Pyrene-fullerene C60 dyads as light-harvesting antennas," *Molecules*, vol. 19, no. 1, pp. 352–366, 2013.

[160] Y. P. Zhang, Z. M. Chen, and M. Sun, "Propagation mechanisms of radio waves over intra-chip channels with integrated antennas: Frequency-domain measurements and time-domain analysis," *Antennas and Propagation, IEEE Transactions on*, vol. 55, no. 10, pp. 2900–2906, 2007.

[161] X.-L. Zhong and Z.-y. Li, "Three-dimensional aluminum nano funnel-antenna for enhanced absorption of near-ultraviolet light by TiO2," in *Metamaterials (Meta), 2012 International Workshop on.* IEEE, 2012, pp. 1–2.

Author's publications

[1] D. Penkin, A. Yarovoy and G. Janssen, "A Study on Communication Aspects of Two-dimensional Large-scale Wireless Sensor Networks Using Percolation Principles," In: 17th IEEE Symposium on Communications and Vehicular Technology, pp. 1-6, 2010.

[2] D. Penkin, G. Janssen and A. Yarovoy, "Estimation of Maximum Communication Distance Between In-vivo Miniature Electronic Implants," In: 5th International Symposium on Medical Information and Communication Technology, pp.33-36, 2011.

[3] D. Penkin, A. Yarovoy and G. Janssen, "Feasibility Analysis of Peer-to-peer Microwave Communications Between Self-powered Miniature Electronic Devices," In: 5th International European Conference on Antennas and Propagation (EUCAP), pp.122-125, 2011.

[4] D. Penkin, G. Janssen and A. Yarovoy, "The Effective Electrically Small Encapsulated Antenna Applied for Communication Between Self-powered Miniature Devices," In: 5th International European Conference on Antennas and Propagation (EUCAP), pp.3801-3803, 2011.

[5] D. Penkin, A. Yarovoy and G. Janssen, "Surface Impedance Model for Nanoscale Device Communications over an Interface," In: 19th IEEE Symposium on Communications and Vehicular Technology (SCVT), pp.1-5, 2012.

[6] D. Penkin, G. Janssen and A. Yarovoy, "Source Node Location Estimation in Large-scale Wireless Sensor Networks," In: 42nd International European Microwave Conference (EuMC), pp.333-336, 2012.

[7] D. Penkin, G. Janssen and A. Yarovoy, "Source positioning in a large-scale tiny-sensor network of arbitrary topology," EURASIP Journal on Advances in Signal Processing, no. 1, pp.1-11, 2014.

[8] D. Penkin, G. Janssen and A. Yarovoy, "Impact of a half-space interface on the wireless link between tiny sensor nodes," Radio Science, 49(9), pp.798-811, 2014.

[9] D. Penkin, A. Yarovoy and G. Janssen, "Electromagnetic properties of fullerene derivatives," submitted to Nanoscale Research Letters, 2015.

[10] D. Penkin, A. Yarovoy and G. Janssen, "Investigation of a Fullerene-based Yagi-Uda-type Antenna," submitted to IEEE Antennas and Wireless Propagation Letters, 2015.

Acknowledgements

Nanonetworking has been a fascinating subject to dedicate 4+ years of my life. My utmost gratitude goes to my promotor, Prof. Alexander Yarovoy, who provided me the opportunity to challenge myself on this ambitious topic. I would like to thank with much sincerity for his scientific support and limitless enthusiasm, for granting me the research freedom and at the same time keeping me focused on my subject through his inspiring guidance. Also, I very appreciate Prof. Yarovoy for all his encouragement, patience and trust in me along all the years required to successfully complete this Ph.D. dissertation.

I would like to express my deepest gratitude to my copromoter Dr.ir. Gerard Janssen, who has been in any moment fully available for discussions and has always provided interesting and stimulating contributions to my research work. I have truly enjoyed the collaboration with Mr. Janssen on various topics and his ability to open up new research perspectives. Also, I wish to thank my committee members, Prof. dr. I. Niemegeers, Prof. ing. F. Le Chevalier, Prof. dr. G. Leus, Prof. dr. W. Serdijn and Prof. dr. A.B. Smolders, for their thorough reviews and suggestions towards the improvement of my academic work.

I would like to extend my gratitude to my former and present colleagues, who have not been directly involved in my Ph.D. project, but who have helped and supported me along this way. Of the many, I would particularly like to thank Nikita Petrov, Yann Dufournet, Francesco Belfiori, Alexey Narykov, Dario Petri, Shenario Valavan, Igor Stepanov, Zongbo Wang, Oleg Krasnov, Dihn Tran, Yuan He, Albert Oude Nijhuis, Shilong Sun, Fotios Katsilieris, Teun de Groot, Inna Ivashko, Nadia Haider, Daniela Vaman, Galina Babur and other from the MS3 group. Also, I would like to thank Pascal Aurby, Fred van der Zwan and the other technicians from MS3 group, who were always very supportive and happy to share their knowledge. A special

acknowledgement goes to Minke van der Put: thank to her endeavours I have merely been busy with my academic activity. I need to further express my gratitude to all the members of the IRCTR Italian team (*precipitevolissimevolmente!*), who have been very friendly and made the best Italian after-lunch coffee. This paragraph would not be complete if I would not acknowledge the fruitful discussions that I have had throughout my Ph.D. period with my officemates Diego Caratelli, Jianping Wang and Harun Cetinkaya.

I am very grateful to my former teammates of the Delft University football team "Op't Randje". Especially, I would like to thank Alexey Andrianov for introducing me to this team. I have enjoyed my time playing in the team and have been proud to win a few medal places with these guys. I would also like to mention all the dear people who have made my stay in The Netherlands enjoyable: Viktor and Svetlana Alefantievy, Ludmila and Evgeniy, Alexandr and Viktoriya, Tobias and Helena, Noa and Bert, Jelmer and Kristina, Slawek, Nicole, Vladimir, Alex and others. Please be ensure of my deep gratitude even if I forgot to mention your names in the lines above.

I am deeply indebted to my parents, Tetiana and Iuriy. Their unconditional love and patience during all these years have continuously supported me despite the fact that they are far away from the Netherlands. I could always feel their backing and greatly appreciate it. Thanks from the bottom of my heart.

And last, best...I would like to say infinitely many thanks to my beloved Oksana for always being there for me and, in particular, for turning a house in Delft into the Home, where I always have comfort, encouragement and love. I want to thank my wife for her support in all the things that I would like to achieve, and for her patience and care. Without her, I would certainly not be able to be the person I am now and I would also not be able to accomplish all the things I have fulfilled so far. I am enormously lucky to have her by my side. A kiss for my beautiful wife and my family, I love you! Thank you for everything!

Dmitriy Penkin,
Delft, October 2015.

About the author

Dmitriy Penkin was born was born in Kharkov, Ukraine, in 1986. He received the M.Sc. degree from the V.N. Karazin Kharkov National University (the graduation work is entitled "Electromagnetic Properties of a Transverse Slot in a Rectangular Waveguide with Local Dielectric Insertion"). Subsequently, he joined the Microwave Sensing, Signals and Systems group, Delft University of Technology (The Netherlands) and worked there towards the Ph.D. degree in the field of wireless communication among nanoscale devices. At present, he performs R&D work applicable to EMC and RF engineering as well as is responsible for the development and improvement of anechoic chambers, reverberating chambers, Faraday cages and other RF shielding facilities.